PREVENTIVE MAINTENANCE OF POROUS ASPHALT PAVEMENT THROUGH SURFACE TREATMENT ASPHALT EMULSION: WORKING MECHANISM AND MATERIAL OPTIMIZATION

BIN YANG

PhD

The Hong Kong Polytechnic University

2025

The Hong Kong Polytechnic University

Department of Civil and Environmental Engineering

Preventive Maintenance of Porous Asphalt Pavement through Surface Treatment Asphalt Emulsion: Working Mechanism and Material Optimization

Bin Yang

A thesis submitted in partial fulfilment of the requirements for
the degree of Doctor of Philosophy

August 2024

CERTIFICATE OF ORIGINALITY

I hereby declare that this thesis is my own work and that, to the best of my knowledge and belief, it reproduces no material previously published or written, nor material that has been accepted for the award of any other degree or diploma, except where due acknowledgement has been made in the text.

_____________(Signed)
___Bin Yang___(Name of student)

To my family

ABSTRACT

Porous asphalt (PA) pavement has been widely applied worldwide because of its numerous merits, such as improved drainage, reduced noise, and enhanced skid resistance. However, the open-graded structure of PA increases the susceptibility of bitumen to aging, which makes PA more vulnerable to the ravelling distress at the early stage compared to conventional dense-graded and gap-graded asphalt pavement. Several measures have been applied to alleviate ravelling, such as using polymer modified asphalt binders, adding fibers/anti-stripping additives, and substituting conventional asphalt binder with epoxy, but the ravelling destress is still of frequent occurrence after a few years of service. Therefore, an effective preventive maintenance technique is necessary to alleviate ravelling during the road service period. Recent field trials in Europe showed that spraying surface treatment (ST) asphalt emulsion to existing PA pavement could mitigate ravelling and extend its service life. However, despite limited field experience and lab results, the interaction mechanisms of ST emulsion in old PA mixture remains unclear. In addition, there is a lack of scientific effort on how to optimize the ST emulsion for this purpose. To fill these research gaps, this study aims to reveal the working mechanism of ST emulsion in PA and optimize the material design of ST emulsion for improving maintenance effectiveness through a multiscale investigation.

At the macroscale, the key factors affecting the recovery efficiency of ST emulsion on the ravelling resistance of damaged PA were first investigated and the optimal application conditions of ST were determined. Subsequently, the effects of ST on the mechanical and functional properties of the damaged PA were systematically evaluated. The results showed that both application rate and solid content of ST emulsion have significant effects on the ravelling resistance recovery of the damaged PA mixtures. The optimum application rate of 0.6 kg/m^2 and solid content of 60% were recommended. The negative effect of ST emulsion on the functional performance (e.g.: noise reduction, permeability, and skid resistance) of PA was

found to be insignificant. Meanwhile, the ST treated PA mixtures achieved superior rutting, fatigue, and cracking resistances.

At the mesoscale, the penetration behavior of ST emulsion in damaged PA was investigated by X-ray Computer Tomography (CT). A series of image-related MATLAB algorithms were developed to identify and quantify the penetration status of three selected ST scenarios. The spatial distribution of ST emulsion in the damaged PA presented a gradient characteristic along the depth direction. The ST application reshaped the interconnected pore microstructure, including the size, number, area, interconnectivity, and tortuosity of air voids. The PA specimen treated by the ST emulsion with an application rate of 0.6kg/m^2 and a solid content of 60% showed the best coating efficiency and the best ravelling resistance among the three ST conditions.

At the microscale, the diffusion phenomena between ST residues and aged asphalt mortars within PA mixtures were observed via the Scanning Electron Microscopy (SEM) with Energy Dispersive Spectroscopy (EDS). TiO_2 nano powder was selected as a tracer to tag the ST emulsion. The PA specimen preparation and analysis method for SEM/EDS testing were developed. The results showed that the diffusion rate at 60 °C was approximately 5 times faster than that at 25 °C. Thus, it is recommended to spray ST emulsions on old PA pavements in hot weather to accelerate the diffusion efficiency.

Due to the nonuniform distribution and slow diffusion efficiency of conventional asphalt emulsion in PA mixture, rejuvenator was added to optimize ST asphalt emulsion. It was suggested to be emulsified first before directly mixing with asphalt emulsion for better compatibility. The optimal dosage of rejuvenator emulsion was determined by balancing the apparent viscosity, wettability, and bonding strength of ST emulsion. The CT images revealed that the rejuvenator-optimized ST emulsion was uniformly distributed in the PA mixture with

a higher coating efficiency, which improved the ravelling resistance of PA. The physicochemical analysis implied that the penetrated rejuvenator-optimized ST residues replenished new asphalt binders and softened aged asphalt binders, decreasing the molecular weight of aged asphalt binder. The rheological results showed the rejuvenator-optimized ST residues improved the stress relaxation property and cracking resistance of aged asphalt binders but might compromise rutting resistance.

LIST OF PUBLICATIONS

Journal papers (Published)

Yang, B., Leng, Z.*, Jiang, J., He, Z. and Li, D., 2022. Recovery efficiency of the damaged porous asphalt mixture with emulsion-based surface treatment: Material optimization and performance verification. *Construction and Building Materials*, *347*, p.128530.

Yang, B., Leng, Z.*, Jiang, J., Chen, R. and Lu, G., 2024. Diffusion characteristics of surface treatment emulsion in aged asphalt mortar of porous asphalt mixture through SEM/EDS analysis. *International Journal of Pavement Engineering*, *25*(1), p.2290093.

Yang, B., Leng, Z.*, Jiang, J., Li, R. and Han, M., 2024. Short-and long-term mechanical performances of damaged porous asphalt mixture treated with asphalt emulsion. *Road Materials and Pavement Design*, pp.1-13.

Yang, B., Jiang, J., Wang, H., Leng, Z.*, Sui, X. and Jiang, X., 2024. Optimization design of asphalt emulsion with rejuvenators towards a uniform distribution inside the damaged porous asphalt mixture for a better ravelling resistance. *Case Studies in Construction Materials.*

Jiang, J., Leng, Z.*, **Yang, B.**, Lu, G., Tan, Z., Han, M. and Dong, Z., 2022. Penetration mechanism of the emulsion-based rejuvenator in damaged porous asphalt mixture: Microstructure characterization and 3D reconstruction. *Materials & design*, *221*, p.111014.

Journal papers (Under review)

Yang, B., Jiang, J., Leng, Z.*, Jiang X., Yan, C., Tan, Z., and Li, G. Maintenance mechanisms of rejuvenator-optimized asphalt emulsion in damaged porous asphalt mixture: morphological, physicochemical, and rheological characterizations. *Under review in Construction and Building Materials.*

ACKNOWLEDGEMENTS

Throughout my doctoral study, I have got tremendous support and help from many individuals.

First of all, I would like to express my sincere appreciation to my supervisor, Prof. Zhen Leng, for his professional guidance, invaluable advice, and substantial support during my PhD study. His rigorous academic attitude and positive learning attitude always inspired me to solve one problem after another in my doctoral research. He often encouraged us to participate in international conferences to practice our presentation skills and share our latest research outcomes as well as exchange minds with other researchers, which enriched my PhD life.

I want to thank Dr. Jiwang Jiang, who is not only an excellent postdoctoral fellow but also a nice mentor in my PhD study. I still clearly remember that at the beginning of the research project, he patiently guided me to dig out and solve the hidden scientific problem from the perspective of engineering practice. His ideas and suggestions are meaningful to this thesis.

I would like to acknowledge the technicians in our transport and highway engineering laboratories, Mr. M.C. Choi, Mr. W.K. Wong, and Mr. W.L. Wong, for their technical support in setting up equipment and daily companionship. I also want to thank the Department of Civil and Environmental Engineering of The Hong Kong Polytechnic University for providing financial support for my doctoral study.

Our research group is a united and loving family. Although the COVID-19 pandemic has trapped us in HK, it has also given us more time to stay together and deepen our friendship. Dr. Li Rui, Dr. Tan Zhifei, Dr. Cai Xing, Dr. Yao Linyi, Dr. Li Danning, Dr. Yan Chuanqi, Dr. Gong Mingyang, Dr. Jiang Xi, Dr. Li Hui, Dr. Yin Binbin, Dr. Zou Fuliao, Dr. Sreeram Anand, Dr. Cao Ruijun, Dr. Wang Haopeng, Dr. Lu Guoyang, Dr. Wang Siqi, Dr. Sun Yubo, Dr. Prabin Kr. Ashish, Dr. Chen Zongwu, Dr. Xia Chengdong, Dr. Guo Feng, Dr. Fang Chenze, Dr. Weng Zihang, Dr. Zhang Xinqiang, Dr. Lu Dong, Mr. Li Gaoyang, Mr. Sui Xin, Mr. Chen Ruiqi, Mr.

Han Meizhao, Mr. Xu Jiaqiu, Ms. Lan Jingting, Mr. Zhang Shaowei, Mr. He Zijian, Mr. Zheng Kunpeng, Ms. Li Hanxi, Mr. Chen Zhaojie, Mr. Fan Yulou, Mr. Wang Yijie, Mr. Shen Mou, … Sincerely appreciate your help and support during my PhD journey.

I also want to thank PolyU for providing us with various sports facilities, so I made many friends from different subjects on the badminton court and in the swimming pool. Thanks Dr. Tian Wei, Dr. Li Yixian, Dr. Zhao Qi, Dr. Li Dongfang, Dr. Wang Xi, Dr. Yan Rui, Dr. He Jionghuang, Dr. Shen Peiliang, Dr. Wang Fei, Mr. Gu Hao, Mr. Wei Yitao, and Mr. Lin Xiaoyu for the colorful life together. Hong Kong has many natural resources for outdoor activities. I am very fortunate to have the opportunity to hike among the mountains and seaside.

Last but not least. I would like to thank my family members for their endless love and support. The daily care and encouragement from my parents have given me the confidence to face life. I also want to thank my elder sister. When I hadn’t accompanied our parents, my elder sister always helped me to share more responsibilities in taking care of the whole family, so that I could complete my doctoral dissertation without distraction. This thesis is also dedicated to them.

LIST OF TABLES

LIST OF FIGURES

LIST OF ABBREVIATIONS

AASHTO	American Association of State Highway and Transportation Officials
AE	Asphalt emulsion
AO	Aromatic oil
AOAE	Aromatic oil optimized asphalt emulsion
ANOVA	A one-way analysis of variance
ASTM	American Society for Testing and Materials
ATR	Attenuated total reflection
BPN	British pendulum number
CSS	Cationic slow-setting
CT	Computed tomography
DAC	Dense asphalt concrete
DCM	Dichloromethane
DLVO	Derjaguin-Landau-Verwey-Overbeek
DSR	Dynamic shear rheometer
FS	Frequency sweep
F-T	Freezing and thawing
FTIR	Fourier transform infrared spectroscopy
GPC	Gel permeation chromatography
G-R	Glover-Rowe parameter
HMA	Hot mix asphalt
HS	Huet-Sayegh
ITFT	Indirect tensile fatigue test
ITSM	Indirect tensile strength modulus
LAS	Linear amplitude sweep
LTA	Long-term aging
MHS	Modified Huet-Sayegh
MSCR	Multiple stress creep recovery
OGFC	Open-graded friction course

PA	Porous asphalt
PAV	Pressure aging vessel
PG	Performance grade (Superpave)
PU	Polyurethane
RAP	Reclaimed asphalt pavements
RALT	Repeated axial load test
SBS	Styrene-butadiene-styrene
SGC	Superpave gyratory compactor
SHRP	Strategic Highway Research Program
SMA	Stone mastic asphalt
ST	Surface treatment
THF	Tetrahydrofuran
TO	Tall oil
TOAE	Tall oil optimized asphalt emulsion
TTSP	Time-temperature superposition principle
UTM	Universal testing machine
WLF	Williams-Landel-Ferry

TABLE OF CONTENTS

CHAPTER 1 INTRODUCTION

1.1 Background

Over the past decades, numerous countries and regions have constructed or expanded extensive networks of highways and municipal roads to accommodate urbanization and rapid economic development. Asphalt pavement has become the predominant paving material due to its various advantages, including convenient construction operation, fast traffic opening, and good driving comfort. Asphalt pavement aggregate gradation can generally be categorized into three typical structures based on varying degrees of skeleton density: dense suspension type, skeleton void type, and skeleton dense type [1, 2]. These correspond to dense asphalt concrete (DAC), stone mastic asphalt (SMA), and porous asphalt (PA) pavements, respectively. DAC and SMA pavements are conventional dense-graded and gap-graded asphalt pavements with a small air void content ranging from 3% to 7%, while the PA pavement is characterized by an open-graded structure with a large air void of at least 15%. PA pavement is often termed as the open-graded friction course (OGFC) in the U.S. [3] or the PA wearing courses in European countries [4]. Owing to its rich surface texture and high air void content, PA pavement offers various attractive functions, such as decreasing tire-road noise [5, 6], reducing water splashing and hydroplaning on rainy days [7, 8], improving pavement surface friction[9], and alleviating urban heat island effects [10, 11]. However, under the combined effects of traffic and weathering, PA mixtures tend to have a shorter service life compared to conventional asphalt mixtures due to rapid ravelling, where aggregate particles dislodge from the pavement surface [12]. The high interconnected air void content in PA mixtures facilitates the ingress of oxygen and water, accelerating asphalt binder aging and weakening the bonding strength between binder and aggregate [13, 14]. Consequently, the ravelling problem has become an inevitable issue that might restrict the widespread application of PA pavements.

To address the ravelling problem of PA pavements, various practical experiences have been explored globally, which can be categorized into three categories based on the material sources and their roles in the PA mixture. Some researchers have introduced fibers [15] and anti-stripping additives [16] into PA mixtures to improve the cohesive strength of binder and the adhesive strength of asphalt binder to aggregate surface. Additionally, high-viscosity asphalt binders have been widely adopted to replace conventional modified asphalt binders in many regions [17, 18]. For instance, in Hong Kong, both virgin and polymer modified asphalt binders have been used to build PA road surfaces, and the PA with polymer modified binder was found more cost-effective due to its superior durability [19]. In Japan, it was observed that PA with a conventional polymer-modified binder containing 5% styrene-butadiene-styrene (SBS) cannot provide sufficient durability. Instead, a highly modified bitumen containing 9% SBS with very high viscosity at 60 °C was developed and found to be able to significantly extend the service life of PA wearing course. This special high-viscosity polymer-modified asphalt has been used in force for PA wearing courses in Japan since 1998 [20]. The Netherlands, features PA wearing courses on over 90% of its main highway network, also has long-term experience with PA pavements. But contradictory to the experience in Hong Kong and many other regions, the Netherlands experience has shown that polymer-modified binder has an insignificant effect on extending the service life of PA wearing courses [21]. It was reported that polymer modified binder was only useful to obtain a higher binder content in PA which led to better behavior in the field, but similar improvements could be achieved with virgin binder and drainage inhibitor [22]. Recently, novel binder materials, such as resins, have been applied in pavement construction, demonstrating excellent mechanical properties. German researchers found that polyurethane (PU) is a promising binder for permeable pavement due to its excellent strength and durability [23, 24]. Epoxy resin was also applied for permeable roads to withstand heavy traffic loads and maintain pavement functional properties [25-27]. However, all the above improvements have focused on enhancing cohesive and adhesive strength through material design and optimization during the pavement construction phase. Although those approaches can prolong the service life of PA pavements to some extent, ravelling is still one of the common distresses that limits the durability of PA wearing courses. Therefore, the development of effective preventive maintenance technologies to alleviate the ravelling post-construction remains a critical challenge.

Recently, spraying surface treatment (ST) asphalt emulsion has been investigated as a preventive maintenance method for PA wearing courses [28, 29]. The main component of ST emulsion is the emulsified asphalt, where asphalt droplets uniformly and stably distribute in water with the help of emulsifiers. Unlike fog seal [30], typically applied to dense-graded and gap-graded asphalt pavements, ST emulsion is designed to penetrate into the PA mixture without clogging air voids and compromising the functional properties. While the application of fog seal on conventional asphalt pavement is relatively well-established, the research and application of ST emulsion as a preventive maintenance method for PA wearing courses remain in the early stages. In 2010, the Netherlands Ministry of Infrastructure and Environment carried out a project entitled “Prolonging the service life of porous asphalt pavement” to investigate the feasibility of using ST emulsions for preventive maintenance of PA wearing courses [31]. The two trial sections involved in this project presented superior durability in the first five years of service without significant distress, which verified that ST emulsions could enhance the ravelling resistance of PA without clogging the voids [22]. They claimed that ST emulsions could add new asphalt binder, fill cracks and rejuvenate aged asphalt binder via diffusion [32, 33]. However, except for some successful field trials and limited laboratory tests, the effects of ST emulsion on the mechanical and functional performances of PA mixtures haven’t been systematically studied. The interaction mechanisms between ST emulsion and the existing PA mixture remain unclear. Suggestions about applying ST emulsion as a preventive maintenance material for PA pavements are still missing. How to optimize ST emulsion to enhance the ravelling resistance of PA needs in-depth research.

1.2 Research Objectives and Scope

Based on the knowledge gaps discussed above, this research aims to multiscale investigate the working mechanism of ST emulsion in PA and optimize the material design of ST emulsion for improving maintenance effectiveness. To achieve such goals, the following research tasks have been conducted:

1. Literature review: to comprehensively review the causes of the ravelling problem in PA, the current research on surface treatment (ST) asphalt emulsion for PA pavements, and the common penetration and diffusion behaviors that happened in asphalt mixtures.

2. Macroscopic evaluation on the recovery efficiency of damaged PA with ST emulsion: to investigate the effects of ST emulsion on the mechanical and functional properties of damaged PA mixtures.

3. Mesoscale investigation on the penetration mechanism of ST emulsion inside PA: to identify and characterize the penetration status of ST emulsion inside damaged PA using X-ray CT imaging.

4. Microscale exploration of the diffusion phenomenon between ST residues and aged asphalt mortar: to investigate the diffusion behavior of new ST emulsion residue in aged asphalt mortar of damaged PA during a long-term curing process by SEM/EDS.

5. Optimization design of ST emulsion with rejuvenator: to optimize the ST emulsion formula with rejuvenator towards a uniform distribution inside the damaged PA mixture for a better ravelling resistance.

6. Comprehensive investigation on the maintenance mechanisms of rejuvenator-optimized asphalt emulsion in damaged PA: to systematically investigate the working mechanisms of rejuvenator-optimized ST emulsion in damaged PA mixture from morphological, physicochemical, and rheological perspectives.

1.3 Significance of This Research

Upon completion of this research, the following contributions were achieved:

1. The effects of ST emulsion on the mechanical and functional performances of damaged PA mixtures were systematically investigated.

2. The penetration depth and coating efficiency of ST emulsion in damaged PA mixture have been proved to significantly affect the ravelling resistance of PA mixture, which inspired the permeability and wettability optimizations of ST emulsion.

3. The diffusion coefficient of ST residues was developed to characterize its diffusion phenomenon in aged asphalt mortar of PA mixture. And it is recommended to apply ST emulsion in hot weather to enhance the maintenance efficiency.

4. The pretreatment method for rejuvenator was proposed, and the optimal dosage of rejuvenator in optimized ST emulsion was determined towards a better ravelling resistance of damaged PA.

1.4 Organization of This Thesis

This thesis consists of 8 chapters as elaborated below.

Chapter 1 presents the background, objectives, scope, and significance of this research.

Chapter 2 presents a comprehensive literature review, including (1) the causes of ravelling in aged PA pavements; (2) the current application status of preventive maintenance technologies for PA pavements; and (3) the current studies on the penetration and diffusion behaviors in asphalt mixtures.

Chapter 3 discusses the effects of ST emulsion on the mechanical and functional properties of damaged PA mixtures at the macroscopic scale. The key factors affecting the recovery efficiency of ST emulsion on ravelling resistance of PA were investigated, and the optimal application conditions of ST were determined. Short- and long-term mechanical performances of damaged PA mixtures treated with ST emulsions were systematically evaluated. The effects of ST emulsion on the functional properties of PA were evaluated for verification purposes.

Chapter 4 presents the distribution of emulsion residue in damaged PA mixture under different ST scenarios and its relationship with the ravelling resistance at the mesoscopic scale. X-ray CT was used to monitor the pore structure of the PA specimen before and after ST. The spatial distribution of ST emulsion residue was back calculated and visualized in 3D through image analysis. The coating efficiency and thickness distribution of emulsion residue were quantitatively estimated to evaluate the penetration status.

Chapter 5 investigates the potential diffusion phenomena between new ST emulsion residues and aged asphalt mortars in PA mixtures at the microscopic scale. The specimen preparation and analysis method for characterizing the diffusion phenomenon through SEM/EDS technology was developed. A quantitative index was proposed to characterize the diffusion degree. Two curing temperatures and several different curing durations were considered.

Chapter 6 presents the optimization design of ST asphalt emulsion with rejuvenator. Three methods for incorporating rejuvenators into ST emulsion were evaluated. The appropriate pretreatment parameters for rejuvenator emulsion were investigated considering the storage stability and homogeneity. Subsequently, the optimal dosage of rejuvenator emulsion in ST emulsion was determined based on the balance design among the viscosity, wettability, and bonding strength.

Chapter 7 discusses the maintenance mechanisms of rejuvenator-optimized ST emulsion in damaged PA mixtures. Maintenance effectiveness is comprehensively characterized using X-ray CT, FTIR, GPC, and DSR tests from morphological, physicochemical, and rheological perspectives.

Chapter 8 summarizes the main findings and recommendations of this thesis study.

The overall research framework is depicted in Figure 1.1. The main research content consists of five chapters. Firstly, the maintenance effectiveness of ST emulsion and its working mechanism in old PA were evaluated through a multiscale investigation. Then, the ST emulsion was further optimized by rejuvenator towards a better ravelling resistance of PA based on the penetration and diffusion mechanisms of ST emulsion. Finally, the maintenance effectiveness of rejuvenator-optimized ST emulsion was comprehensively investigated and verified.

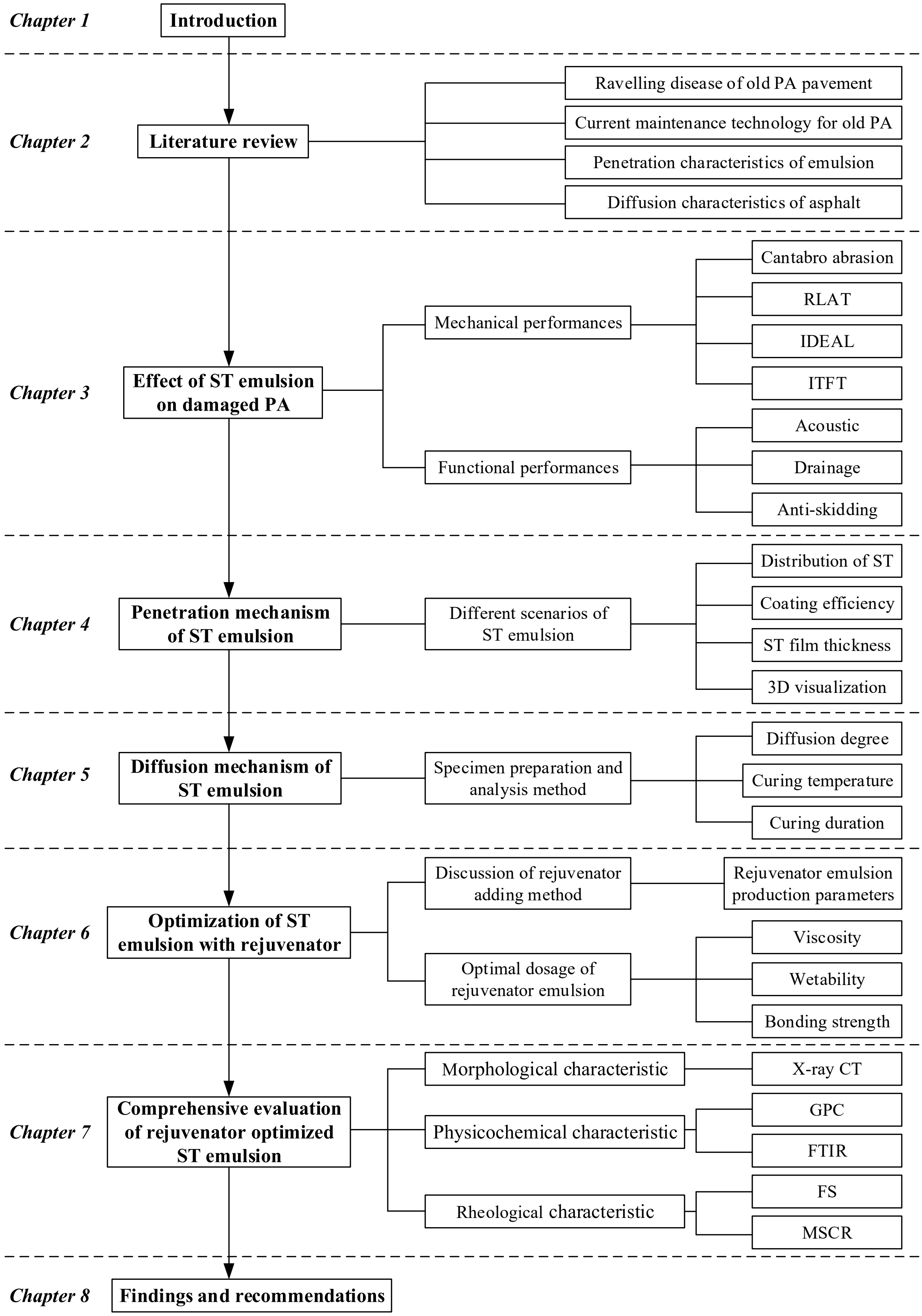

Figure 1.1 Research framework

CHAPTER 2 LITERATURE REVIEW

This chapter provides a comprehensive review of previous studies on the application and maintenance of PA pavement. Section 2.1 presents the origin and development of PA pavement. Section 2.2 summarizes common diseases that occurred in PA pavement and the corresponding maintenance strategies. Section 2.3 reviews current research on penetration behavior observed in PA pavement. Section 2.4 discusses the current research on the diffusion phenomenon that happened in PA pavement.

2.1 Porous Asphalt Pavement

The concept of creating porosity in pavement was first introduced in the 1800s to alleviate the stormwater in European cities. During World War II (WWII) and the post-war period, porous pavement gained renewed attention and application in Europe due to shortages of construction materials such as cement [34]. This type of pavement was subsequently adopted in the United States. By the 1960s, porous pavement, including porous asphalt (PA) and porous concrete, began to see widespread use across several states, driven by the U.S. Environmental Protection Agency's recognition of its potential to address urban waterlogging issues [35, 36]. Due to its open-graded structure, PA mixture was also referred to as an open-graded friction course (OGFC) in the U.S.

Compared to conventional dense graded asphalt pavement, PA pavement has lots of interconnected pore structures with an air void content of no less than 15% [37]. Beyond its effectiveness in stormwater management and runoff control, PA pavement offers additional benefits. For example, PA pavement also is a kind of low-noise pavement as it can significantly reduce the traffic noise at the source by controlling the tyre-road interaction noise [38]. The tyre-road interaction noise mainly consists of pumping, rolling, and vibration noise [39-41]. Although rapid contact and compression between the tire tread and road surface during high-speed driving generate air compression, most of this energy dissipates as frictional heat and other kinetic energy along the pavement's interconnected pores. Only a small portion of the energy results in cavity resonance, thereby significantly reducing pumping noise [42, 43]. Besides, PA pavement functions as a cooling surface in "sponge cities" [44, 45]. Rainwater can quickly infiltrate the PA pavement and permeate the road base, potentially replenishing groundwater. Some of this rainwater remains within the PA mixture and evaporates on sunny or cloudy days, helping to lower surface temperatures [46]. This contributes to alleviating the urban heat island effect. Also, the relatively rough surface of PA pavement provides tires with enough roughness, which significantly enhance driving safety, especially in wet conditions. In Japan, PA pavement has been shown to reduce the risk of traffic accidents by more than 80% in critical sections during rainy conditions, leading to an increased application of PA pavement across the national expressway network [47-49].

However, with the widespread adoption of PA pavement, some limitations have become apparent. Firstly, the air voids in PA tend to become clogged after PA road was opened to traffic for about 4 to 5 years [50, 51]. The reduction in air void can be attributed to two main factors: the accumulation of soil and debris within the voids through rainfall [52, 53] , and the densification of the pavement under continuous traffic loads, particularly at high service temperatures, which causes the aggregate structure to compress [54, 55]. These factors diminish the attracting functions of PA. Besides, ravelling is another common disease for PA pavement, which refers to the aggregate particles stripping from the pavement surface. It could be attributed to the failures of cohesion among asphalt binders and adhesion between asphalt binders and aggregates [56-58]. The open-graded structure of PA, where coarse aggregates are in direct contact, transmits traffic loads through a skeleton structure. This creates higher stress at the contact points between aggregates compared to conventional dense asphalt pavement [59]. Consequently, PA pavement is more susceptible to repeated loading, leading to microcracking in mortar areas. The high air void content also facilitates the diffusion of heat and oxygen, accelerating the ultraviolet and oxidative aging of the asphalt binders. Aging typically results in binder brittleness and reduced ductility, increasing the risk of ravelling.

2.2 Current Maintenance Technology for Ravelling of Old PA

As introduced in Section 2.1, long-term observations have identified two main pavement diseases in old PA roads: clogging and ravelling. To address clogging, apart from using a high-performance binder with a high polymer modifier content or changing aggregate gradation during the construction period, regular maintenance is essential. This includes cleaning the air voids in PA pavements using the combined high-pressure vacuum/washing methods [60-62]. While as for the ravelling disease, although appropriate high-performance materials were adopted to alleviate this problem, PA road still suffered from ravelling distress after it was opened to traffic for several years. Recent studies indicated that timely spraying surface treatment (ST) emulsion to PA pavement, before the beginning of ravelling disease, can effectively delay the need for extensive rehabilitation and extend the pavement's service life. The detailed literature reviews about this preventive maintenance material were summarized as follows.

2.2.1 Surface treatment (ST) asphalt emulsion

2.2.1.1 Composition of ST asphalt emulsion

ST emulsion is mainly comprised of asphalt emulsion, which typically contains asphalt, emulsifiers, water, and stabilizers [63, 64]. Although some specific functional additives are added to asphalt emulsion to improve its workability in some performances, the commonly used emulsion is introduced here first. Other kinds of ST emulsion will be introduced later. Asphalt emulsion is a typically oil-in-water (O/W) system where asphalt droplets stably distributed in water with the help of emulsifiers [65]. The solid content in asphalt emulsion generally ranges from 40% to 75% [66]. Some asphalt emulsions with low solid contents around 30% were prepared by directly diluting the common asphalt emulsion with water. Those asphalt emulsions with low solid contents are usually used as the prime coat or tack coat to achieve a more uniform distribution without applying excessive mass of asphalt binders [67-69].

The average particle size of asphalt droplets generally spans 2 to 10 μm [70]. The particle size of the asphalt droplet shouldn't be too large as the viscosity of the emulsion cannot provide it with enough supporting force. Otherwise, the coalescence and separation will occur. The particle size of asphalt droplets shouldn't be too small as it requires a high-performance colloid mill to produce the asphalt emulsion, and it will increase the risk of flocculation in asphalt emulsion.

An emulsifier typically consists of a hydrophobic (water-repellent) head and a hydrophilic (water-attracting) tail [71]. Emulsifiers can be classified as amphoteric, anionic, cationic, or non-ionic type according to the charge of the polar head group [72]. Most current cationic emulsifiers are nitrogen-containing organic substances, which often derive from organic amines [73-76]. The hydrophilic part of these emulsifiers mainly includes amidogen, which is rich in nitrogen atoms. These nitrogen atoms exhibit strong adsorption and affinity with both acidic and alkaline aggregates. By contrast, the hydrophobic part of anionic emulsifiers is similar to that of cationic emulsifiers, comprising straight-chain alkyl or alkyl phenyl groups. However, the hydrophilic part of anionic emulsifiers is distinct, containing more oxygen atoms and a larger molecular structure [77, 78]. The oxygen atoms attract the hydrogen atoms in the water molecules and form hydrogen bonds to form bound water, which might be a little bit difficulty to demulsify when it contacts with aggregates. Cationic asphalt emulsion is widely used in cold recycling asphalt mixtures and other preventive maintenance applications [79, 80].

Because the cationic asphalt emulsion usually has a superior adhesive property with aggregates and a higher demulsification efficiency than other types of asphalt emulsion.

2.2.1.2 Stability of ST asphalt emulsion

Stability is a critical property of ST asphalt emulsion. When asphalt binders are emulsified by anionic or cationic emulsifiers, asphalt droplets acquire a charge (negative or positive), attracting oppositely charged ions in the aqueous phase. According to the established Derjaguin-Landau-Verwey-Overbeek (DLVO) theory [81, 82], both repulsive and attractive forces exist between the asphalt droplets simultaneously. This theory postulates that the electrostatic double layer forces and Van der Waals’ forces independently exist, which can be superimposed along different distances between the asphalt droplet particles. Take the commonly used cationic asphalt emulsion as an example (Figure 2.1), the surface of asphalt droplet is surrounded by cationic emulsifiers, creating in a positively charged surface that generates surface potential. A thin layer of ions with a negative charge is subsequently adsorbed onto the droplet surface, forming the stern layer. While the remaining cationic and anionic ions are distributed in the outside, forming the diffusion layer. The zeta potential refers to the electric potential at the boundary of the electrical double layer (stern layer and diffusion layer) [83, 84]. This parameter plays a crucial role in evaluating asphalt emulsion stability. Many studies showed that the zeta potential has a good correlation with the storage stability of the asphalt emulsion [85, 86]. A zeta potential absolute value exceeding 30 mV typically indicates a stable emulsion. The zeta potential can be calculated based on the Smoluchowski theory [87].

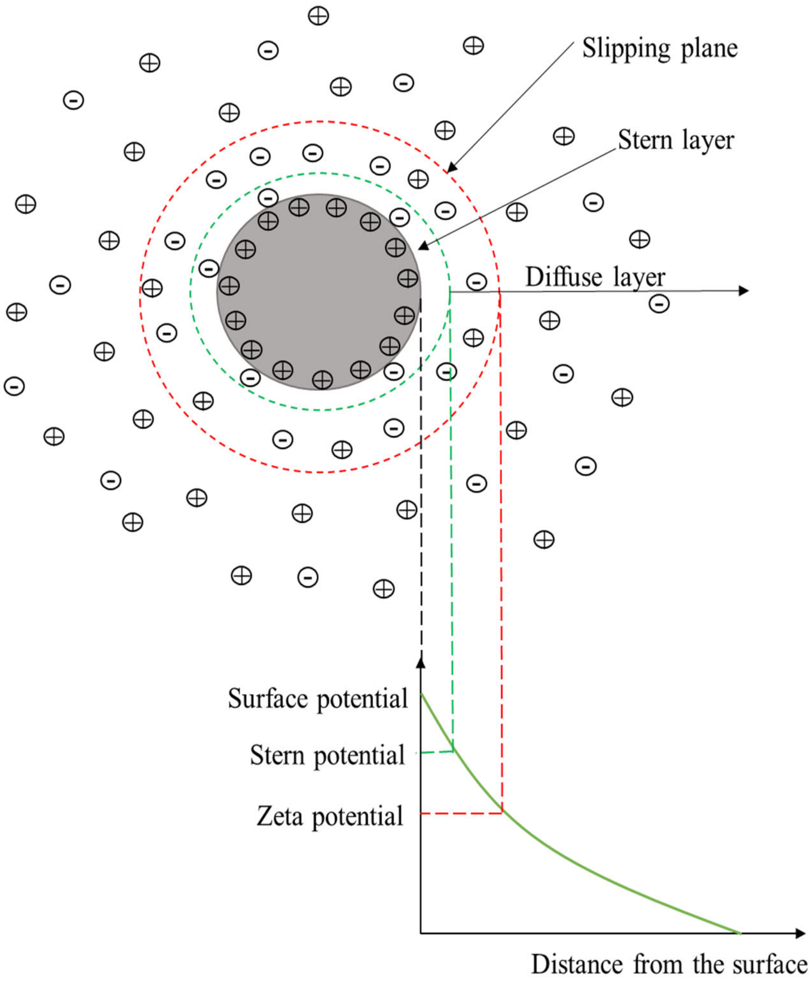

Figure 2.1 Electrical double layer of DLVO theory [88]

$$U_e = \frac{V_p}{E_x} \tag{2-1}$$

$$\zeta = (\frac{\eta}{\varepsilon})U_e \tag{2-2}$$

where U_e represents the electrophoretic mobility V_p and E_x are the particle velocity and the applied electrical field, respectively; η and ε represent the dispersant viscosity and dielectric permittivity, respectively.

2.2.1.3 Demulsification of ST asphalt emulsion

Based on the application scenarios, the demulsification of asphalt emulsion can be categorized into two types. The first type occurs when asphalt emulsions come into contact with original aggregates, as seen in micro-surfacing and sand fog sealing. The second type occurs when emulsions interact with Reclaimed Asphalt Pavement (RAP) aggregates, such as in cold recycling asphalt pavement and tack coat applications. These two demulsification processes can sometimes occur simultaneously [89].

Here uses the cationic asphalt emulsion as an example to explain the first kind of demulsification of asphalt emulsion. When dry or slightly wet aggregates are mixed with asphalt emulsions, water initially contacts the aggregates. Subsequently, emulsifier molecules, both free in the aqueous phase and attached to asphalt droplets, migrate to the aggregate surfaces due to concentration gradients. The hydrophilic group of each emulsifier orients itself toward the aggregate surface. Then, asphalt droplets gradually move closer toward the aggregate surface due to the directional movement of hydrophilic groups. The hydrophobic groups of cationic emulsifiers, containing nitrogen atoms with strong adsorption and affinity for aggregates, displace the water film previously in contact with the aggregate. As water gradually evaporates, the electrical double layer around the asphalt droplets becomes disrupted, reducing the average distance between droplets and leading to their coalescence into an asphalt film on the aggregate surfaces.

Besides, the RAP aggregates were selected to explain another demulsification type of asphalt emulsion. When the asphalt emulsions contact with RAP aggregates which are already coated by aged asphalt binders, the demulsification process can be divided into three stages as depicted in Figure 2.2 [90-92]. In the initial stage, the water evaporation rate remains relatively stable, and the average distance between asphalt droplets decreases (Figure 2.2 (a)). As evaporation continues, the electric field within the aqueous phase strengthens, and the attractive forces between asphalt droplets begin to surpass the repulsive forces, leading to flocculation and eventual coalescence (Figure 2.2 (b)). In the final stage, coalesced asphalt droplets further merge as residual water slowly diffuses through capillary pores or are squeezed out by the rearrangement of asphalt droplets (Figure 2.2 (c)). Accordingly, the water evaporation rate is very slow in the final stage, indicating the demulsification of asphalt emulsion is almost finished.

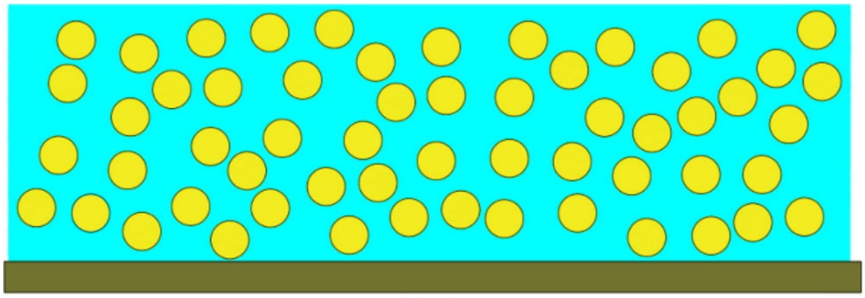

(a) The first stage

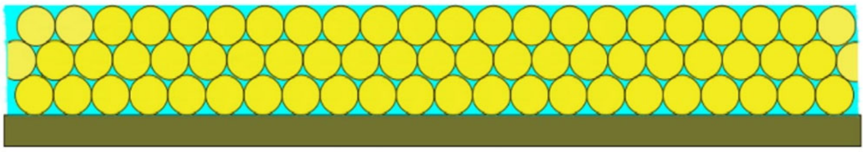

(b) The intermediate stage

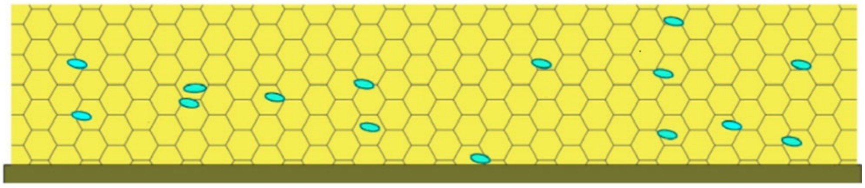

(c) The final stage

Figure 2.2 Schematic picture of the three-stage demulsification of asphalt emulsion on RAP aggregate surface [90]

2.2.2 Application status of ST emulsion

Recent studies showed that before the dislodgement of aggregate particles from PA mixtures, timely spraying surface treatment (ST) emulsions to PA roads could effectively alleviate the ravelling distress [22, 33, 93]. This method is similar to the fog seal, which is a preventive maintenance method for conventional asphalt pavements. In both methods, asphalt emulsions will be applied for the purpose of repairing micro-cracks and softening/rejuvenating aged asphalt binders. However, the fog seal method is expected to seal the conventional pavement surface, thus preventing the air and water from penetrating [94], while the ST emulsion for PA wearing course is designed to penetrate the voids of the PA without clogging them, thereby maintaining the functional performance of PA.

In 2010, the Netherlands Ministry of Infrastructure and Environment launched a research project titled "Prolonging the Service Life of Porous Asphalt Pavement" [32, 93]. The project aimed to assess the feasibility of preventive maintenance for PA pavements using ST emulsions, which were expected to penetrate aged asphalt mixtures without compromising their performance. Three surface treatment products (STPs) were selected and their properties are summarized in Table 2.1. The project was conducted on two Dutch PA roads, A53 and A73, both approximately five years old. A53 featured a single layer PA pavement with a design air void of 20%, while A73 had a top and bottom layer with air voids of 20% and 25%, respectively. Before and after the STP materials were sprayed to the surfaces of A53 and A73 highways, cores were drilled out from the trial sections for laboratory testing. The morphological distribution, ravelling resistance, bending stiffness, fracture properties, and indentation modulus were evaluated in this study [32, 95]. The key findings of this project were summarized as follows:

(1) The treated PA specimen showed a thickened mortar film thickness, and the grayscale histogram of CT image scanned from STP B and STP C treated road sections showed statistical differences in air void contents as well as mortar contents between the treated and untreated specimens, indicating that STP B and STP C materials have penetrated into PA mixtures.

(2) Fresh bituminous binders were observed from the thin slices of STP B and STP C treated PA specimens through the optical microscope, which was consistent with CT scanning analysis.

(3) STP A was sprayed to the artificially aged PA mixture and there were no statistical differences in stiffness modulus or indirect tensile strength compared to the untreated specimens. Also, no significant changes were observed in the rheological and shear fatigue properties of the artificially aged mortar treated with STP A and STP C.

(4) The treated road sections demonstrated improved ravelling resistance and higher bending stiffness compared to the untreated sections, although fracture properties showed no clear difference.

(5) The nano-indentation test results showed an increased modulus percentage in bitumen-rich areas and filler-rich regions, indicating new bituminous binders were added into the mortar areas of PA mixtures.

Table 2.1 Basic information of three kinds of surface treatment products used in Zhang's study [22]

Type	Main components	Construction conditions	Working mechanism
STP A	Volatile fraction, oily fraction, bitumen	A product was sprayed at ambient temperature without special requirements. The application rate is 0.80 kg/m^2.	Volatile fraction was expected to work as an activator of the old binder. It has a very fast diffusion rate to temporarily soften old binders. The oily fraction was expected to rejuvenate the old binder. And the bitumen was expected to fill cracks and replace lost binders.
STP B	Polymer modified binder	B product was sprayed at 180 ºC with a spraying truck, followed by a rubber scraper to scratch the sprayed binder into the surface of the pavement. The application rate is 0.40 kg/m^2.	The newly added bitumen was expected to fill cracks and replenish fresh binder.
STP C	Cationic rapid setting bituminous emulsion (containing non-volatile rejuvenating agents and a biopolymer stabilized bituminous emulsion)	C product was sprayed at 75 ºC with a spraying truck, followed by a rubber scraper and a steek brush to scratch the sprayed emulsion into the pores at the pavement surface. Meanwhile, an air-jet turbine was used to blow hot air at approximately 300 ºC into PA to promote coating efficiency. The application rate is 0.80 kg/m^2.	The rejuvenating agents, containing maltene-like and asphaltene compatible molecules, could rejuvenate aged bitumen. The modified biopolymer additive occurred in the emulsion to help improve the storage stability of an emulsion.

At the same time, Xu, et al. [96] also investigated the preventive maintenance technology for PA pavement. They developed three preventive materials—RJ (rejuvenation-based), CEM (cohesive reinforcement-based), and GL1 (polymerization-based)—and selected a commonly used asphalt emulsion as a control group. Long-term aged asphalt mixtures were fabricated in the laboratory. A modified Cantabro Abrasion test, named single-side ravelling test was conducted in this study. As the ravelling distress mainly occurred on the pavement surface, the bottom and sides of each cylindrical specimen were wrapped with tape, exposing only 2 cm of the upper layer of the specimen. Four kinds of preventive materials were applied to the surfaces of specimens with different application rates. It was found that all materials can improve the ravelling, with the rejuvenator-based material RJ performing the best. Meanwhile, the CT scanning results showed that the RJ and GL1 materials presented deeper penetration depths and lower clogging degrees of air voids than the other two materials due to the flowability differences of different materials.

Although the ravelling problem could be alleviated by spraying this preventive maintenance material, the effects of ST emulsions on other mechanical properties of PA mixtures, crucial for pavement durability, are rarely investigated. To some extent, previous studies relevant to the fog seal can give some insights [97-99]. Because the fog seal is similar to the surface treatment emulsion from the perspective of the application scenario. Both methods aim to repair micro-cracks and rejuvenate/soften aged bitumen binders. However, the main objective of fog seal is to seal the conventional pavement surface, thus preventing moisture and oxygen from penetration. Estakhri and Agarwal [100] found that around 20% reduction in tensile strength and a 50% increment in the strain at failure were observed in the indirect tensile tests for fog seal treated specimens. It indicated that the fog seal material could significantly decrease the bituminous pavement stiffness, thereby improving the cracking resistance. However, they are also concerned that this might enhance the potential for permanent deformation at high temperatures. Similarly, some researchers conducted the indirect tensile test on the lab-prepared PA specimens before and after immersing them in ST emulsions with rejuvenating components. Unlike the fog seal, they haven't observed the decreasing trends of the stiffness moduli and facture strengths [101]. This lack of effect may be due to the poor compatibility of the selected rejuvenator with the aged binder or insufficient usage to soften the binder. Later, the same researcher performed the three-point bending beam test on field-cored PA specimens before and after ST emulsion treatment. They found an increase in bending stiffness post-treatment, though bending strength remained unchanged [22]. In addition, Xu, et al. [28] conducted low-temperature cracking tests at -10°C to assess the impact of four preventive maintenance materials on PA specimens. They found that both the flexural modulus and flexural strain energy of treated specimens increased, indicating low temperature cracking resistance of aged PA specimens was improved.

2.3 Penetration Behavior in Asphalt Mixture

In pavement fields, penetration refers to the seepage behavior of liquid (such as rainwater or asphalt emulsions) or a mixture of liquid and small solid particles (like clay, fine aggregate, or debris) in asphalt concretes. Many studies have investigated the penetration behavior in asphalt mixtures, which can be divided into three categories based on the material sources.

Some studies have focused on the water permeability of porous asphalt (PA) mixtures, which are widely used in permeable pavement systems, particularly in sponge city projects aimed at mitigating urban waterlogging. At the macroscopic level, permeability velocities in horizontal and vertical directions can be measured using custom-developed devices to evaluate the anisotropy property of permeability in PA mixture [102, 103]. Generally, the permeability velocity in the horizontal direction is higher than that in the vertical direction due to the relatively low flow resistance of transverse flow [104]. Comprehensive permeability velocity is also often used to investigate the overall water permeability of PA mixture. The mathematical relationship between comprehensive permeability velocity and hydraulic gradient follows Darcy's law at low gradients, while the Forchheimer equation more accurately models non-Darcy flow at higher gradients [104, 105]. Recently, there has been growing interest in studying water migration at the microscopic level, which is crucial for understanding and mitigating moisture-induced damage in pavements [106, 107]. The pore structures could significantly affect water seepage characteristics. Like in the DAC and SMA mixtures with small pore sizes, water prefers horizontal migration to vertical migration due to its initial inertia [108].

Besides, some studies investigated the clogging characteristics of different clogging materials with the help of water in PA pavements [109, 110]. Clogging material particle sizes typically range from 0.15mm to 2.36mm. Meng, et al. [111] described that the clogging process of PA pavement consists of four stages: fast clogging, clogging recovery, gradual clogging, and clogging acceleration. The distribution of clogging materials in PA mixture depends on its grading composition and particle type. Generally, a relatively small particle size could induce a deeper distribution. The retained clogging materials in the mixture typically share similar shape and angularity with the original aggregate particles used in the asphalt mixture, whereas outflowed materials do not. Therefore, investigation of the common types and morphologies of local clogging materials is recommended before designing anti-clogging gradations for PA mixtures [112].

In addition, there are also some studies investigating the penetration status of emulsion-based material in pavement. The prime coat is typically applied to the base layer so as to improve the adhesion between the base and asphalt layers. It also provides a waterproof seal to prevent water from penetrating the base layer. So, it can be seen that the penetration ability of prime coat material is critical to achieving above mentioned objectives [113]. Due to the significant color contrast between the dark prime coat and the lighter cement-treated base layer, the side view image can effectively observe and quantify the penetration status of the prime coat material (Figure 2.3) [114]. Rejuvenator seal material (RSM) is another preventive maintenance material, used to rejuvenate aged asphalt binders and is typically applied to old asphalt pavement surfaces [115]. The penetration depth of RSM is a key factor in its maintenance effectiveness. Currently, the common practice to detect the penetration depth of RSM is cutting the treated specimen into several thin slices. Then, the solvent-washing method is used to extract the residual mixture of asphalt binders and RSM (if any). Subsequently, some physical and chemical experiments are carried out to compare the performance differences between extracted samples of treated and untreated asphalt mixtures. The RSM penetration depth is inferred from the layer where no performance difference is detected [116, 117]. However, because test methods vary in their sensitivity to performance differences, it is recommended to conduct multiple experiments simultaneously to reduce experimental errors and gain a comprehensive understanding of penetration depth.

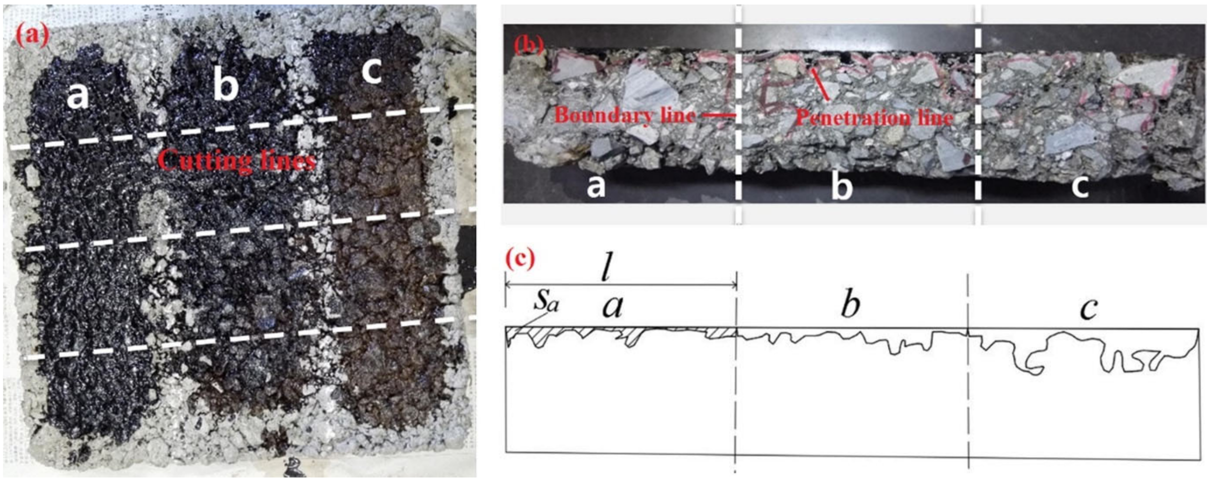

Figure 2.3 Penetration test of asphalt emulsion into cement-treated base [114]

2.4 Diffusion Phenomenon in Asphalt Mixture

Aged asphalt binders form over time due to the combined aging effects of UV exposure, heat, and oxygen, leading to embrittlement and increased rigidity. One purpose of applying preventive maintenance materials to pavement surfaces is to replenish these binders with new asphalt binders or rejuvenator materials. Those newly added materials are expected to soften aged asphalt binders and restore their viscoelastic properties through diffusion. The following is a summary of studies on diffusion phenomena in asphalt mixtures.

Numerous studies have explored the diffusion of soft virgin binders or rejuvenators into aged binders within reclaimed asphalt pavement (RAP) at high construction temperatures. When the contact surfaces between virgin and aged binders are established during the mechanical mixing process, binder diffusion becomes the dominant process that governs the blending quality of RAP [118, 119]. Research has spanned from microscopic and rheological investigations of diffusion in aged binders to studies on laboratory-prepared mixture specimens. One of the earliest studies of diffusion in aged binders was performed by Oliver [120], and the radioactive material was chosen to mark rejuvenators. It was found that adding more rejuvenators or increasing the temperature could increase the diffusion rate. Attenuated total reflectance-Fourier transform infrared spectrophotometry (ATR-FTIR) was also used to characterize the diffusion of rejuvenator in aged binder [121, 122], which indicated that temperature had a significant effect on the diffusion coefficient, which follows the Arrhenius-type relationship. Later on, the same researchers characterized the diffusion using the dynamic shear rheometer (DSR) and claimed that the diffusion phenomenon could be described by Fick's law [123], which is consistent with the findings of their early studies. For the characterization of diffusion in asphalt mixture in the laboratory, as shown in Figure 2.4, a multistep staged solvent washing and extraction method has been widely used for analysing the different binder layers around RAP aggregate particles [124, 125]. Then, the properties of different binder layers were characterized by various chemical and rheological tests such as gel permeation chromatography (GPC), DSR, and FTIR tests to evaluate the diffusion degree of virgin binder or rejuvenator in the aged binder of RAP [126-128]. It was found that the diffusion of virgin binder in aged binder could be accomplished in hot mix asphalt (HMA) containing 50% RAP, which can also be improved by adding the warm mix additive (WMA) [128]. Besides, some researchers selected molecular dynamics simulations to investigate the diffusion between virgin binder/rejuvenator and aged binder [129, 130]. However, the abovementioned studies largely focus on the diffusion of virgin binders or rejuvenators in RAP mixtures at elevated temperatures over a few hours. Few studies have examined potential diffusion at room temperature over extended durations, which is crucial for understanding the interaction between surface treatment (ST) emulsion residue and aged asphalt mortar in PA mixtures from a microscopic perspective.

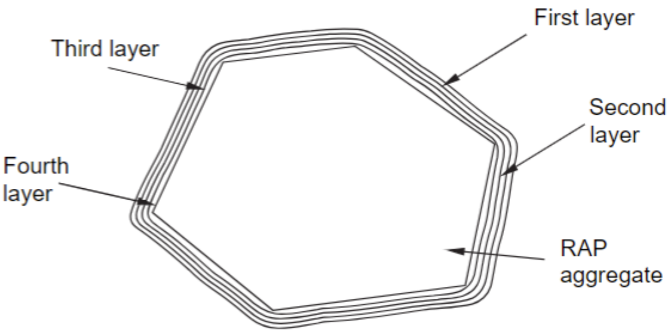

Figure 2.4 Layers of asphalt binder coating RAP aggregate [124]

Some studies have demonstrated that Scanning Electron Microscopy (SEM) with Energy Dispersive Spectroscopy (EDS) was an effective tool to investigate the blending efficiency between virgin and aged binders in RAP mixtures [131, 132]. For example, titanium dioxide (TiO_2) was used as a tracer to mark virgin asphalt binder. Two kinds of RAP aggregates (dark basalt) and virgin aggregates (light-colored limestone) with two different colors were selected for distinguishment purposes. A total of 14 mixture schemes including 4 different RAP contents and 4 different aging levels were designed in this study [133]. The EDS tests were conducted on the virgin aggregate surfaces with a 30 μm range to detect the mass ratio of the element titanium to sulfur (Ti:S). Initially, virgin aggregates are coated with virgin asphalt binder, where the Ti:S mass ratio is set as the initial value. The blending ratio, calculated from the Ti:S mass ratios, was then used to evaluate the blending degree across different mixture schemes. This study provides an alternative approach to characterize binder diffusion at actual ambient temperatures.

2.5 Summary

Porous asphalt pavement is an environmentally friendly pavement with many promising functions, but its susceptibility to ravelling distress restricts its widespread application. Through the literature review, the current preventive maintenance technologies for PA pavement were summarized. Related studies about the penetration and diffusion behaviors that occurred in asphalt mixtures were expected to inspire the research of this dissertation. The following points are summarized based on the literature review:

(1) The solar radiation heat and oxygen can easily diffuse into PA mixture due to its open-graded structure, leading to the fast aging of asphalt binders compared with conventional dense asphalt pavements. The skeleton structure of PA makes it more sensitive to repeated traffic loading, resulting in micro-cracks. Both variations can account for the onset of ravelling destress of PA pavement.

(2) Cationic asphalt emulsion is the most popular type in the asphalt pavement field due to its faster demulsification time and better compatible with different aggregates. Zeta potential is a reliable indicator, strongly correlated with the storage stability of the asphalt emulsion.

(3) Timely spraying ST asphalt emulsion to old PA pavement could alleviate the ravelling distress. The applied asphalt emulsion residues were expected to repair micro-cracks and soften/rejuvenate aged asphalt binders without clogging the air voids or compromising the functional performances of PA pavements.

(4) A series of physical and chemical experiments could be used to detect the penetration status of emulsion-based material, but the sensitivities of different experimental methods to the performance differences should also be considered to minimize the test errors.

(5) The SEM/EDS technique might be a feasible microscopic method to investigate the potential on-site diffusion phenomenon between asphalt emulsion residues and old asphalt binders of asphalt mixture under actual ambient temperatures.

Meanwhile, the research gaps were summarized as follows:

(1) Except for some successful field trials and limited laboratory tests, the effects of ST emulsion on the mechanical and functional performances of PA mixtures haven’t been systematically studied.

(2) The interaction mechanisms between ST emulsion and the existing PA mixture remain unclear.

(3) Suggestions about applying ST emulsion as a preventive maintenance material for PA pavements are still missing.

(4) How to optimize ST emulsion to enhance the ravelling resistance of PA needs in-depth research.

Therefore, the following works were conducted with the expectation of minimizing those research gaps.

CHAPTER 3 EFFECTS OF ST EMULSION ON THE MECHANICAL AND FUNCTIONAL PERFORMANCES OF DAMAGED PA MIXTURES

This chapter investigates the effects of ST asphalt emulsion on the mechanical and functional performances of damaged PA mixtures. Section 3.1 introduces several material design and treatment factors which might affect the ravelling resistance recovery of damaged PA. It also details the preconditioning methods used to prepare the damaged PA mixtures and the experimental techniques employed to assess their mechanical and functional properties. Section 3.2 presents the test results and discussion. The optimal application parameters of ST emulsion were determined based on the recovery efficiency of ravelling resistance of damaged PA under different ST scenarios. Additionally, the durability of PA mixtures treated with ST emulsion was systematically evaluated, focusing on their resistance to cracking, rutting, and fatigue. Meanwhile, the noise absorption, permeability, and skid resistance of ST treated PA mixtures were investigated for verification purposes.

3.1 Experimental Programs

3.1.1 Materials and specimen preparation

One commonly used PA mixture with a nominal maximum aggregate size of 13.2 mm, denoted as PA-13, was selected in this study. A styrene-butadiene-styrene (SBS) polymer-modified asphalt binder satisfying the Superpave performance grade of 76-16 (PG76-16) was used. The coarse and fine aggregates for PA-13 were both granites. Calcium hydroxide was used to improve the anti-stripping property of the PA mixture with a content of 1.5% by the weight of aggregate. The optimum asphalt content was 4.1% by the weight of aggregates and the target air void content was 23% (± 0.5%). The gradation of PA-13 is shown in Table 3.1.

Table 3.1 Mixture gradation of PA-13

Retained on sieve size (mm)	Weight percentage (%)	Passing percentage (%)	Lower and upper limitations (%)

16	-	100	-
13.2	7.4	92.6	90-100
9.5	25.6	67.0	40-71
4.75	52.5	14.5	10-30
2.36	2.8	11.7	9-20
1.18	3.1	8.6	7-17
0.6	2.1	6.5	6-14
0.3	1.4	5.1	5-12
0.15	0.9	4.2	4-9
0.075	1.0	3.2	3-6
Filler	1.7	-	-
Calcium hydroxide	1.5	-	-
Total aggregate	100	-	-
Asphalt content	4.1		

A cationic slow-setting (CSS-1) type asphalt emulsion was prepared as the ST emulsion. The composition by mass of the ST emulsion included 60% asphalt binder, 3% emulsifier, 36.8% deionized water, and 0.2% stabilizer. Firstly, a virgin asphalt binder with a penetration grade of 60/70 (Pen60/70) was heated to 135 °C for later mixing. The emulsifier was mixed with deionized water at 60 °C to prepare the soap solution. Calcium chloride powders were subsequently added to the soap solution as the stabilizer. Hydrochloric acid was then gradually dropped into the soap solution while stirring with a glass rod until the pH value reached 2.0–2.5. It should be noted that the well-prepared soap solution needs to be stored in the oven at 60 °C for several minutes. After that, the soap solution was poured into a colloid mill operating at a shearing rate of 2,870 rpm. Finally, the heated asphalt binder with a temperature of 135 °C was gradually added into the soap solution and emulsified by the colloid mill within 2 minutes. The basic properties of the asphalt emulsion are detailed in Table 3.2. Two petrol-based rejuvenators and three bio-based rejuvenators were selected in this study, which were designated as EO, AO, TO1, TO2, and WCO. These commercial rejuvenators were directly added to asphalt emulsion with the expectation of further enhancing the recovery and rejuvenation effects. Table 3.3 presents the basic information of the rejuvenators. The dosage of each rejuvenator is in terms of the weight of the residual binder of the asphalt emulsion, which are recommended by the producer. Table 3.4 outlines four variables and a total of 16 ST conditions are considered in this study. Based on the literature review [22, 69, 114, 115], four factors were considered as they might directly affect the maintenance effectiveness of ST emulsion on damaged PA mixtures.

Table 3.2 Basic properties of asphalt emulsion

	Evaporated residue				Storage stability	
	Residue content (%)	Penetration (25 ºC, 0.1 mm)	Softening point (ºC)	Ductility (5 ºC, cm)	1 day (%)	5 days (%)
Asphalt emulsion	60	64	50	67.2	0.3	2.1

Table 3.3 Basic information about rejuvenators

No.	Rejuvenator type	Dosage (%)	Viscosity at 135 ºC (mPa·s)	Petroleum or organic	Refined or waste	Molecular structure	Polarity
EO	Extract oil	5	98.4	Petroleum	Refined	Aromatic ring	High
AO	Aromatic oil	7	6.3	Petroleum	Refined	Aromatic ring	High
TO1	Tall oil 1	2.5	4.1	Organic	Waste	Ring and strand	Mild
TO2	Tall oil 2	2.5	3.8	Organic	Refined	Ring and strand	Mild
WCO	Waste cooking oil	5	3.6	Organic	Waste	Strand	Slight

Table 3.4 Summary of ST conditions

Variables	Conditions
Solid content (%)	40, 50, 60
Application rate (kg/m^2)	0.4, 0.6, 0.8, 1.0
Curing duration (days)	0, 3, 7, 14
Rejuvenator type	EO, AO, TO1, TO2, WCO

3.1.2 PA specimen preconditioning

To evaluate the treatment effects of emulsions, all PA specimens were subjected to aging and freezing-thawing (F-T) conditioning to create micro-damages inside the mixture. It is worth noting that the main purpose of aging and environmental conditioning is to create micro-damages, instead of completely simulating the field damage. As shown in Figure 3.1(a), all specimens tested in this study were subjected to the long-term aging (LTA) before the compaction. Based on the previous study of Wisconsin Highway Research Program (WHRP) 17-04 [134], the LTA condition is an oven aging of loose mixtures at 135 °C for 8 h, which has been confirmed that the aging degree of asphalt binder in the mixture processed by this method could well represent the asphalt binder after the standard pressure aging vessel (PAV) test for 20 h [135]. Then, all tested mixtures were fabricated using the Superpave gyratory compactor (SGC). Two kinds of SGC specimens with two different diameters, 100 mm and 150 mm, were prepared for mechanical and functional properties tests.

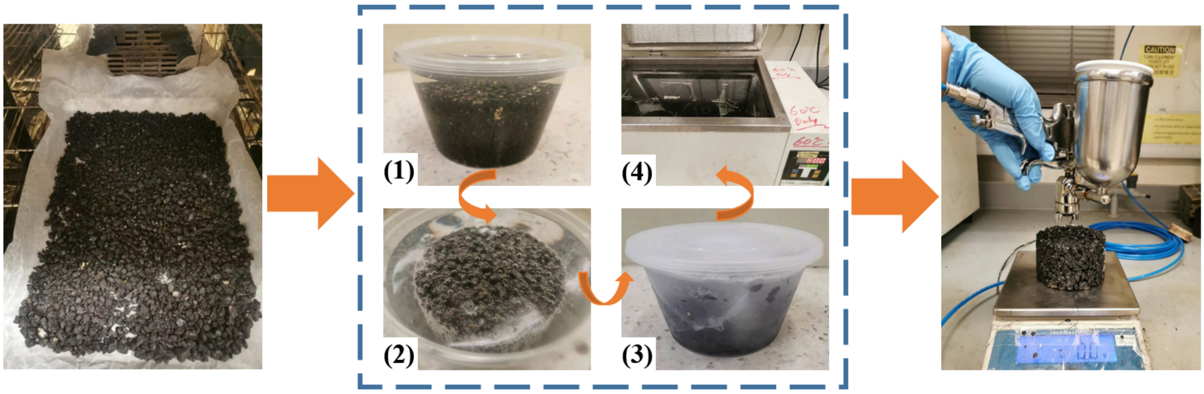

(a) (b) (c)

Figure 3.1 Specimen preconditioning: (a) long-term aging; (b) freezing and thawing; (c) spraying ST emulsion to the specimen's surface.

Figure 3.1(b) illustrates the F-T procedure, which was implemented after the aged specimens were compacted. First, each specimen was placed into a plastic container filled with water and they were saturated under a vacuum of 87.8 kPa for 10 min. Subsequently, the plastic containers containing the specimens were placed in a freezer at a temperature of -18 ± 3 °C for 16 h. Finally, all specimens were put into a water bath at 60 °C for 24 h.

To determine the appropriate number of the F-T cycles, the indirect tensile stiffness modulus (ITSM) test was conducted as it's a non-destructive testing method. As shown in Figure 3.2, the ITSM values of the aged specimens first rapidly decreased and then remained stable after three F-T cycles, indicating that some micro-cracks occurred inside mixtures leading to a nearly 20 % reduction of the ITSM. Similar variation trends about the effect of F-T cycle number on mechanical properties of PA mixture were also found in other studies [136-138]. Under the freezing condition, water in a specimen was frozen and the volume swelled, leading to some micro-cracks in the asphalt mortar area, which interferes with the transmission of force and deformation between coarse aggregates. Those micro-cracks might further extend and even connect with other micro-cracks to form small cracks or voids with the increase of F-T cycles. However, after three cycles of F-T conditioning, the internal pore structure of PA mixture has been adjusted accordingly to resist F-T conditioning. Its internal pore structure is less and less sensitive to F-T treatment. Therefore, three cycles of F-T tests were adopted in the following study.

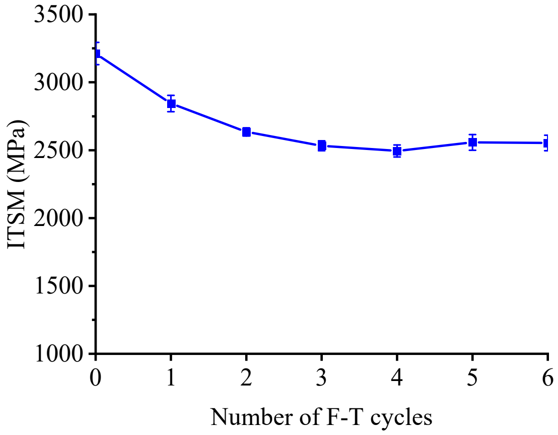

Figure 3.2 The variation of the ITSM under different F-T cycles

After the aged and damaged PA specimens were prepared, ST emulsion was applied to them. Two methods had been commonly used to apply ST emulsion to PA specimens in the lab, i.e., directly dipping specimens into asphalt emulsion, and brushing emulsion onto the specimens with a brush. However, these methods cannot accurately control the application of the ST emulsion and may easily cause inhomogeneity problems. Moreover, these indoor methods are quite different from the field practice, where asphalt emulsions are usually sprayed under high pressure, and sometimes at a high temperature if necessary. Therefore, the spraying method by using a spray gun was adopted in this study as shown in Figure 3.1(c). This method can precisely control the ventilation pressure, airflow volume, and the mass of the ST emulsion sprayed on the surface of the specimens.

3.1.3 Testing program

In this chapter, the Cantabro abrasion test was conducted as the main approach to evaluate the ravelling resistance recovery of damaged PA mixture after the application of ST emulsion, considering various factors, such as the rejuvenator type, curing duration, application rate and solid content of asphalt emulsion. The statistical analysis was carried out to compare the significance of different factors and optimal application parameters of ST emulsion were determined. Then, four curing durations (3, 14, 30, and 90 days) were selected to investigate the short-term and long-term mechanical performances of the specimens treated with ST emulsions. Besides, the maintenance effect could be affected by the pavement surface temperature, which is related to local weathering conditions. Hong Kong has a hot summer and mild winter, which is a typical subtropical climate [139]. So the curing temperatures of 25 °C and 60 °C were selected as a normal temperature and a higher temperature for the road surface, respectively. Finally, functional performance tests were conducted on the PA mixtures to characterize the noise absorptions, permeabilities, and skid resistances before and after the application of ST emulsion. The flowchart of the testing scheme is presented in Figure 3.3.

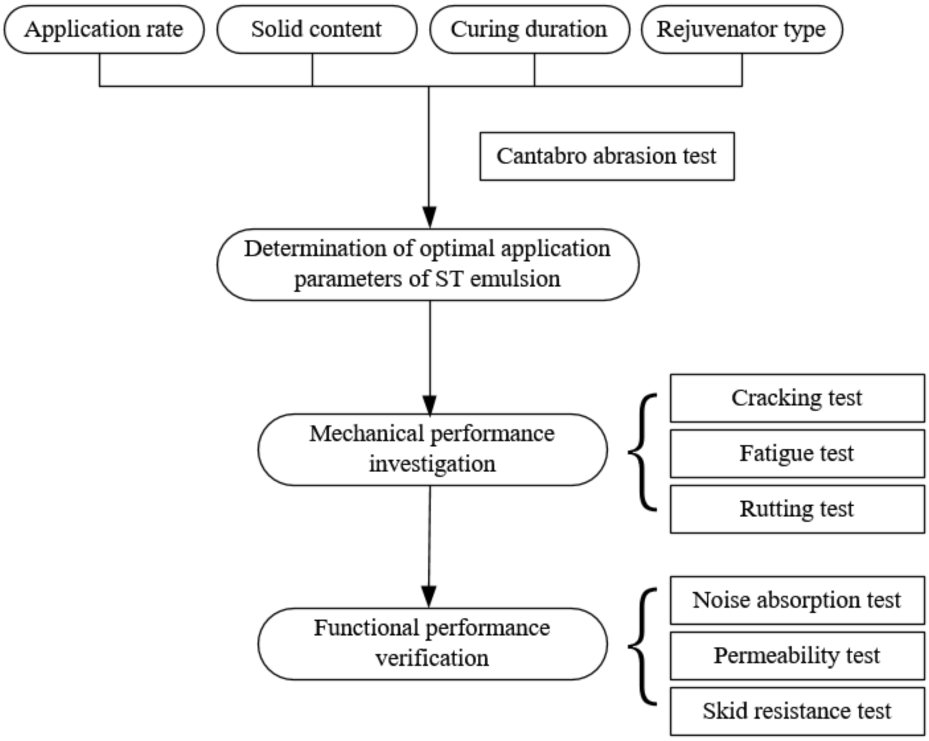

Figure 3.3 Testing scheme of Chapter 3

Cantabro abrasion test

According to standard ASTM D7064 [140], Cantabro abrasion test measures the ravelling resistance of the PA specimen, which is carried out in the abrasion machine as shown in Figure 3.4 (a). Each time, one specimen is placed into the steel drum of the machine. The specimen will be picked up by a shelf plate and carried around until it is dropped to the opposite side of the drum. During this process, some aggregates may fall off depending on the adhesive and cohesive strength of PA mixtures. Figure 3.4(b) shows the specimens after the Cantabro tests.

(a) (b)

Figure 3.4 Cantabro abrasion test: (a) abrasion machine; (b) specimens after test.

According to standard ASTM C131 [141], the abrasion machine is operated for 300 revolutions with a speed of 30 to 33 rpm at 25 ºC. At least three replicates were prepared for each ST condition. The following formula was used for calculating the mass loss ratio (M_r):

$$M_r = \frac{m_1 - m_2}{m_1} \times 100\% \qquad (3\text{-}1)$$

where m_1 and m_2 represent the original and final mass of the tested specimen before and after the abrasion test, respectively, g.

Indirect tensile cracking test

The indirect tensile asphalt cracking test (IDEAL-CT) is widely used due to its simplicity, practicality, and efficiency in characterizing crack propagation in asphalt mixtures [135, 142, 143]. In Texas, the cracking tolerance index (CT_{index}) was proposed to evaluate the cracking resistance of the asphalt mixture, which is calculated from the fracture energy (G_f), specimen dimensions, post-peak slope ($|m_{75}|$), and displacement at 75% of the peak load after the peak (l_{75}). According to the standard ASTM D6931 [144], IDEAL-CT tests were conducted at 25 ºC with a constant load-line displacement rate of 5 cm/min using a closed-up, feedback-controlled servo-hydraulic loading machine. Figure 3.5 shows the schematic of the IDEAL-CT test. The CT_{index} is calculated using Equations (3-2) - (3-4). The parameter $|m_{75}|$ is typically associated with the rate of crack propagation, with higher values indicating a faster cracking rate. Fracture energy (G_f) represents the energy needed to make a specimen broken. The peak load corresponds to the maximum value of the loading force during the test.

$$G_f = \frac{W_f}{D \times t} \cdot 10^6 \tag{3-2}$$

$$|m_{75}| = \left|\frac{P_{85} - P_{65}}{l_{85} - l_{65}}\right| \tag{3-3}$$

$$CT_{index} = \frac{t}{62} \frac{l_{75}}{D} \frac{G_f}{|m_{75}|} 10^6 \tag{3-4}$$

where CT_{index} is the cracking tolerance index; G_f is the fracture energy (J/m^2) calculated as the work of failure (the area under the load versus the average load-line displacement curve) divided by the cross-sectional area of the specimen (the product of the specimen thickness and diameter); $|m_{75}|$ is the slope of the tangential zone around the 75% peak load point after the peak; and t as well as D are the thickness of 62 mm and the diameter of 150 mm for the test specimen, respectively.

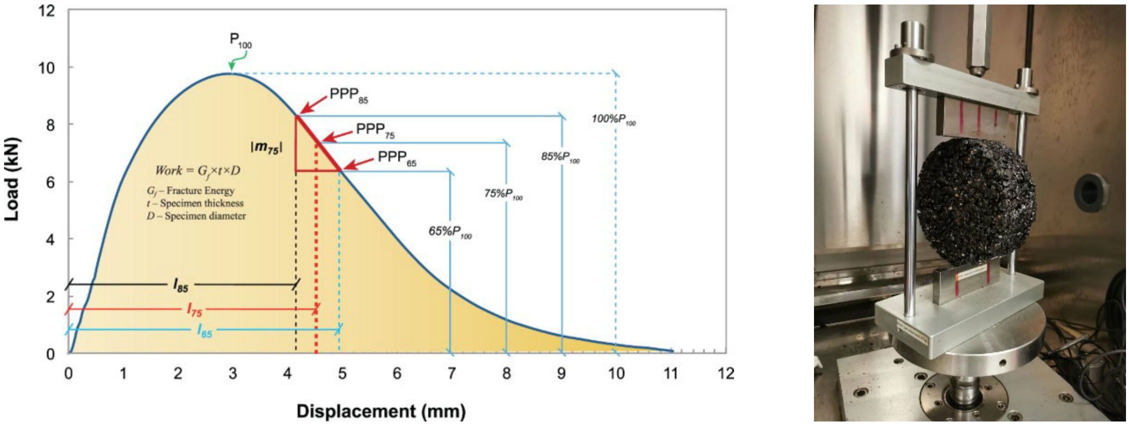

(a) (b)

Figure 3.5 Schematics of the IDEAL-CT test: (a) typical load-displacement curve of IDEAL-CT test [142]; and (b) set-up of IDEAL-CT test.

Indirect tensile fatigue test

The indirect tensile fatigue test (ITFT) was performed at 20 °C to evaluate the fatigue resistance of the PA mixture as shown in Figure 3.6(a). The test employed a stress-controlled mode, applying a repeated haversine load with a loading time of 0.1 seconds and a rest time of 0.4 seconds, resulting in a loading frequency of 2 Hz. According to EN 12697-24, the initial tensile strain should range from 70 με to 400 με during the first 10 applications. Following load adjustments, three stress levels were established in this study for the lab-compacted specimens: 220 kPa, 320 kPa, and 420 kPa. Cylindrical specimens with a diameter of 100 mm and a thickness of 60 mm were prepared for the ITFT test. The fatigue life was determined by analyzing the relationship between the decimal logarithm of the number of load cycles and the energy ratio, with the peak energy ratio point being identified, as shown in Figure 3.6(b). The energy ratio is calculated using Equation (3-5).

$$w_n = \frac{n}{\varepsilon_{R,n}} \cdot 10^6 \tag{3-5}$$

where w_n is the energy ratio at the load cycle of n; n is the number of load cycles; and $\varepsilon_{R,n}$ is the resilient strain at the load cycle number of n.

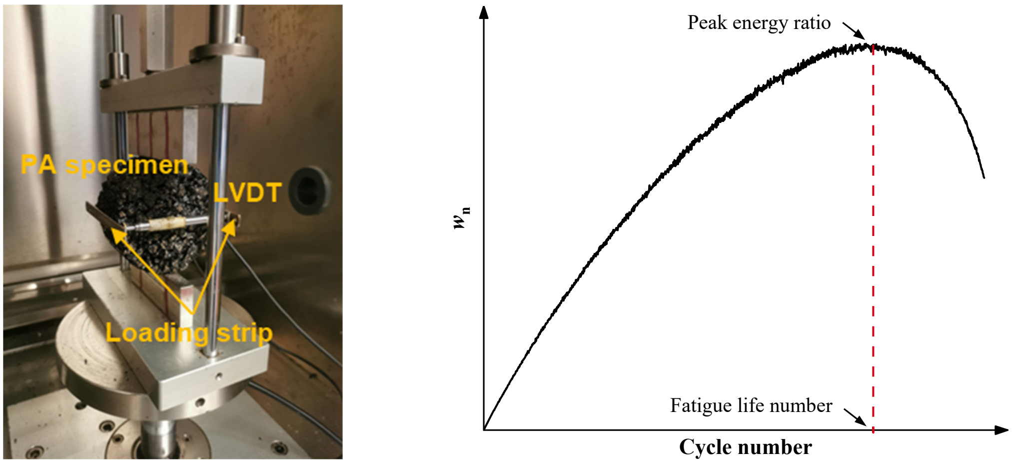

(a) (b)

Figure 3.6 Schematics of the ITFT test: (a) set-up of ITFT test; and (b) determination of the fatigue life based on energy concept.

Repeated axial load test

When ST emulsions are applied to the surface of old PA pavement, fresh ST asphalt residues will be added to existing aged pavements. It could lead to a potential risk of rutting distress, which cannot be overlooked in practice. The repeated axial load test (RALT) was selected to assess the rutting resistance of the asphalt mixture. A rectangular and periodical vertical stress pulse is applied to the specimen with a loading duration of 1 s and a rest period of 1 s. The loading stress, frequency, and loading cycles were set at 100 kPa, 0.5 Hz, and 3600 pulses, respectively. To simulate the worst-case scenario for the rutting behavior of the PA specimen, the maximum test temperature specified in EN 12697-25, which is 50 °C, was selected. Cylindrical specimens with a diameter of 150 mm and a thickness of 60 mm were prepared for this test. Figure 3.7 presents the schematic of the RALT test. The creep rate was determined from the slope of the curve during the steady creep stage. The cumulative axial strain and creep modulus are calculated using the following equations.

$$\varepsilon_n = 100 \cdot \frac{u_n}{t} \tag{3-6}$$

$$f_c = \frac{\varepsilon_{n1} - \varepsilon_{n2}}{n_1 - n_2} \cdot 10^4 \tag{3-7}$$

$$E_n = \frac{\sigma}{10 \cdot \varepsilon_n} \tag{3-8}$$

where ε_n is the final cumulative axial strain of specimen; f_c is the creep rate (με per loading cycle); E_n is the creep modulus (MPa); u_n is the permanent deformation of the specimen (mm); n_1 and n_2 are the numbers of repetitive loading pulses; and σ is the loading stress which is 100 kPa.

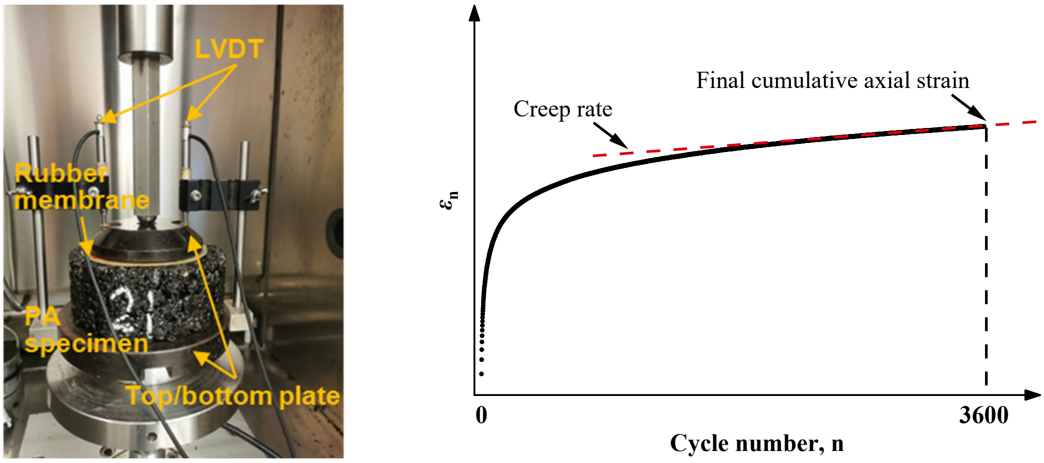

(a) (b)

Figure 3.7 Schematics of the RALT test: (a) set-up of RALT test; and (b) typical loading cycle number - cumulative axial strain of RALT test.

Noise absorption test

The noise absorption of PA mixtures was measured by the impedance tube test in accordance with EN 10534-2. The difference in the noise-reduction ability of a PA specimen before and after the application of ST emulsion can be detected by this method. As Figure 3.8(a) shows, the impedance tube shall be straight with a uniform cross-section and with smooth, rigid, and non-porous walls in the test section. As shown in Figure 3.8(b), the test specimen is mounted in the tube at one end, and plane waves are generated by a sound source at the other end. The acoustic pressure is measured at two fixed locations using wall-mount microphones.

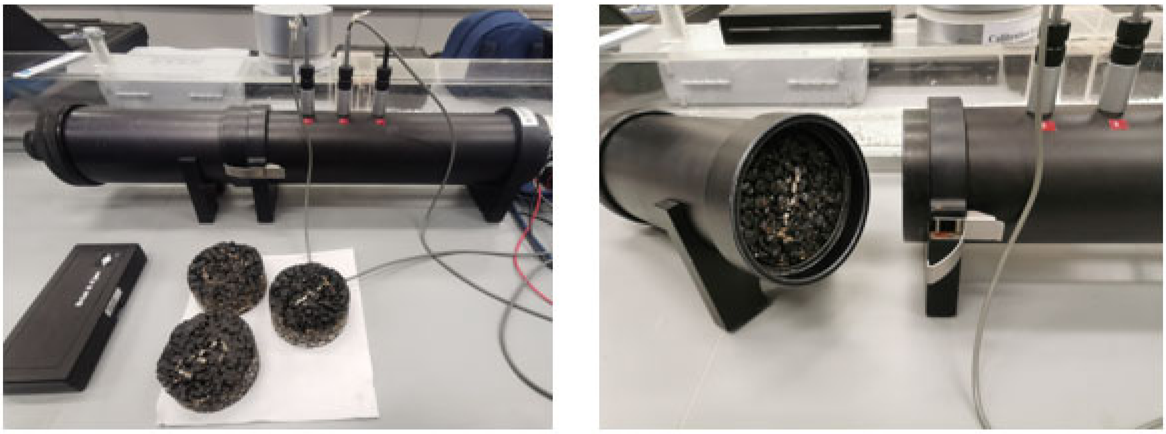
(a) (b)

Figure 3.8 Noise absorption test: (a) impedance tube; (b) PA specimen in the tube.

Considering that the diameter of the tube and the distance between the microphone positions have an obvious influence on the usable frequency range, the specimen with a diameter of 100 mm and a thickness of 40 mm was used in this test, which can detect the frequency range between 50 Hz and 1600 Hz. The complex acoustic transfer functions are used to calculate the reflection factor, r, and normal-incidence absorption coefficient, α, of the test material, using Equations (3-9) and (3-10), respectively.

$$r = |r|e^{j\emptyset_r} = r_r + jr_i = \frac{H_{12}-H_I}{H_R-H_{12}}e^{2jkx} \tag{3-9}$$

$$\alpha = 1 - |r|^2 \tag{3-10}$$

where α represents the noise abortion coefficient; r is the reflection factor, r_r and r_i are its real and imaginary components; $\emptyset_r$ is the phase angle of the normal incidence reflection factor; j is an imaginary unit; x represents the distance between the specimen and the further microphone location, mm; k is the wave number; H_{12} is a complex acoustic transfer function; and H_I and H_R are the transfer functions for the incident wave and reflected wave, respectively.

Permeability test

As Figure 3.9(a) shows, the specimen used for the permeability test has a diameter of 100 mm and a thickness of 40 mm. Before this test, each specimen was wrapped by tapes to ensure that water only infiltrated vertically through the specimen. As Figure 3.9(b) illustrates, a constant head permeameter was used to measure the hydraulic conductivity based on Darcy's law [145]. The vertical permeability coefficient is calculated by Equation (3-11).

$$K_V = \frac{4 \times Q_V \times L}{h \times \pi\ D^2 \times t} \tag{3-11}$$

where K_V is the vertical permeability coefficient, mm/s; Q_V is the volume of water vertically flowing through the specimen during the test period, mm^3; L and D are the thickness and diameter of the specimen, respectively, mm; h is the actual height of the water column and equals 150 mm here; and t is the test time of collecting water, s.

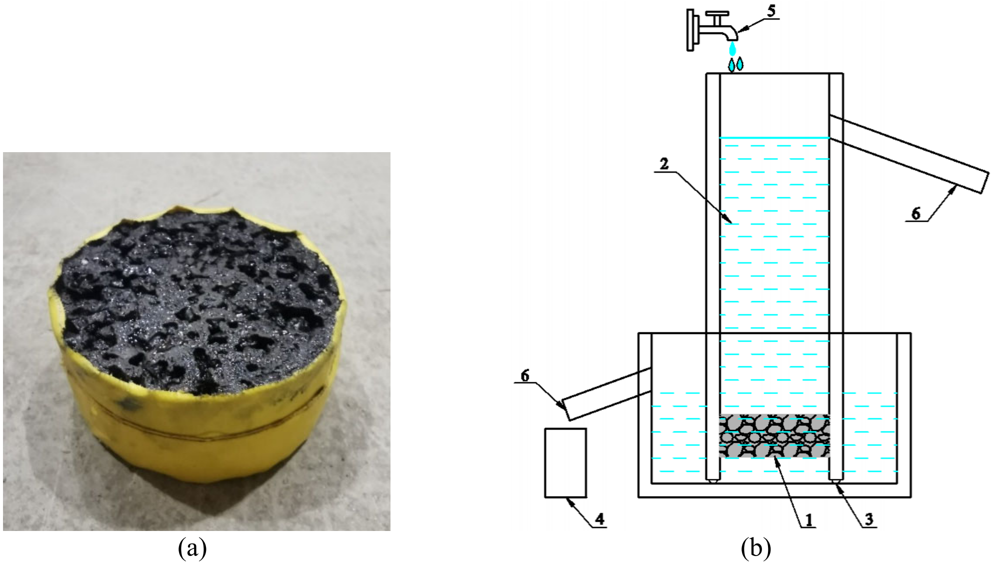

(a) (b)

Figure 3.9 Permeability test: (a) PA specimen wrapped with a tape; (b) permeameter, where 1 = specimen, 2 = water, 3 = mold, 4 = water collector, 5 = tap, and 6 = plastic tube.

Skid resistance test

According to ASTM E303 [146], a British pendulum tester was used to measure the frictional properties of the PA surface before and after ST conditions. As shown in Figure 3.10, a 75 mm rubber strip with a slider contact path length of 126 mm was provided by the tester for measuring the friction between the slider and the specimen surface. The skid resistance of the PA mixture is represented by the measured value of the British pendulum number (BPN), with a lower value indicating a more slippery surface condition. At the beginning of each swing, adequate water is sprayed onto the test area, and the test is repeated four times for each specimen.

Figure 3.10 British pendulum tester

3.2 Results and Discussions

3.2.1 Recovery efficiency of the damaged PA after emulsion-based ST

As aforementioned, ravelling is one of the main distresses for PA pavement at the early stage. To evaluate the performance of emulsion-based ST on improving the ravelling resistance of PA, the Cantabro tests were conducted, and the effects of different material design factors, such as the application rate, the solid content of ST emulsion, the curing duration, and the rejuvenator type, on the M_r index were analyzed.

Effect of the application rate of ST emulsion

Based on the actual construction experience [147], four different application rates of the ST emulsion ranging from 0.4 to 1.0 kg/m^2 were selected in this study. The solid content of the ST emulsion was 60%. After being treated with the ST emulsion and cured for 14 days, the PA specimens were used for the Cantabro abrasion test.

Figure 3.11 presents the mass losses of the specimens with different ST emulsion application rates. It can be seen that the M_r values of all specimens treated with ST emulsions were lower than that of the untreated PA, which indicates that the application rate could significantly affect the recovery efficiency of the damaged PA mixture. In addition, M_r decreased rapidly from 28.7% to 17.4% when the application rate increased from 0.4 kg/m^2 to 0.6 kg/m^2. Then, the downtrend of M_r flattened out with the increase of the application rate within the range of 0.6 kg/m^2 to 1.0 kg/m^2. These results suggested that after ST emulsions penetrated into PA mixtures and flowed through connected voids, some ST emulsion coated on the surface of aged asphalt mortar and the newly added emulsion residues might fuse with aged asphalt binders. Meanwhile, some micro-cracks inside the specimens might be filled. All the above changes are helpful to improve the cohesion of the binder and the adhesion between the binder and aggregates. However, too much ST emulsion showed no additional recovery efficiency enhancement for the damaged mixtures. Because the redundant emulsion residue not only filled the air voids but also directly flowed out from the bottom of the specimen through the interconnected voids, leading to the waste. When the application rate increased from 0.6 kg/m^2 to 0.8 kg/m^2, some ST emulsions were found at the bottom of the specimens. Taking material cost into consideration, the application rate of 0.6 kg/m^2 was selected in the following tests.

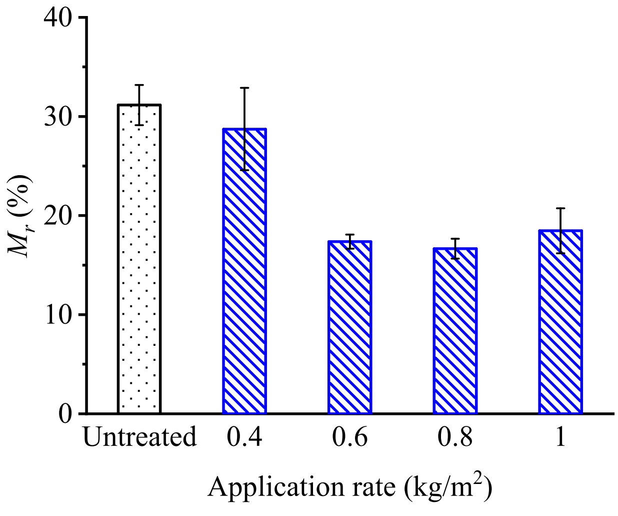

Figure 3.11 M_r of PA mixtures with different application rates of the ST emulsion

Effect of the solid content of ST emulsion

The solid content of ST emulsion could affect its viscosity, which further influences the recovery efficiency of damaged PA mixtures. In the laboratory tests, three emulsion solid contents were selected, including 40%, 50%, and 60%. The asphalt emulsion with a solid content of 60% was first prepared by the collide mill as the raw emulsion. The emulsions with lower solid contents were obtained by directly diluting the raw emulsion. To better reveal the effect of solid content, the application rate of ST emulsion with different solid contents was set to be the same as 0.6 kg/m^2.

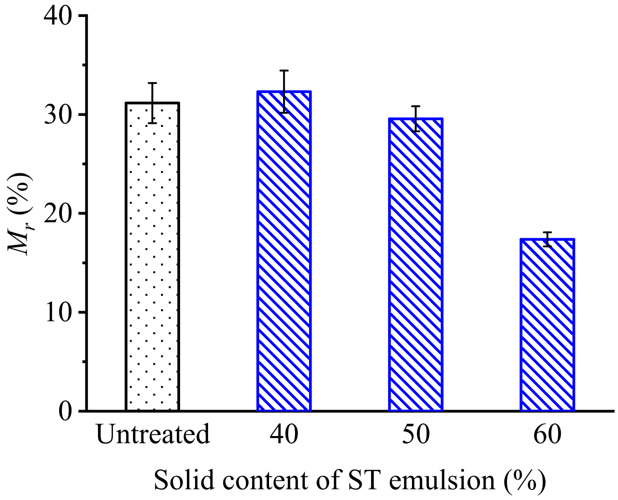

Figure 3.12 M_r of PA mixtures with different solid contents of the ST emulsion

Figure 3.12 shows that the PA mixture treated with the ST emulsion with a solid content of 60% had the lowest material loss. When the solid contents were diluted to 50% and 40%, the material losses sharply increased to around 30%, which is similar to that of the untreated specimens. It suggested that the solid content may significantly affect the recovery efficiency of the damaged mixtures. There are two possible reasons for this phenomenon. On one hand, under the same application rate of ST emulsion, the smaller the solid content, the fewer emulsion residues left inside a specimen after the water of the emulsion evaporated. The effective fresh binders were too few to improve the ravelling resistance of damaged PA specimens. On the other hand, ST emulsions with smaller solid contents usually have relatively lower viscosities, which will make the emulsion quickly flow through a specimen, resulting in the draindown and waste of ST emulsion. Therefore, it is recommended to use the ST emulsion with a solid content of 60% in the following study.

Effect of curing duration

Figure 3.13 shows the M_r of the specimens at different conditioning and ST stages. The application rate and solid content of the ST emulsion were 0.6 kg/m^2 and 60%, respectively. Compared with the unaged and no FT treated specimens, the M_r of the specimens subjected to the LTA and three cycles of FT conditioning gradually increased. However, after applying ST emulsion, the M_r decreased first sharply and then slowly as the curing duration increased. To balance the curing duration and recovery efficiency, it is recommended to maintain 14 days to get a better ravelling resistance. It is worth noting that the 14-day curing period is for the emulsions inside the mixture to cure and form strength, but for the emulsion stayed at the pavement surface, its moisture can be quickly evaporated to form the initial strength, which allows for traffic opening after several hours.

In addition, it is interesting to notice that the M_r of the ST specimens after 7 days' curing became lower than that of the LTA-conditioned specimens, which indicates that the asphalt emulsion not only filled up the micro-cracks inside the mixtures but also possibly diffused into the aged binder.

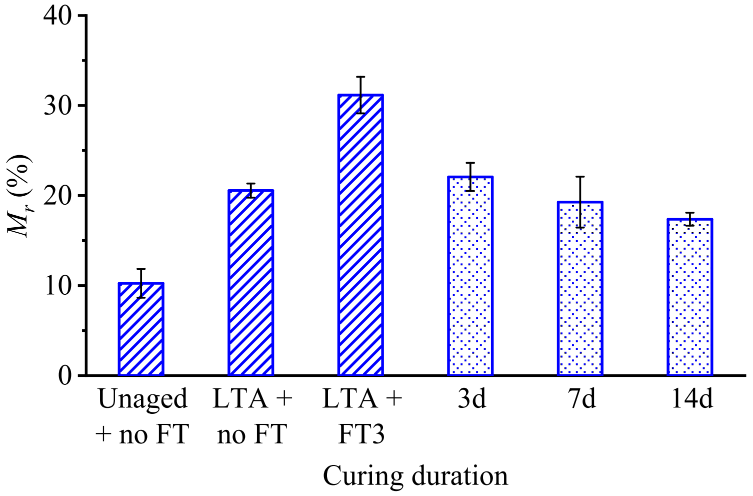

Figure 3.13 M_r **of PA mixtures with different curing durations**

Effect of the rejuvenator type

Rejuvenators have been widely used in asphalt pavement recycling. Five types of rejuvenators were evaluated in this study. Each type of rejuvenator was directly mixed with asphalt emulsion in advance, and then the emulsion was applied to the damaged specimens, which were tested after 14 days of curing. The damaged specimens with the ST application rate of 0.6 kg/m^2 and solid content of 60% were set as the control group. Figure 3.14 shows that most rejuvenators weakened the recovery efficiency of the ST emulsion except for one bio-based rejuvenator of TO2. One possible explanation is that those rejuvenators have slightly higher viscosities than the pure ST emulsion, leading to the non-uniform penetration effect. It reminds us that the rejuvenator might need appropriate preconditioning before being directly added to the ST asphalt emulsion, which will be further discussed in section 6.1. Another possible reason is that the diffusion effect of rejuvenators is very slow, which needs longer-term observation.

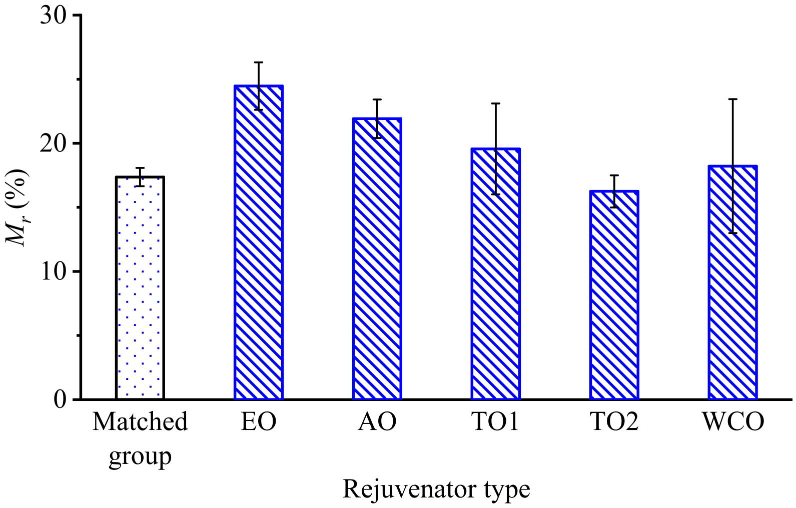

Figure 3.14 M_r of PA mixtures with different rejuvenators

Significance analysis

To further analyze the effects of different ST emulsion design factors on the M_r index, a one-way analysis of variance (ANOVA) was carried out and the results are summarized in Table 3.5. It can be seen that only the rejuvenator type has a significance value greater than the threshold of 0.05, indicating that the rejuvenator type is not a significant factor. This result is consistent with the analysis based on Figure 3.14. However, the other three factors all had significance values less than 0.05, which means that there is a statistically significant difference between the experimental groups. Moreover, the significance values of the application rate and solid content were all less than the threshold of 0.01, suggesting that the application rate and solid content had a significant effect on the M_r at the 99% confidence level. Therefore, it is critical to control these design factors of the ST emulsion in practice to achieve a better recovery efficiency for the PA mixture.

Table 3.5 The ANOVA results between different ST emulsion design factors on the M_r index

Factors	Source of difference	SS	df	MS	F	Sig.
Application rate	Between groups	288.649	3	96.216	16.618**	0.001
	Within groups	46.320	8	5.790	-	-
	Total	334.9692	11	-	-	-
Solid content	Between groups	377.509	2	188.754	86.939**	0.000

	Within groups	13.027	6	2.171	-	-
	Total	390.536	8	-	-	-
Curing duration	Between groups	33.012	2	16.506	7.382*	0.024
	Within groups	13.416	6	2.236	-	-
	Total	46.428	8	-	-	-
Rejuvenator type	Between groups	123.215	4	30.804	1.805	0.204
	Within groups	170.630	10	17.063	-	-
	Total	293.844	14	-	-	-

** means a high significance at the 99% confidence interval; * means a high significance at the 95% confidence interval.

Note: SS represents the sum of squares; df represents the degrees of freedom, F represents the F statistic, and Sig. represents the significance value.

3.2.2 Effects of ST emulsion on the mechanical performances of damaged PA

Cracking resistance of PA mixture

Figure 3.15 depicts the load-displacement curves of the new PA specimen, aged and F-T conditioned specimen, and ST treated specimen. Four replicates were prepared for each scenario, and the average values of the IDEAL-CT test results were summarized in Table 3.6. After undergoing long-term aging and F-T conditioning, the vertical peak load of the damaged specimen was significantly higher than that of the unconditioned specimens. This increase in fracture load can be attributed to the stiffening of the asphalt binders due to aging. Although the aged PA specimen was then subjected to F-T conditioning, the reduction in fracture load was limited compared with the effects of long-term aging resulting in a peak load that exceeded that of the new specimens. The decreasing trend of CT_{index} also indicates a deterioration in the cracking resistance of the damaged specimen. Meanwhile, the damaged specimen showed a higher value of $|m_{75}|$, indicating a faster deterioration rate of the post-peak load. Accordingly, the fracture energy of G_f decreased significantly in the damaged specimen, as the asphalt became stiffer and more brittle after aging, and some micro-cracks occurred within mortars during the F-T cycle conditioning.

Besides, for ST-treated specimens, the peak loads gradually increased over 14 days of curing at both temperatures. This increase could be due to the ST emulsion residue replenishing fresh asphalt binders and filling micro-cracks within the mixtures, thereby enhancing the cohesive strength of the aged mortar and the adhesive strength between aggregates and asphalt. After 90 days of curing, the peak load of the specimens cured at 60 ºC significantly increased to 8,343.67 N, while those cured at 25 ºC showed only a slight increase compared to the 3- and 14-day curations. The disparity between the test specimens cured at two temperatures could be attributed to two reasons. One explanation is the diffusion efficiency between emulsion residue and old asphalt binder is higher at 60 ºC than that at room temperature, aiding in rejuvenating the aged asphalt binder and recovering its bonding strength [148]. On the other hand, a relatively higher curing temperature might accelerate the oxidation of asphalt binder over a long-term curing period, further increasing the peak load.

It should be noted that four indicators, CT_{index}, peak load, $|m_{75}|$, and G_f, were derived from the loading-displacement curve, which were expected to evaluate the cracking resistance from different perspectives. It’s reasonable to conclude that the ST emulsion improved the damaged PA specimens' ability to withstand heavier traffic loads, as indicated by the higher peak load results compared to untreated specimens. However, except for the peak load, the $|m_{75}|$ and G_f didn’t show significant improvements between ST treated and untreated PA specimens. Particularly, the CT_{index} values of ST treated specimens even exhibited worse cracking performance than untreated specimens, which is contradictory to the findings based on the peak load results. So, additional replicates and alternative cracking tests are necessary to comprehensively assess the cracking resistance of ST-treated specimens. Nonetheless, based on peak load as an indicator, the treated PA specimens generally exhibited better cracking resistance than untreated ones.

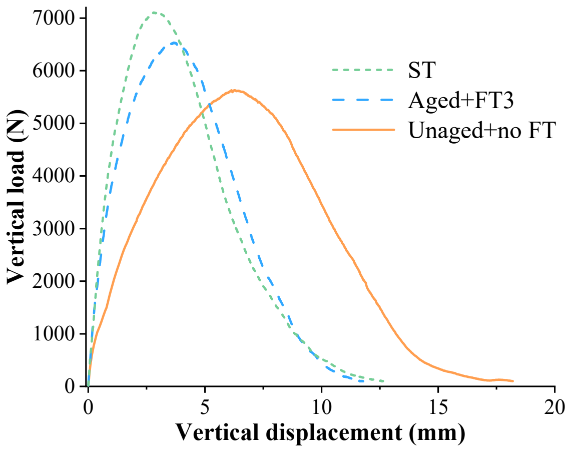

Figure 3.15 Load-displacement curves of IDEAL-CT

Table 3.6 Results of IDEAL-CT

Item	CT_{index}	Peak load N	$\lvert m_{75} \rvert$ N/m	G_f J/m^2
unaged+no FT	371.11	5,911.79	871,035.79	5,814.49
aged+FT3	120.95	6,388.90	1,301,823.81	4,277.25
25 °C-3d-ST	105.30	6,823.95	1,339,479.94	4,445.45
25 °C-14d-ST	117.54	6,603.13	1,269,357.05	4,197.15
25 °C-90d-ST	86.94	6,985.65	1,456,925.05	4,211.32
60 °C-3d-ST	104.05	7,067.94	1,412,321.41	4,412.44
60 °C-14d-ST	109.90	6,720.70	1,297,424.58	4,461.94
60 °C-90d-ST	56.57	8,343.67	1,939,906.03	4,256.10

Fatigue resistance of PA mixture

Fatigue tests were conducted to investigate the short- and long-term effects of ST emulsion on the fatigue resistance of damaged PA specimens. The load cycle number at the maximum energy ratio was collected to estimate the fatigue life of the test specimen. Figure 3.16 shows the ITFT results of ST treated PA mixtures after the short-term curing. The fatigue lives of damaged specimens at the stress levels of 220 kPa, 320 kPa, and 420 kPa were 17,636, 3,899, and 1,121 cycles, respectively. Compared to the damaged specimens subjected only to aging and F-T conditioning, the ST-treated specimens exhibited significantly better fatigue resistance. When the curing temperature is 25 °C, the fatigue lives of the treated specimens at the stress levels of 220 kPa, 320 kPa, and 420 kPa increased to 19,642, 4,446, and 1,730 cycles, respectively. This improvement is attributed to the penetration of ST emulsions into the damaged PA specimens, which replenished fresh asphalt binders and filled micro-cracks within the asphalt mixtures. Moreover, when the curing temperature is 60 ºC, the fatigue lives of ST treated specimens at the low, medium, high stress levels (220/320/420 kPa) were 28,686, 4,921, and 1,855 cycles, respectively, which were 63%, 26% and 65% higher than those of the damaged specimens without emulsion treatment. This indicates that a high curing temperature can improve the recovery efficiency of fatigue resistance in the short term.

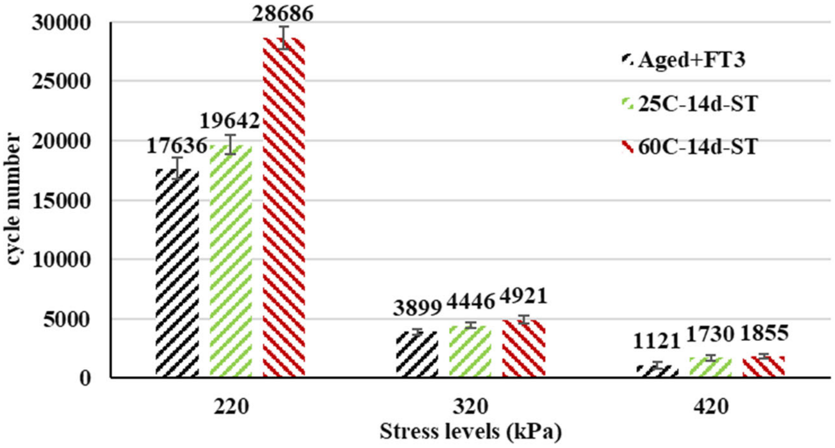

Figure 3.16 Fatigue lives of PA specimens after a short-term curing period

Figure 3.17 shows the fatigue lives of different specimens after 90 days of curing. Even after a long-term curing, specimens treated with ST emulsion maintained better fatigue resistance than untreated specimens, indicating that the recovery efficiency of ST emulsion on fatigue resistance has good durability. In addition, compared with Figure 6, specimens cured for 90 days showed longer fatigue lives than those cured for 14 days as shown in Figure 7. One possible explanation is that long-term curing leads to asphalt aging, which increases the resilient modulus of a PA specimen [149]. Consequently, when the same stress level was applied to specimens, the 90-day cured specimens exhibited a lower initial resilient strain as shown in Table 3.7. This lower strain suggests that the specimens had a greater ability to withstand the applied loading conditions. Therefore, compared with the short-term cured specimen, the long-term cured specimen showed a longer fatigue life under the controlled-stress loading mode.

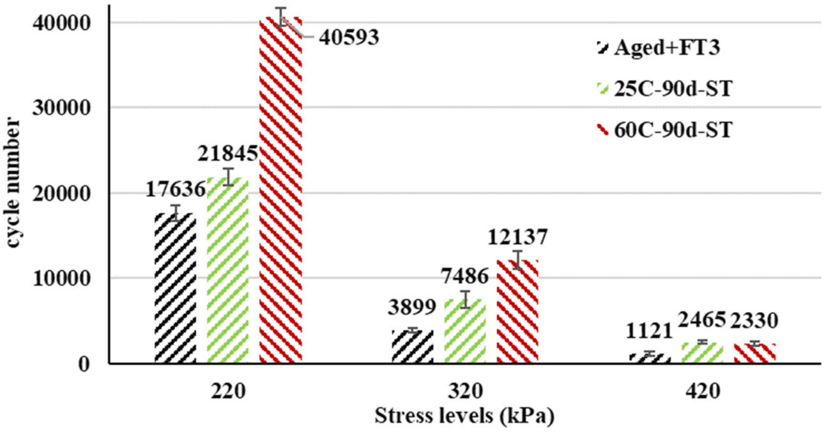

Figure 3.17 Fatigue lives of PA specimens after a long-term curing period

Table 3.7 Initial tensile strains of PA specimens after a long-term curing period

Item	Initial tensile strain at different stresses (με)		
	220 kPa	320 kPa	420 kPa
Aged + FT3	117.3	183.9	277.0
25 °C-14d-ST	106.5	165.8	229.6
25 °C-90d-ST	105.6	161.0	223.8
60 °C-14d-ST	98.8	164.5	213.1
60 °C-90d-ST	89.0	140.8	200.4

Rutting resistance of PA mixture

From the RALT test, the following three performance parameters of the PA specimens are commonly obtained: cumulative axial strain (ε_n), creep rate (f_c), and creep modulus (E_n). Figure 3.18 shows the RALT test results of ST treated specimens cured at two different temperatures over three months. The ε_n and f_c of ST treated specimens were notably lower than those of untreated PA specimens, indicating enhanced rutting resistance in the treated specimens. This outcome was unexpected, as previous studies have suggested that applying ST emulsion to asphalt pavement could increase the asphalt content in the mixture, potentially leading to rutting issues on the top layer of asphalt pavement [100, 150]. A possible explanation is that asphalt emulsion was usually applied to the dense-graded pavement as a preventive maintenance technology, like the fog seal, while the ST emulsion used in this study was applied to the PA pavement. The emulsion likely penetrated the mixture without clogging the voids or accumulating on the pavement surface. Thus, as long as the application rate and the viscosity of ST emulsion are well controlled, the potential rutting problem may not be aggravated. A similar phenomenon was also observed in another study [151].

In addition, the treated specimens cured at 60 ºC showed higher ε_n values compared to those cured at room temperature throughout the whole curing period, which means a deeper cumulative permanent deformation. This may be due to the diffusion of newly added ST residue with aged mortar, with the higher curing temperature accelerating the diffusion rate. This hypothesis is supported by the variation in the indicator E_n. During the short-term curing period, both treated specimens cured at two temperatures showed higher creep moduli than untreated specimens after 14 days of curing. This suggests that the application of ST emulsion to damaged PA specimens can enhance cohesive and adhesive strengths by filling micro-cracks and thickening mortar films. Interestingly, the E_n of treated specimens cured at 60 ºC is 6.91 MPa, while that at 25 ºC is 9.69 MPa, which implies a high curing temperature can improve the diffusion efficiency of the new ST residue in the aged asphalt mortar, then further softens the aged asphalt binders. However, during the long-term curing period, the treated specimens cured at 60 ºC were more sensitive to aging, so the E_n of treated specimens gradually increased to 7.65 MPa after 90 days of curing. By contrast, the treated specimens cured at room temperature were less affected by the aging problem, and the diffusion phenomenon likely continued at the same time, so the E_n of treated specimens gradually decreased to 8.18 MPa after 90 days of curing. Overall, the application of ST emulsion improved the rutting resistance of the damaged PA specimens.

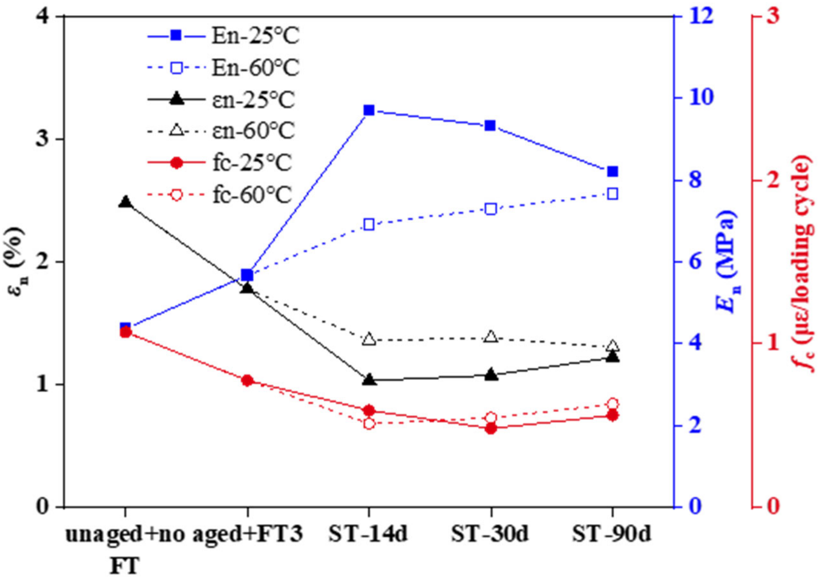

Figure 3.18 RALT test results of PA specimens

Significance analysis

To statistically evaluate the effects of ST emulsion on the mechanical properties of damaged PA specimens, significant difference analyses were conducted 1) between specimens treated with and without ST emulsions, 2) between different curing temperatures. Table 3.8, Table 3.9, and Table 3.10 summarize the statistical results of cracking, fatigue, and rutting properties of different PA specimens, respectively. Codes N, S, and HS represent no significant difference ($P > 0.05$), significant difference ($0.01 < P < 0.05$), and highly significant difference ($P < 0.01$), respectively.

It can be seen from Table 3.8 that all damaged PA specimens treated with ST emulsion had highly significant differences in peak load values compared to those damaged PA specimens treated without any maintenance material, highlighting the effectiveness of ST emulsion. And curing temperatures have significantly different peak load values among ST treated specimens. However, different evaluating indicators may vary in their sensitivity to maintenance effectiveness. Insignificant differences were found in several comparison scenarios when using CT_{index}, $|m_{75}|$ or G_f as indicators to evaluate the effect of ST emulsion and curing temperature effect on cracking performance. Table 3.9 shows that, regardless of the applied stress levels and curing periods, the fatigue properties of PA specimens treated with and without ST emulsions indicated significant differences. Fatigue resistance differences were also found at the low/medium stress levels under different curing temperatures. Finally, statistical results in Table 3.10 suggest that the ST emulsion significantly improved the rutting properties of damaged PA specimens. The curing temperature also had a significant impact on the rutting properties of ST treated specimens. Overall, the ST emulsion statistically improved the cracking, fatigue, and rutting resistance of damaged PA specimens. Moreover, applying the ST emulsion to the road in hot weather can promote the recovery efficiency of the mechanical properties of PA.

Table 3.8 Significant analysis of cracking performance of different PA specimens

Item	Cracking performance			
	CT_{index}	Peak load	$\|m_{75}\|$	G_f
ST emulsion effect				
aged+FT3 vs 25 °C-3d-ST	S	HS	S	S
aged+FT3 vs 25 °C-14d-ST	N	HS	S	N
aged+FT3 vs 25 °C-90d-ST	HS	HS	S	S
aged+FT3 vs 60 °C-3d-ST	S	HS	S	S
aged+FT3 vs 60 °C-14d-ST	S	HS	N	S
aged+FT3 vs 60 °C-90d-ST	HS	HS	HS	N
Curing temperature effect				
25 °C-3d-ST vs 60 °C-3d-ST	N	S	S	N
25 °C-14d-ST vs 60 °C-14d-ST	N	S	S	S
25 °C-90d-ST vs 60 °C-90d-ST	HS	HS	HS	N

Note: N: no significant difference ($P > 0.05$); S: significant difference ($0.01 < P < 0.05$), HS: highly significant difference ($P < 0.01$).

Table 3.9 Significant analysis of fatigue performance of different PA specimens

Item	Fatigue life		
	220 kPa	320 kPa	420 kPa
ST emulsion effect			
aged+FT3 vs 25 °C-14d-ST	HS	S	S
aged+FT3 vs 25 °C-90d-ST	HS	HS	HS

aged+FT3 vs 60 °C-14d-ST	HS	HS	HS
aged+FT3 vs 60 °C-90d-ST	HS	HS	HS
Curing temperature effect			
25 °C-14d-ST vs 60 °C-14d-ST	HS	S	N
25 °C-90d-ST vs 60 °C-90d-ST	HS	HS	N

Note: 220/320/420 kPa means the stress level of fatigue test.; S: significant difference ($0.01 < P < 0.05$), HS: highly significant difference ($P < 0.01$).

Table 3.10 Significant analysis of rutting performance of different PA specimens

Item	Rutting performance		
	ε_n	f_c	E_n
ST emulsion effect			
aged+FT3 vs 25 °C-14d-ST	HS	S	HS
aged+FT3 vs 25 °C-30d-ST	HS	S	HS
aged+FT3 vs 25 °C-90d-ST	HS	S	HS
aged+FT3 vs 60 °C-14d-ST	HS	S	HS
aged+FT3 vs 60 °C-30d-ST	HS	S	HS
aged+FT3 vs 60 °C-90d-ST	HS	S	HS
Curing temperature effect			
25 °C-14d-ST vs 60 °C-14d-ST	HS	S	HS
25 °C-30d-ST vs 60 °C-30d-ST	HS	S	HS
25 °C-90d-ST vs 60 °C-90d-ST	S	S	S

Note: S: significant difference ($0.01 < P < 0.05$), HS: highly significant difference ($P < 0.01$).

3.2.3 Effects of ST emulsion on the functional performances of damaged PA

Although it is expected that ST emulsion can help extend the service life of PA pavements in terms of its ravelling resistance recovery, it is also very important to ensure that the ST emulsion will not compromise the functional performances of PA mixtures. Figure 3.19 shows the test results of three functional performances, including noise absorption, permeability, and skid resistance. All tests were carried out before and after emulsion ST.

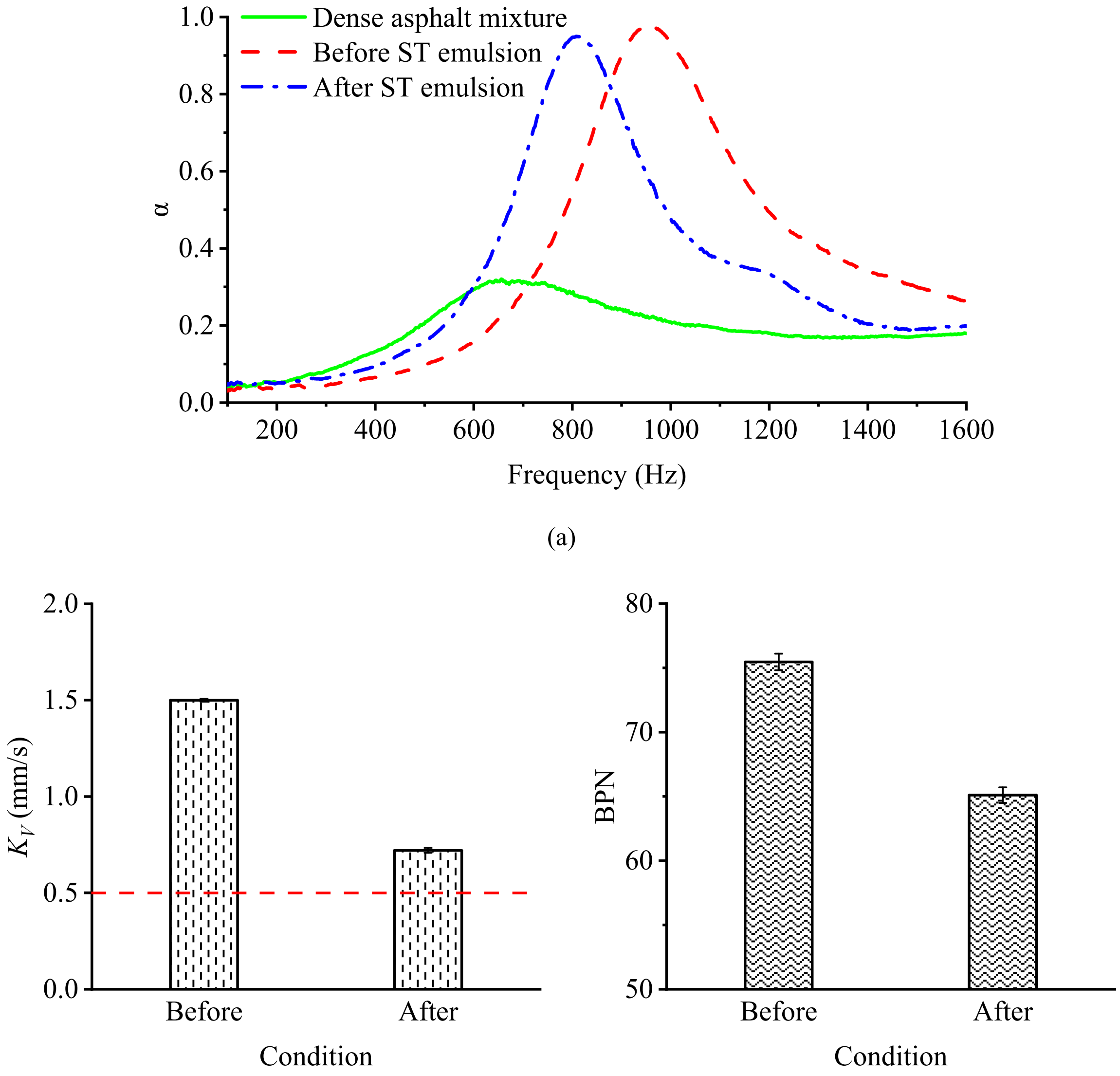

(a)

(b) (c)

Figure 3.19 Functional performance: (a) noise absorption; (b) permeability; (c) skid resistance

Figure 3.19 (a) shows the noise absorption coefficients of the PA specimens in comparison to that of a conventional dense-graded asphalt mixture used in Hong Kong. After the damaged specimens were treated by ST emulsions, the noise absorption curve shifted horizontally to the left. However, the peak value of the noise absorption coefficient for the treated PA mixture is slightly lower than that of the untreated one. The absorption coefficients of the treated PA specimen were still within the range of 35-95% between 800 Hz to 1200 Hz, which is the sensitive frequency range for human auditory perception. In addition, even after the PA mixtures were treated with the ST emulsion, they still had much better noise absorption properties than the dense-graded asphalt mixtures. As **Figure 3.19**(b) shows, the vertical permeability coefficients of the untreated and treated specimens obviously decreased from 1.50 mm/s to 0.72 mm/s, indicating that some pores, especially the connected pores, might have been clogged or partially clogged by the ST emulsions. However, according to EN 12697-19, the vertical permeability coefficient of the treated PA specimens can still meet the minimum requirement of 0.5 mm/s. The BPN values from the skid resistance tests are shown in Figure 3.19(c). After the damaged specimens were treated by ST emulsions, the BPN values of the PA mixtures were also reduced from 75.5 to 65.1, but it can still meet the minimum requirement of 45 in accordance with the Chinese standard JTG 5142-2019. The previous studies indicated that BPN values can quickly recover after the roads are open to traffic for several months [152, 153]. Therefore, the ST emulsion may only negatively affect the functional performances of the PA mixtures in the short term, but the effect is considered overall acceptable.

3.3 Summary

In this chapter, the Cantabro abrasion test was carried out to investigate the ravelling resistance recovery of damaged PA mixture with ST emulsion. Several material design and treatment factors were considered, and the optimal application parameters were determined. The effects of ST emulsion on both the mechanical and functional performances were systematically evaluated. The major findings of this chapter are summarized as follows:

(1) Both the application rate and solid content of the ST emulsion significantly affect the ravelling resistance recovery in damaged PA mixtures. In practice, controlling these factors is crucial to ensure the effectiveness of this preventive maintenance method.

(2) The recovery efficiency of the rejuvenator on the damaged PA mixtures was not obvious within 14 days of curing. But in the long term, it is still possible for the rejuvenator to soften the aged binder by diffusion, which needs further study.

(3) For the CSS-1 emulsion and PA mixture evaluated in this study, the optimum application rate of 0.6 kg/m^2 and solid content of 60% were recommended, which could reduce the M_r from 31.2% to 17.4%. At the same time, the negative effect of the ST emulsion on functional performance is limited. This confirms that the ST emulsion can serve as a promising preventive maintenance material for PA pavements.

(4) After the ST emulsion was applied to the damaged PA specimen, the treated specimen exhibited a higher indirect tensile strength, a longer fatigue life, and a better anti-rutting performance than the untreated PA specimen in the short term. Compared with the damaged PA specimen, the ST treated PA specimen maintained a good mechanical performance over 3 months, indicating strong durability and the potential to extend the service life of PA pavement.

(5) Although a relatively high curing temperature can accelerate the recovery efficiency of mechanical properties of damaged PA in the short term, a relatively fast aging phenomenon also accompanies it, which cannot be neglected. Therefore, a ST emulsion with an excellent anti-aging property is expected to achieve a better maintenance outcome for PA.

(6) When the appropriate ST emulsion material and application conditions are well designed, the rutting resistance of the treated PA specimen was not compromised in the scenarios considered in this study.

(7) While the application of ST emulsion may have a slight short-term impact on functional performance, verification is necessary during material design to balance the recovery of mechanical performance with the preservation of functional performance.

CHAPTER 4 PENETRATION MECHANISM OF ST EMULSION IN DAMAGED PA MIXTURE: MICROSTRUCTURE CHARACTERIZATION AND 3D RECONSTRUCTION

As a promising preventive maintenance material for PA road, ST emulsion functions as a time-dependent phase transition material. When sprayed to the surface of old PA pavements, ST emulsions initially acted as the liquid phase penetrating into the PA mixtures along the void structures. Following the water evaporation and ST emulsion demulsification, ST residues worked as the solid phase filling microcracks and replenishing new asphalt binders within PA pavements. It can be seen that the distribution status of ST residues inside PA mixtures could significantly affect the maintenance effects of ST emulsion. However, despite the positive outcomes of the studies and applications of ST emulsion for PA wearing courses, most of these outcomes are based on macroscopic laboratory tests and empirical field trials, as discussed in Chapter 2 and Chapter 3. Fundamental studies exploring the penetration mechanism of the ST emulsion in PA are still limited.

To understand such a mechanism, it is important to know how the emulsion penetrates the pore structure and how the ST emulsion residue is distributed spatially in damaged PA. ST emulsions are liquids with certain viscosities during the penetration stage. Several studies have been conducted to characterize the clogging [26] or water flow [27] of PA at the micro-scale using the image analysis approach, which are solid particle and pure water penetration process, respectively. For the interaction between the ST emulsion and PA, it is expected that the additional emulsion residue may fill some micro-cracks and thicken the aged asphalt binder film, but no quantitative evidence is available. To fill this gap, this chapter aims to investigate the penetration behavior of the ST emulsion in damaged PA with the help of X-ray CT. Section 4.1 describes the image acquisition and analysis methods, including the air void identification and morphological analysis, back-calculation of the ST emulsion residue, and quantifications of film thickness and coating area of the ST emulsion residue. Section 4.2 presents the analysis results of the penetration status of ST emulsion residue in a damaged PA mixture. X-ray CT scanning was performed to monitor the changes in the pore microstructure of PA specimens under three selected ST conditions. The spatial distribution of the ST emulsion residue was back-calculated and visualized in 3D through CT image analysis. The coating efficiencies and thickness distributions of ST emulsions were quantitatively estimated to characterize their penetration status. The outcomes of this chapter are expected to help optimize the performance of the ST technology for PA, thus contributing to more durable PA pavements.

4.1 Experiments and Methods

4.1.1 Materials and sample preparations

The ST asphalt emulsion and damaged PA specimens were prepared following the same methods as described in Section 3.1. Based on the preliminary test results, three ST conditions with different emulsion application rates and solid contents were considered in this study, as shown in Table 4.1. Three damaged PA specimens were selected for the X-ray computed tomography (CT) scanning before and after ST with a curing time of 7 days at room temperature.

The effects of different ST conditions on the performance recovery of the damaged PA were evaluated by the Cantabro abrasion test [141]. In addition, the permeability coefficients of the damaged PA before and after ST were also measured by a constant head permeameter. Three replicates were prepared for each ST condition. The mass loss ratio and permeability coefficient were calculated by Equations (3-1) and (3-11), respectively.

Table *4.2* presents the detailed test results for three different ST application scenarios. The PA specimens with an emulsion application rate of 0.6kg/m^2 and solid content of 60% provided the highest recovery efficiency. Its permeability coefficient was lower than that of the control material, but still higher than the lower limit of 0.5mm/s for PA as standardized in EN 12697-19.

Table 4.1 Basic properties of the ST emulsion

Specimen ID	Application rate (kg/m^2)	Solid content (%)	Evaporated residue		
			Penetration (25°C, 0.1mm)	Softening point (°C)	Ductility (5 °C, cm)
ST 0.4-60%	0.4	60%	60	64	50
ST 0.6-60%	0.6	60%			
ST 0.6-40%	0.6	40%			

Table 4.2 Performance of the damaged PA before and after different ST application scenarios

Specimen ID	Mass loss ratio (%)		Permeability coefficient (mm/s)	
	Mean	St.d	Mean	St.d
Control	31.2	2	1.50	0.01
ST 0.4-60%	28.7	4.1	-	-
ST 0.6-60%	17.4	0.7	0.72	0.01
ST 0.6-40%	32.3	2.1	-	-

4.1.2 Image acquisition and analysis methods

Cross-sectional images of the damaged PA before and after different ST conditions were acquired by an X-ray computed tomography (CT) scanning system of Phoenix v |tome |xs. Table 4.3 presents the detailed scanning parameters. The horizontal resolutions of different specimens ranged from 0.061 to 0.067 mm/pixel, which could be explained by the slight absorbance variance. The CT slices are 8-bit grayscale images with 256 levels of intensity, which reflect the densities of objects inside the specimen.

Table 4.3 Summary of the XCT scanning parameters

Specimen ID	Scanning time	Voltage (kV)	X-ray tube current (mA)	Vertical resolution (mm/pixel)	Horizontal resolution (mm/pixel)
ST 0.4-60%	Before ST	190	110	0.1	0.067
	After ST				0.061
ST 0.6-60%	Before ST				0.067
	After ST				0.061
ST 0.6-40%	Before ST				0.065

After ST	0.061

Air void identification and morphological analysis

As can be seen in Figure 4.1(a) and (b), the air void in each CT slice can be separated from the aggregates and asphalt mortar using the image processing methods of enhancement, filtering, and thresholding. The white region of the binary image shown in Figure 4.1(b) represents the air void of one PA specimen cross-section. Then, the volume, size, and number of air voids in the PA specimen were statistically analyzed considering different ST conditions and scanning timings. The air voids inside PA can be divided into two types: interconnected air voids and closed air voids [154], which have different effects on the flow path of the ST emulsion. Thus, it is important to differentiate the two types of air voids. A series of MATLAB codes were programmed to analyze the interconnectivity of binary images from top to bottom in the vertical direction. As **Figure 4.1**(c) illustrates, a top-down processing program followed by a bottom-up processing was used to distinguish the interconnected air voids from the closed air voids [155]. Each white region in two consecutive CT images was compared starting with the top surface image. If they continuously overlapped from top to bottom, they would be labeled as candidate interconnected air voids. The procedure was then repeated, starting from the bottom surface image, to rule out the closed air voids with a downward dead-end. Finally, the interconnected pores and the closed air voids could be successfully identified. The reconstructed 3D models of both types of air voids are shown in Figure 4.1(d) and (e), respectively.

Two indexes, namely interconnected factor (F_i) and tortuosity (T), were used to quantify the interconnectivity of the PA's pore-structure. As Equation (4-1) shows, F_i is defined as the ratio of the interconnected air voids to the total air voids, representing the drainage efficiency of the pores in PA. As Equation (4-2) shows, T is calculated by dividing the actual length of the flow path by the shortest distance between the two ends of the interconnected porous structure. A larger T value indicates that the movement of the fluid through the interconnected pores is more difficult.

$$F_i = \frac{P_i}{P_t} \times 100 \tag{4-1}$$

$$T = \frac{L_e}{L} \tag{4-2}$$

where P_i = the voxel number of the interconnected air void; P_t = the voxel number of all air voids in the specimen; L_e = the distance between the centroids of two interconnected air voids from two target images, mm; and L = the shortest distance between the two images, mm.

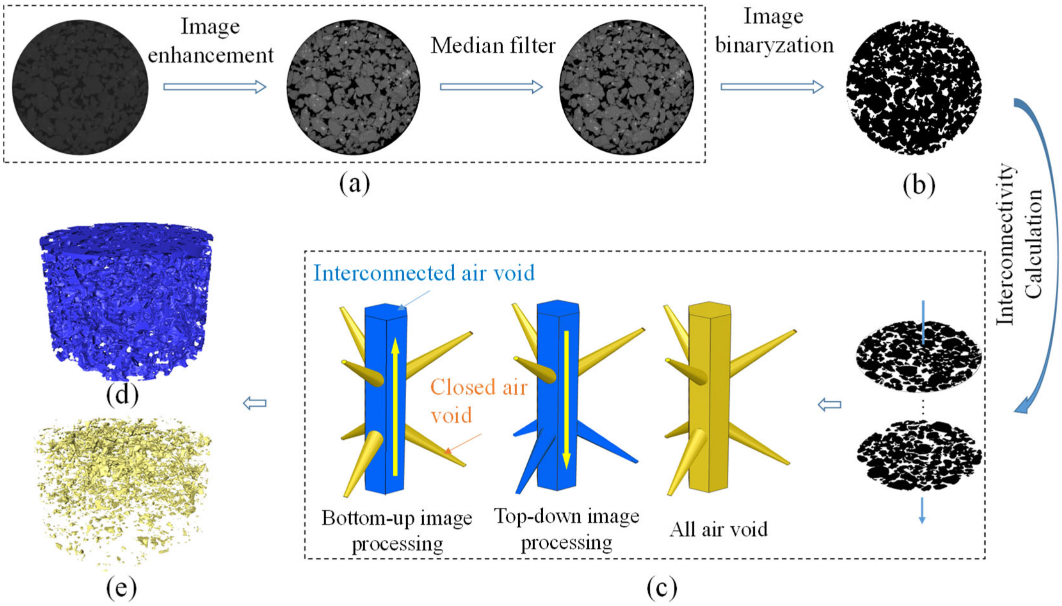

Figure 4.1 Procedures for air void identification from the CT slices: (a) pro-processing; (b) binary image; (c) interconnectivity analysis; (d) interconnected air void and (e) closed air void.

Back-calculation of the ST emulsion residue

It is assumed that the volume of the ST emulsion residue is equal to the volume of the reduced air void regions in PA. Based on this assumption, the ST emulsion residue was back-calculated using a set of customized MATLAB codes. The corresponding CT images of PA before and after ST were determined by feature matching. As Figure 4.2(a) and (b) illustrate, the original binary images were resized to the same resolution, and the center of both circular cross-sections were relocated to the same position. Following that, a rotation operation was performed on the binary images of the treated PA specimen. It should be noted that the rotated angle and center position should be calculated backward by maximizing the overlap between the white areas of the corresponding binary images before and after ST. Finally, through image subtraction, the ST emulsion residue could be successfully identified as shown in Figure 4.2(c). The gold area represents the ST emulsion residue, the black area represents the air voids after ST, and the gray area represents the coarse aggregates and mortar in the PA specimen.

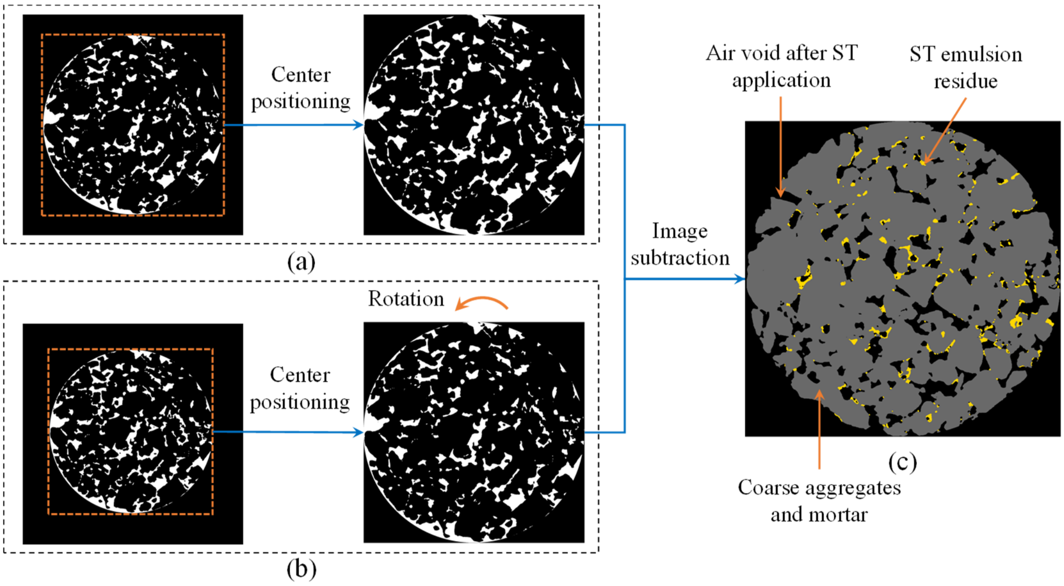

Figure 4.2 Images of: (a) air voids before ST; (b) air voids after ST; and (c) ST emulsion residue.

Film thickness and coating area of the ST emulsion residue

All the ST emulsion residue in the cross-sectional images from the top surface to the bottom were highlighted and labeled. The ST emulsion residues are randomly dispersed over the surface of the aged mortar, as illustrated in Figure 4.3(a), but not all of them are fully coated. The black, gray, and yellow colors depicted in Figure 4.3(b) represent the air void, aggregate, and ST residue, respectively. The newly added ST residues are generally distributed around the air voids and the coated boundary is marked as the red color. To quantify the coating efficiency of the ST emulsion residue, a new index called the percentage of coating area (P_c) was proposed and calculated by Equation (4-3). For each CT slice, it is defined as the ratio of the coated boundary length to the total boundary length of the air voids before ST, which is proposed to evaluate the coating efficiency of ST residue in damaged PA.

Besides, as can be seen in Figure 4.3(a), the shapes of the emulsion droplets are complicated, and the thickness values of the coating layer on the aged mortar vary. Therefore, the coating film thickness was calculated to quantify the spatial distribution of the ST emulsion residue. A similar approach has been implemented to effectively investigate the meso-structure of the asphalt mortar [156]. A series of image-related MATLAB algorithms were implemented to collect the coating film thickness, as shown in Figure 4.3(c) and (d). The binary images of the ST emulsion residue were first prepared. Then, the centre line of each emulsion droplet was extracted. After that, a distance transformation was applied on the centre line to calculate the shortest distance between the centre line pixels to the boundary of the corresponding droplet. As shown on the right side of Figure 4.3(d), the centre lines were assigned with different grayscales to represent different distance values, with darker indicating shorter distance. Finally, the coating film thickness was determined as twice the shortest distance. For each CT slice, thousands of coating film thickness values were collected from different centre line pixels. Two parameters, namely the mean value (T_c) and standard deviation (SD_c), were introduced to characterize the distribution of the coating film thickness.

$$P_c = \frac{\sum_{i=1}^{i=n} L_c^i}{\sum_{i=1}^{i=n} L_a^i} \times 100 \tag{4-3}$$

where n is the number of CT images; L_c^i means the total lengths of the coated boundaries of ST for the number i image, mm; and L_a^i is the perimeters of all air voids before the ST condition for the number i image, mm.

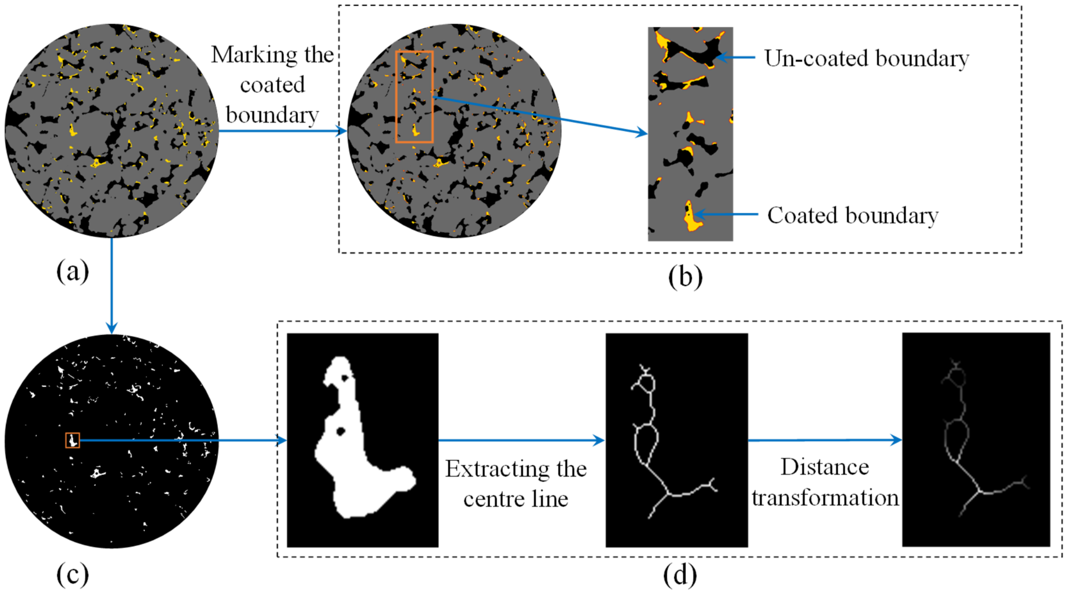

Figure 4.3 Calculation methods for the coating area and film thickness of the ST emulsion residue: (a) RGB image; (b) coated boundary; (c) binary image of the ST emulsion residue; and (d) thickness counting.

4.2 Results and Discussions

4.2.1 Air void reduction in the depth direction

The addition of ST emulsions occupies a certain portion of the air voids. The air void content of each CT slice is equal to the area proportion of the white area to the total cross-sectional area. Figure 4.4 illustrates the air void content of PA before and after ST as well as the decreased air void content induced by the ST emulsion residue. The vertical volume distribution of the air void in PA before and after ST are both in bathtub shape, which is consistent with the findings of the previous study [157]. Figure 4.4 also shows that the distribution of the ST emulsion residue in PA has a vertical gradient profile, with more accumulating near the top of the specimen. The black lines immediately surged around the bottom in Figure 4.4(b) and (c), suggesting that only a tiny proportion of the ST emulsion could travel through the interconnected flow path, and it is still reasonable to deduce that the majority of the ST emulsion has limited penetration depth. As shown in Figure 4.4(b), the majority of the ST emulsion could penetrate approximately 20mm, but for the other two ST conditions (Figure 4.4(a) and (c)), the ST emulsion could only penetrate nearly 10mm.

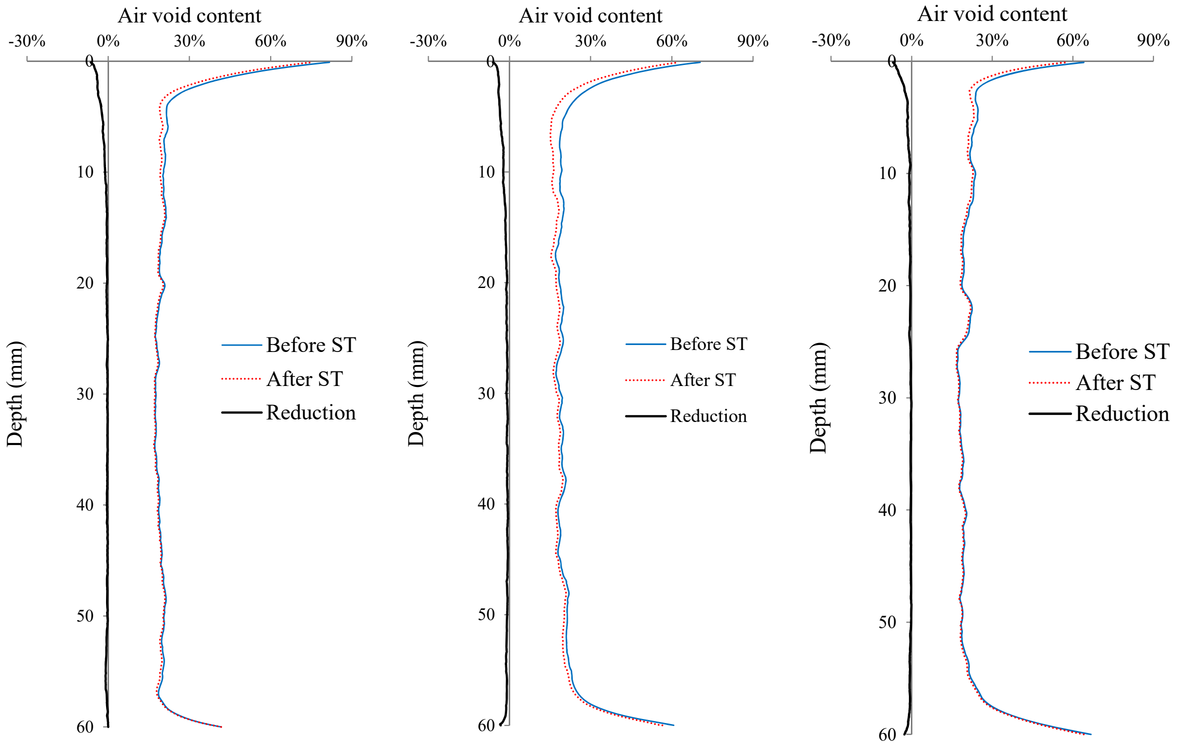

(a) (b) (c)

Figure 4.4 The gradient distribution of the air void content along the depth direction before and after different ST conditions: (a) ST 0.4-60%; (b) ST 0.6-60%; and (c) ST 0.6-40%.

In Figure 4.4, the absolute values of the air void reduction are quite small and may relate to the value of the total air void content. So, the percentage reduction in air voids (P_{ra}) was also calculated using Equation (4-4) to further characterize the air void decreasing patterns for different ST conditions. P_{ra} is defined as the ratio of the reduced air void content to the total air void content without ST. Figure 4.5 shows the P_{ra} of the PA specimens subjected to different ST conditions with a depth interval of 5 mm. P_{ra} is larger than 5% when the penetration depth is less than 25 mm for ST 0.6-60% condition, but only 10 mm for ST 0.6-40% condition and 5 mm for ST 0.4-60% condition.

$$P_{ra} = \frac{\sum_{i=1}^{i=n}(V_{tb}^{i} - V_{ta}^{i})}{\sum_{i=1}^{i=n} V_{tb}^{i}} \times 100 \qquad (4\text{-}4)$$

where n = number of CT slices; V_{tb}^{i} = air void content of number i image before ST condition, %; and L_{ta}^{i} = air void content of number i image after ST condition, %.

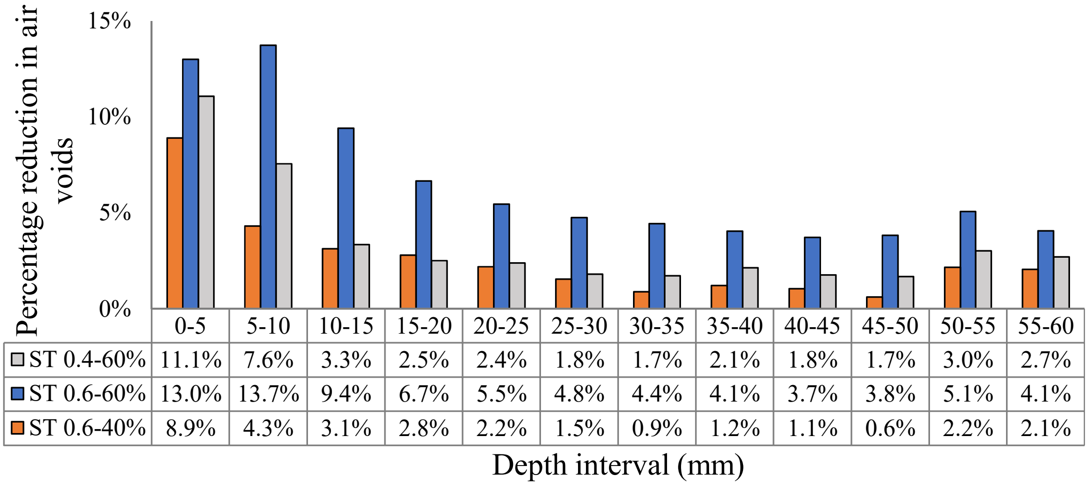

	0-5	5-10	10-15	15-20	20-25	25-30	30-35	35-40	40-45	45-50	50-55	55-60
□ ST 0.4-60%	11.1%	7.6%	3.3%	2.5%	2.4%	1.8%	1.7%	2.1%	1.8%	1.7%	3.0%	2.7%
🟦 ST 0.6-60%	13.0%	13.7%	9.4%	6.7%	5.5%	4.8%	4.4%	4.1%	3.7%	3.8%	5.1%	4.1%
🟧 ST 0.6-40%	8.9%	4.3%	3.1%	2.8%	2.2%	1.5%	0.9%	1.2%	1.1%	0.6%	2.2%	2.1%

Figure 4.5 Percentage reduction in air voids (P_{ra}) of PA due to ST in depth direction

4.2.2 Pore morphology of PA before and after ST

The air void contents (V_a) of the three damaged PA specimens before ST were measured by the dimensional method [158] as shown in Table 4.4. The total and interconnected V_a of PA before and after ST calculated through the image analysis are also presented. Besides, to characterize the size and number of the air voids within the PA specimen, the average equivalent diameter (D_e) and number of air voids (N_a) are also summarized in Table 4.4. The equivalent diameter of each air void is defined as the diameter of an equivalent circle that has the same area as the air voids. The overall interconnected factor (F_i) and tortuosity (T) were also calculated as presented in Table 4.4. The V_a values calculated by the CT image processing are all slightly less than those measured by the dimensional method, which may be caused by the limited resolution of CT images. After ST, the total and inter-connected V_a of the PA specimens were all decreasing with the deviations ranging from 0.7% to 1.4% and 0.9% to 1.7%, respectively. Accordingly, the F_i values of each PA specimen also decreased after ST with varying deviations, indicating varying effects of ST on the permeability of PA. In addition, after ST, D_e of each PA specimen decreased, while N_a increased, indicating that more air voids with smaller D_e showed up in the treated PA specimen. As for the tortuosity, after ST, the T value of each PA specimen reduced somewhat, so the penetrated ST emulsion may first block or fill the branches along the flow path with little impact on the main fluid channels. Overall, it is noticed that the ST 0.6-60% specimen had the most significant change in all morphological indexes after ST.

Table 4.4 Summary of the morphological properties of the air voids in PA

Specimen ID		Measured V_a	V_a of the images	Inter-connected V_a	Mean value of each CT slice			
					D_e (mm)	N_a	F_i	T
ST 0.4-60%	Before ST	22.7%	21.2%	19.8%	2.375	179	0.932	1.403
	After ST	--	20.4%	18.9%	2.286	183	0.924	1.384
	Deviation	--	0.8%	0.9%	0.089	-4	0.008	0.019
ST 0.6-60%	Before ST	23.1%	21.6%	20.2%	2.461	157	0.944	1.454
	After ST	--	20.2%	18.5%	2.339	162	0.914	1.403
	Deviation	--	**1.4%**	**1.7%**	**0.122**	**-5**	**0.030**	**0.051**
ST 0.6-40%	Before ST	22.8%	22.0%	20.8%	2.388	162	0.934	1.424
	After ST	--	21.3%	19.9%	2.310	164	0.929	1.418
	Deviation	--	0.7%	0.9%	0.078	-2	0.005	0.006

Size, number, and area distribution of the air voids

Based on the air void volume analysis, it can be confirmed that the penetration of the ST emulsion shows gradient characteristics. Taking ST 0.6-60% as an example, the D_e and N_a values of the air voids in PA before and after ST were further statistically analyzed along the depth direction with an interval of 5mm as shown in Figure 4.6. After ST, the top 20 mm of PA specimen presents decreasing D_e but increasing N_a. The middle 20 mm of PA specimen presents relatively minor fluctuation of D_e and N_a. For the bottom 20 mm, D_e showed an increasing trend while N_a decreased. Therefore, the size distribution of the air voids in PA should have different changes at different depths. To further characterize the effects of ST emulsion residue on the pore structure, the area percentage of the air voids in each CT slice less than 25 mm^2, falling between 25 and 200 mm^2 and larger than 200 mm^2 were counted as shown in Figure 4.7. The counting was conducted for PA specimen before and after ST with a depth interval of 20 mm. By contrast, the area percentage of the air voids less than 25 mm^2 increased sharply for the top 20 mm, and considering that N_a also increased, it could be inferred that some large air voids (>25 mm^2) were partially occupied by the ST emulsion residue and became smaller or were separated into several smaller ones. For the bottom 20 mm, the area percentage of air voids falling between 25 and 200 mm^2 decreased, and given that N_a also decreased but D_e increased, it could be inferred that some medium size air voids (25-200 mm^2) were totally filled by the ST emulsion.

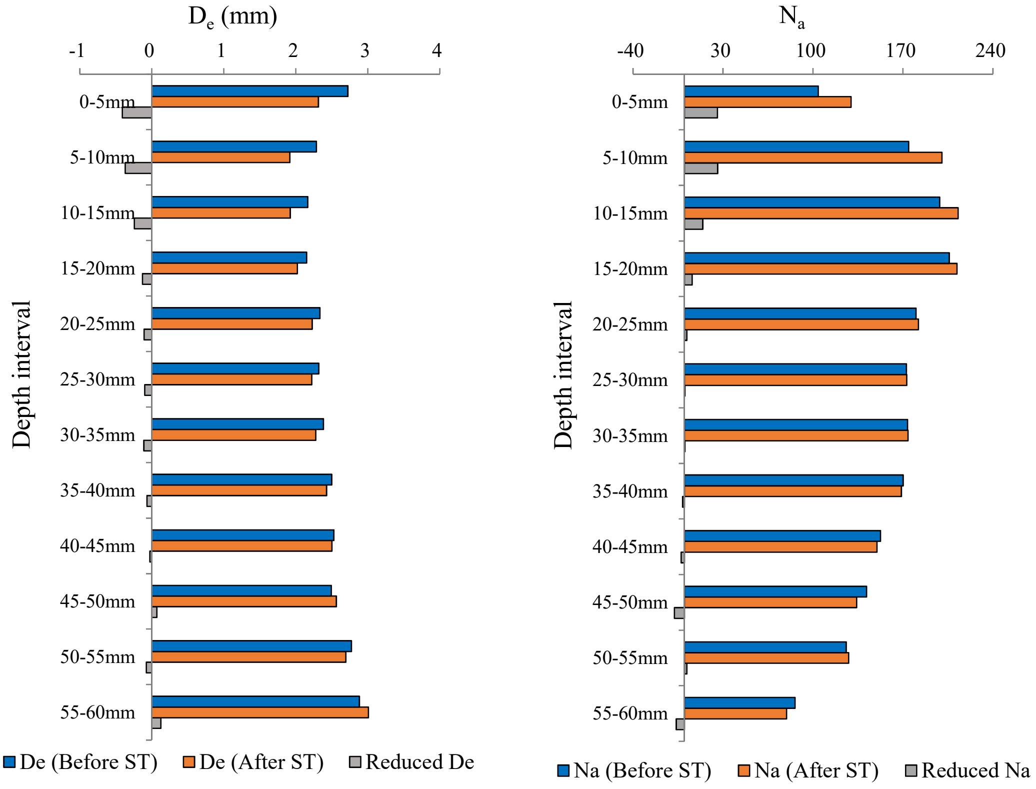

(a)

(b)

Figure 4.6 Morphological properties of air voids in PA before and after the ST 0.6-60% condition: (a) D_e; (b) N_a.

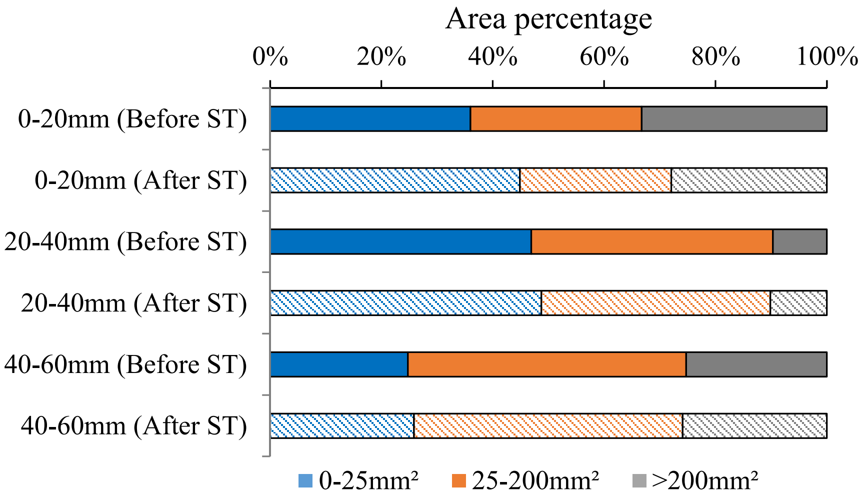

Figure 4.7 The area distribution of the air voids in PA before and after the ST 0.6-60% condition

Typical profiles of the air voids at different depths

The micro-pore structure of PA is affected by the ST emulsion, and the penetration process has obvious gradient characteristics. To better illustrate such an effect, several typical profiles of the air voids after the application of ST 0.6-60% were randomly selected as presented in Figure 4.8. The black area is the air voids after ST, and the gold area is the back-calculated ST emulsion residue. Figure 4.8(a) is one of the profiles of the treated PA at the depth of 9.9 mm from the top surface. It can be observed that several large air voids, marked by the red circles, were partially filled by the ST emulsion residue and were turned into several smaller voids. As Figure 4.8(b) shows, for the middle part of the specimen, most of the ST residue can only fill the micro-pores around the main pore-structure because a limited volume of ST emulsion could penetrate to and remain in this depth. As Figure 4.8(c) demonstrates, the ST emulsion residue around the bottom part could completely fill some small air voids while leaving most of the big pores intact. The observation from the typical profiles could well verify the findings obtained from the size, number, and area analysis for air voids, and it can be concluded that the penetrated ST emulsion would definitely reshape the micro-pore structure, which is supposed to be one of the key factors influencing the mechanical and functional performance of the damaged PA.

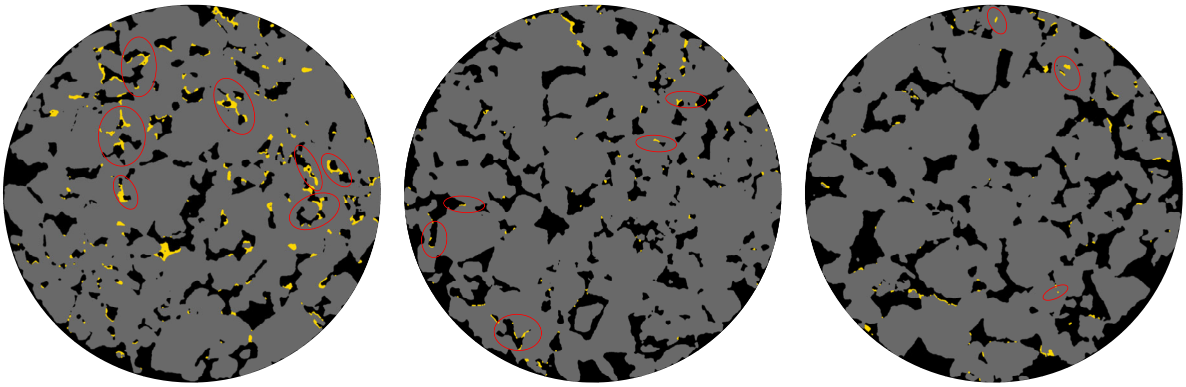

(a) Depth 9.9 mm (b) Depth 28.2 mm (c) Depth 56.6 mm

Figure 4.8 The RGB images of the back-calculated ST emulsion residue within PA

Interconnectivity and tortuosity of the air voids

The overall interconnectivity and tortuosity of the air voids in PA after ST are also changed. For example, the F_i and T value along the depth direction for the specimen of ST 0.6-60% are shown in Figure 4.9. As illustrated in Figure 4.9(a), after ST, the F_i value presents a significant drop when the depth is less than 20 mm, while keeping almost the same when the depth is more than 20 mm. Figure 4.9(b) shows the tortuosity of the PA specimen before and after ST. The distribution of the T value varied in the range of 1 to 2 due to the inhomogeneous structure of the interconnected pore. After ST, the T value decreased at both ends of the PA specimen. The flow path with higher F_i and lower T value should have better permeability. Therefore, the reduced permeability caused by the ST emulsion should be mainly attributed to the lower F_i near the top portion of the PA specimen.

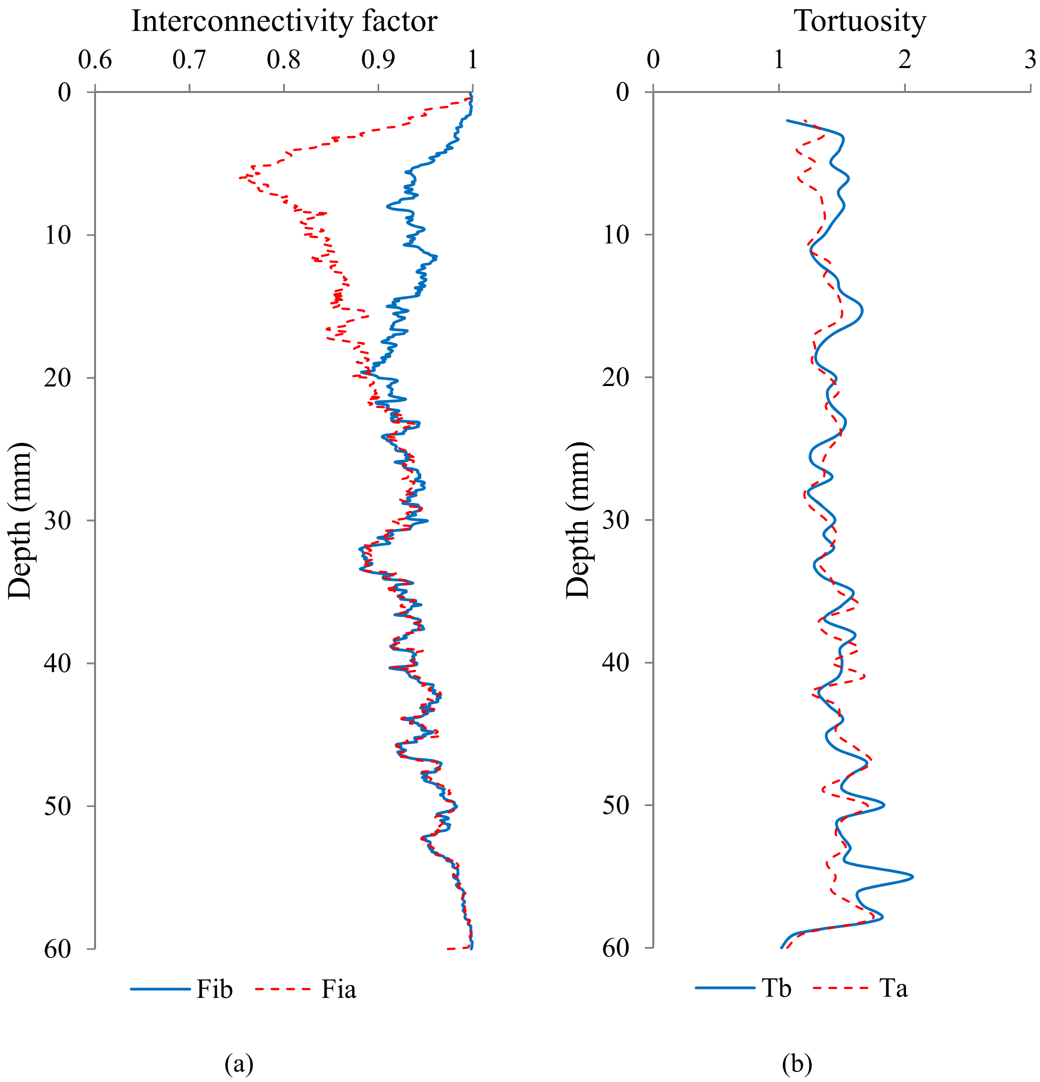

Figure 4.9 Interconnectivity and tortuosity of PA before and after ST: (a) F_i; (b) T.

4.2.3 Back-calculated distribution of the ST emulsion residue

3D model visualization

The 3D models of the ST emulsion residue within the PA specimens were reconstructed by stacking the continuously back-calculated binary images of the ST emulsion residue. Based on the visualization shown in Figure 4.10, most of the ST emulsion residues are concentrated near the top surface of the PA specimens. The shape of the residue droplet is complex and the distribution is non-uniform.

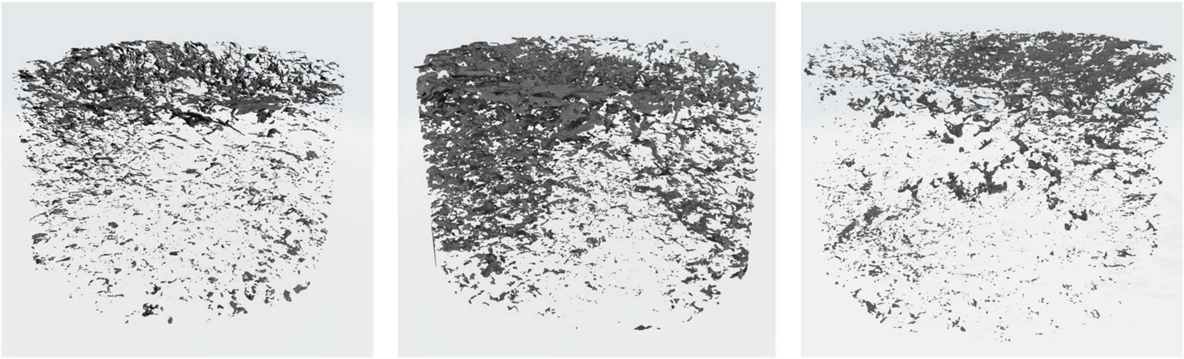

(a) (b) (c)

Figure 4.10 The back-calculated 3D models of ST emulsion residues of the three ST conditions: (a) ST 0.4-60%; (b) ST 0.6-60%; (c) ST 0.6-40%.

Coating area gradient

Apart from the changed pore-structure, it is also expected that the soft emulsion residue could coat and adhere to the surface of the aged mortar. More coating area indicates a higher possibility for the soft binder (or even some recycling agents if added) to diffuse into the aged mortar, which benefits the long-term performance of the damaged PA. Figure 4.11 presents the P_c values of the ST emulsion in different PA specimens at depths with an interval of 5mm. An obvious gradient characteristic could be observed for each ST condition. As Figure 4.11(b) shows, the PA specimen of ST 0.6-60% presents the best coating efficiency with P_c value in the range of 6.34% to 36.6%. However, for the ST 0.4-60% and ST 0.6-40% specimens, the P_c values are in the range of 2.50% to 30.41% and 2.71% to 21.53%, respectively. The lower P_c value range indicates an insufficient coating from the ST emulsion residue. It is worth noting that the P_c value could be well correlated with the mass loss ratio as shown in Table 4.2. Considering the clear physical meaning of P_c index, it shall be a promising micro-scale index to characterize the coating efficiency of ST emulsions in PA.

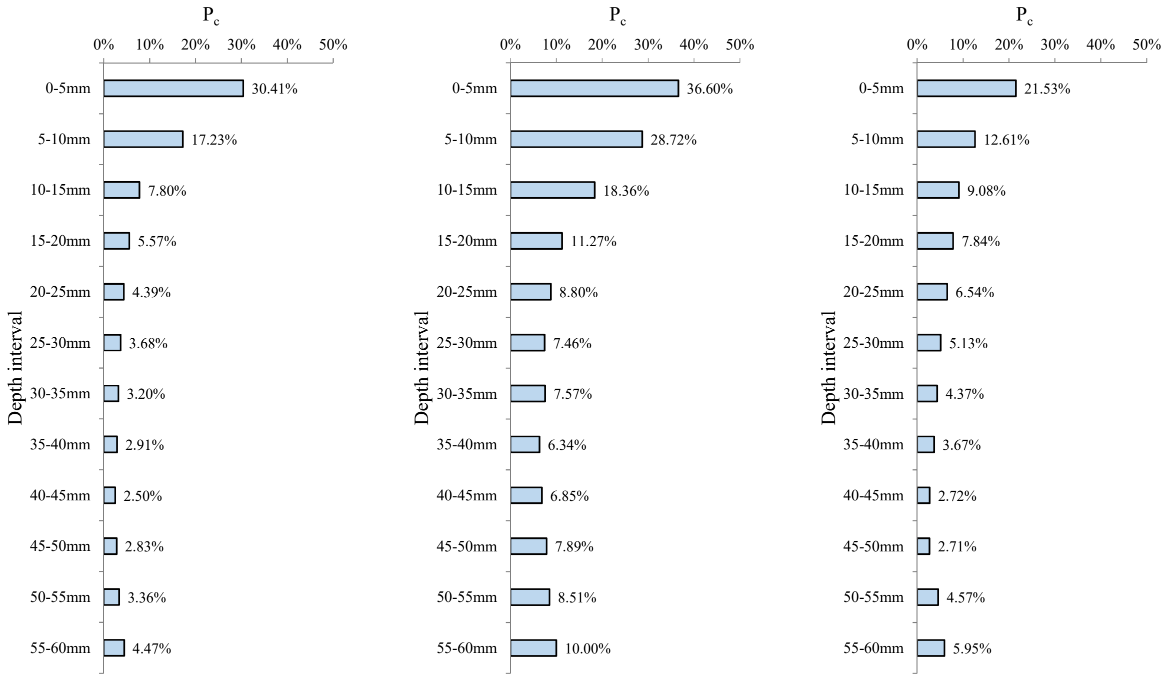

(a) (b) (c)

Figure 4.11 The P_c value of the ST emulsion at depths for each PA specimen: (a) ST 0.4-60%; (b) ST 0.6-60%; (c) ST 0.6-40%.

Binder film thickness distribution

From the 3D visualization, the spatial distribution of the ST emulsion is complex and non-uniform. So, the binder film thickness distribution of the ST emulsion residue was also evaluated. Figure 4.12 shows the frequency histograms of the binder film thickness distribution of the three ST emulsion residues. At each interval (0.1 mm), the frequency is in terms of a percentage of the number of certain coating film thickness to the total number of calculated coating film thickness. The curves present a double-peak pattern with a higher peak at around 0.3 mm and another peak at around 0.7 mm. However, it is noticed that the film thickness distribution of the ST emulsion residue varies from each other.

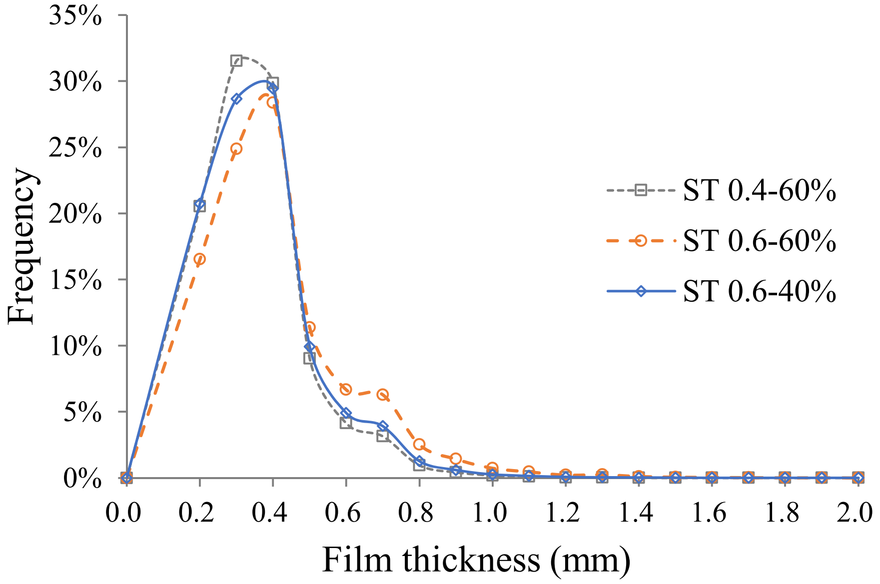

Figure 4.12 Binder film distribution curve of the ST emulsion residues

Two statistical indexes, namely the mean value (T_c) and standard deviation (SD_c), of the emulsion residue film thickness were also calculated as presented in Table 4.5. A smaller T_c means a thinner coating layer for the aged mortar. A larger SD_c indicates a wider distribution of the thickness value and less uniformity. Noteworthy, the specimen of ST 0.6-60% exhibits the largest T_c and SD_c value, indicating a thicker coating thickness but less uniformity. A thicker coating layer would reduce the aging rate of the mortar film, which is beneficial to the durability of the mixture [159]. Furthermore, to achieve a better coating efficiency, it is expected that the ST emulsion residue could distribute as uniformly as possible, so a smaller SD_c is also preferred.

Table 4.5 Indexes of the binder film thickness distribution of the ST emulsion residue

Specimen ID	T_c (mm)	SD_c (mm)
ST 0.4-60%	0.32	0.13
ST 0.6-60%	0.37	0.18
ST 0.6-40%	0.31	0.14

4.3 Summary

In this chapter, the 3D models of air voids and ST emulsion residues were reconstructed from the X-ray CT images of the PA specimens before and after ST. The changed pore-microstructure in PA induced by the sprayed ST emulsion was then characterized based on the morphology analysis. The complicated and non-uniform spatial distribution of the ST emulsion residue was quantified by calculating the coating surface area and coating film thickness. Moreover, statistical micro-scale indexes: P_c, T_c, and SD_c, were defined to indicate the emulsion residue coating efficiency, mortar thickening, and spatial homogeneity, respectively. The following points summarize the main findings and conclusions of this chapter:

(1) The penetration of the ST emulsion presents gradient characteristics, and the penetration depths of different ST emulsions vary. According to the air void reduction and P_c values, the asphalt emulsion under the ST condition of 0.6-60% had the deepest penetration depth of around 20 mm, while the emulsion penetration depths were only approximately 10 mm for the other two conditions.

(2) The ST application alters the size, number, and area distribution of the air voids in PA. Both N_a and D_e reduced at the bottom of each PA specimen after ST, N_a increased while D_e decreased at the top of the specimens. Based on image analysis, the ST emulsion droplets can fill the micro-pores and separate the large air voids into multiple smaller ones.

(3) The ST emulsion can considerably lower the interconnected factor (F_i) across the top surface of the PA specimen and the tortuosity (T) at both ends of the specimen. The smaller F_i value should be primarily responsible for the decreased permeability of the PA specimen caused by the ST emulsion.

(4) The P_c value has a strong relationship with the mass loss ratio of the treated PA specimen. A larger P_c value implies improved coating effectiveness on the aged mortar surface and, potentially, improved recovery efficiency for the damaged PA.

(5) Among the three ST conditions, the PA specimen conditioned by the ST emulsion with an application rate of 0.6 kg/m^2 and a solid content of 60% exhibited the greatest P_c and T_c values, as well as the best performance recovery.

(6) Apart from the P_c value, a more uniform (smaller SD_c value) coating film thickness is also expected for the ST emulsion to achieve a better penetration status in PA.

CHAPTER 5 DIFFUSION CHARACTERISTICS OF ST EMULSION IN AGED ASPHALT MORTAR OF PA MIXTURE THROUGH SEM/EDS ANALYSIS

When the ST emulsion penetrated into the damaged PA mixture along the air voids, its residue coated on the aged mortar area, potentially diffusing into and fusing with the aged binders over time. However, previous studies on the diffusion of virgin binder/rejuvenator in aged binder were mainly focused on RAP mixture at a higher temperature within a few hours. Very few studies have been conducted on the potential diffusion phenomenon at room temperature with a long duration, which is important to understand the interaction mechanism between ST emulsion residue and aged asphalt mortar of PA from a microscopic perspective. Little is known about whether the applied ST emulsion residue diffuses into aged asphalt mortar of PA, and there is no quantitative indicator available to characterize the diffusion behavior. To fill these knowledge gaps, this chapter aims to: 1) develop a specimen preparation method for observing the diffusion phenomenon by SEM/EDS; 2) investigate the diffusion of ST emulsion in aged asphalt mortar of PA under different curing conditions (e.g., temperatures and curing durations); and 3) propose a quantitative index to characterize the diffusion degree. The findings are expected to provide guidance for applying ST to PA for preventive maintenance and promote its application.

5.1 Experiments and Methods

5.1.1 Materials preparations and pre-test of specimens

The raw materials used in this chapter are the same as those introduced in Section 3.1. Nano TiO_2 powder was selected as a tracer to tag the ST emulsion, and its basic physical properties are shown in Table 5.1. Following recommendations from previous studies [131, 132], the tracer content was set as 10% by mass of the virgin binder. TiO_2 was first mixed with virgin binder using a high-speed shear mixer, and then the TiO_2 modified asphalt binder was emulsified by the soap to produce ST emulsion for spraying. To ensure precise control over the application dosage of the ST emulsion, each specimen was placed on a balance throughout the spraying period. The emulsion was sprayed to the specimen's surface using a spraying gun, a device commonly applied in the coating field [160-162], which simulates on-site spraying conditions on asphalt pavement. Compressed air was used to atomize ST emulsion and direct its particles, allowing for uniform coverage on the specimen's surface. The application rate of 0.6 kg/m^2 for ST emulsion was used based on the findings of Chapter 3.

Table 5.1 Physical properties of TiO_2

Color	Appearance	Purity (wt%)	Specific surface area (m^2/g)	Granularity (nm)
White	Powder	99.90	78	500

Besides, the PA specimens were fabricated in accordance with the same preparation method as described in Section 3.1.1. All PA specimens were subjected to long-term aging [163] and freeze-thaw conditioning (ASTM D7064) to artificially induce internal micro-cracks. Then, ST emulsions were sprayed onto those damaged PA specimens, which were subsequently cured for different durations at 25 °C or 60 °C. The mass loss ratio of the treated PA specimen was determined through the Cantabro Abrasion test according to the ASTM C131 to evaluate the effects of curing conditions (duration and temperature) on the recovery efficiency of ST emulsion. The mass loss ratio was calculated by Equation (3-1). Three replicates were prepared for each condition.

Figure 5.1 shows the variations in mass loss ratio as a function of curing time at different curing temperatures. At the very beginning (without curing), the mass loss ratio was about 32%. With the increase of curing of ST emulsion, the mass loss ratios of PA specimens rapidly decreased and gradually flattened out. Specifically, a higher curing temperature appeared to accelerate the demulsification and water evaporation of ST emulsions, so the specimens cured at 60 °C showed a lower value of mass loss ratio than those at 25 °C at the early stage. After 14 days of curing, it could be speculated that all water in PA mixture has evaporated. Specimens cured at two different temperatures should have exhibited a similar recovery efficiency of ravelling resistance. But the mass loss ratio still indicated a relatively lower value at 60 °C than that at 25 °C, which is about 1%. It can be attributed to a more efficient diffusion of ST residue in aged asphalt mortar at the higher curing temperature, which benefits the rejuvenation of aged asphalt binder in PA. It should be noted that the diffusion phenomenon likely happens once the ST residue covers aged asphalt mortar or fills micro-cracks within the PA mixture. Next, the SEM/EDS was adopted to investigate the potential diffusion of new ST emulsion residue in aged asphalt mortar from the microscopic perspective.

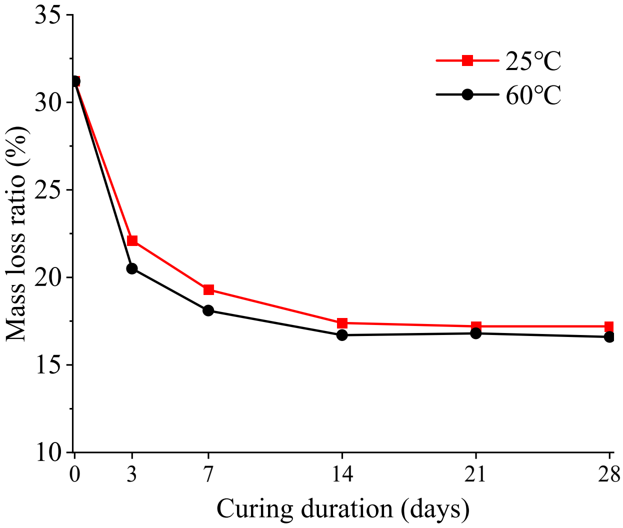

Figure 5.1 Temporal variations of mass loss ratios at 25 °C and 60 °C

5.1.2 SEM/EDS specimen preparation

A procedure with multiple steps was followed to prepare the specimens for the SEM/EDS test. The damaged PA specimens with a diameter of 150 mm and a height of 40 mm were first prepared by the Superpave gyratory compactor (SGC). Small PA specimens with a diameter of 30 mm were then drilled out from the SGC specimens (Figure 5.2(a)). After that, these small specimens were sawed into several slices with a thickness of 5 mm (Figure 5.2(b)). ST emulsion containing TiO_2 was sprayed on the surface of the thin slices, which penetrated into PA through the interconnecting pores (Figure 5.2(c)). After ST, the thin slices were dried in a vacuum drying oven for 24 hours of curing to accelerate the demulsification of emulsified asphalt and evaporation of water. Then, the specimens were immersed in epoxy resin under a vacuum of 90 kPa for 10 min. This process not only helps get a clear boundary between the epoxy and mortar film for the convenience of quickly locating the added ST emulsion, but also improves the strength of the whole mixture to avoid the dislodgement of aggregate particles and the slippage of mortar during specimen grinding and polishing. Subsequently, the specimens were ground and polished until the smooth surface was exposed (Figure 5.2(d)). The reason is that a sloping and rough surface may prevent the electronic signal from bombarding the specimen to form shadow areas or hinder the detector from collecting the excited electronic signal. Finally, the surface of each specimen was sputter-coated by Au to make it conductive for microscopic observation (Figure 5.2(e)). It’s also recommended to draw some silver paint lines from the specimen surface to the carbon tape at the bottom of the specimen to improve the specimen’s conductivity. Besides, pre-marking of the air void peripheries on the specimen surface can help locate the target test areas quickly.

The specimen preparation procedures shown in Figure 5.2 not only preserve the original morphology of the PA specimen as much as possible but also allow direct in-situ observation of the diffusion of ST emulsion residue in aged asphalt mortar of PA.

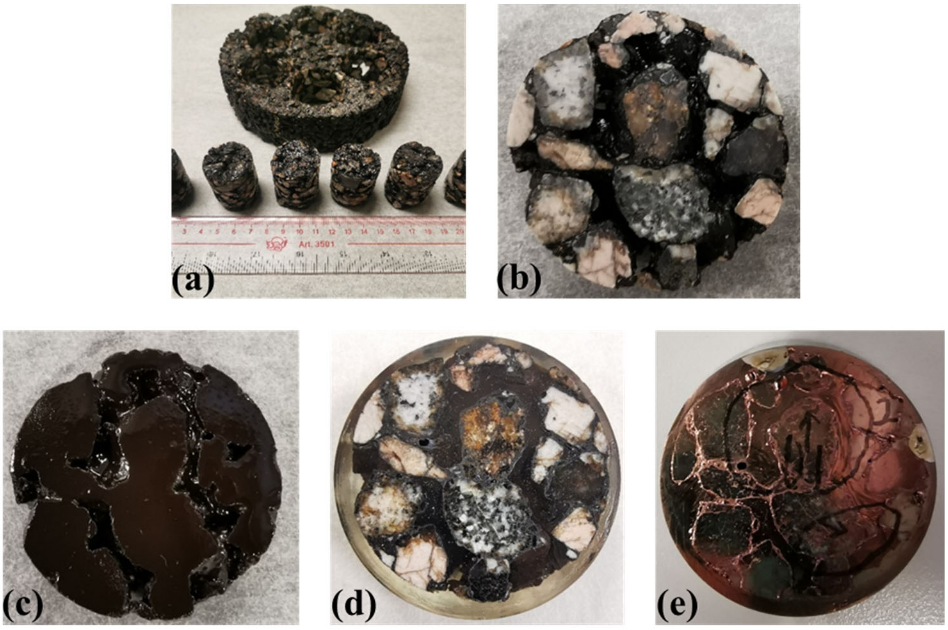

Figure 5.2 Procedures for specimen preparation: (a) Drilling cores; (b) A slice of PA; (c) Spraying ST emulsion; (d) Grinding and polishing; (e) Sputter coated by Au.

5.1.3 Identification and analysis of characteristic elements

A TESCAN VEGA3 scanning electronic microscope (SEM) equipped with an Oxford energy-dispersive X-ray spectroscope (EDS) was used to investigate the diffusion of ST emulsion in aged asphalt mortar (Figure 5.3(a)). The accelerating voltage was 20 KV and the backscattered electron (BSE) imaging was performed on the PA specimen after ST.

Four specimens were prepared according to the aforementioned method (Figure 5.3(b)). Two curing temperatures (25 ºC and 60 ºC) and five curing durations (0d, 7d, 14d, 21d, and 28d) were considered. Two replicates were prepared at each temperature for periodic observation and three different locations were selected for each specimen to conduct the EDS tests.

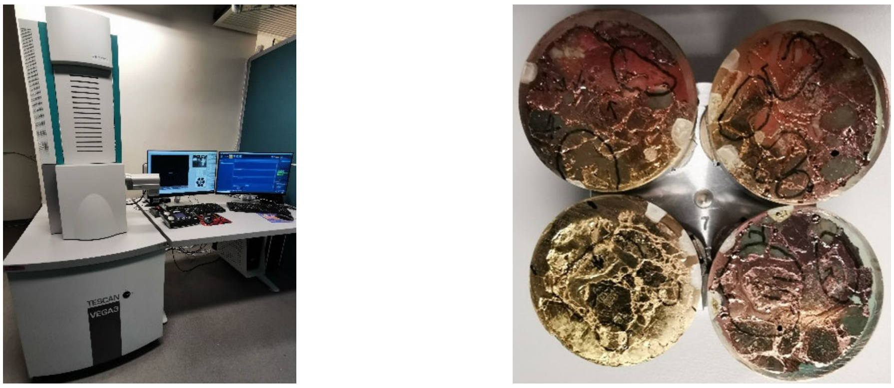

(a) (b)

Figure 5.3 SEM/EDS testing: (a) SEM equipment; (b) Final prepared specimens.

Selection of test areas and consistency verification

The morphology of a test area on a specimen's surface is shown in Figure 5.4(a). Fine aggregates, mortar, and epoxy resins can be clearly distinguished in each SEM image based on their colors and relative positions. Meanwhile, the location of the mortar film can be inferred according to the relative position of the other components of specimens, which is critical for the EDS line scanning test later. Because each component of PA mixtures has a unique characteristic element, chemical analysis of a test area by EDS allows the identification of mechanically similar but chemically distinct phases. The silicon (Si), titanium (Ti), and sulfur (S) are the characteristic elements of the aggregates, added ST emulsion, and aged asphalt binder, respectively. Epoxy resin is an organic material consisting of carbon, hydrogen, and oxygen, which are also the main elements in asphalt binder. Therefore, no particular element can be selected to represent the epoxy resin. Figure 5.4(b) shows the EDS map scanning results. The main distribution areas of the aggregates, new and aged asphalt binder are illustrated by green, red, and blue colors, respectively. A red contour line was observed along the boundary between epoxy resin and PA, suggesting that the applied ST emulsion was distributed around the contact zone between epoxy and mortar.

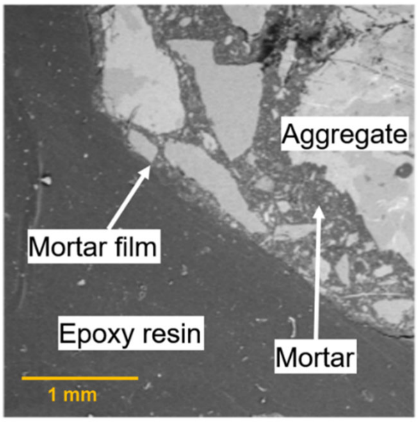

(a)

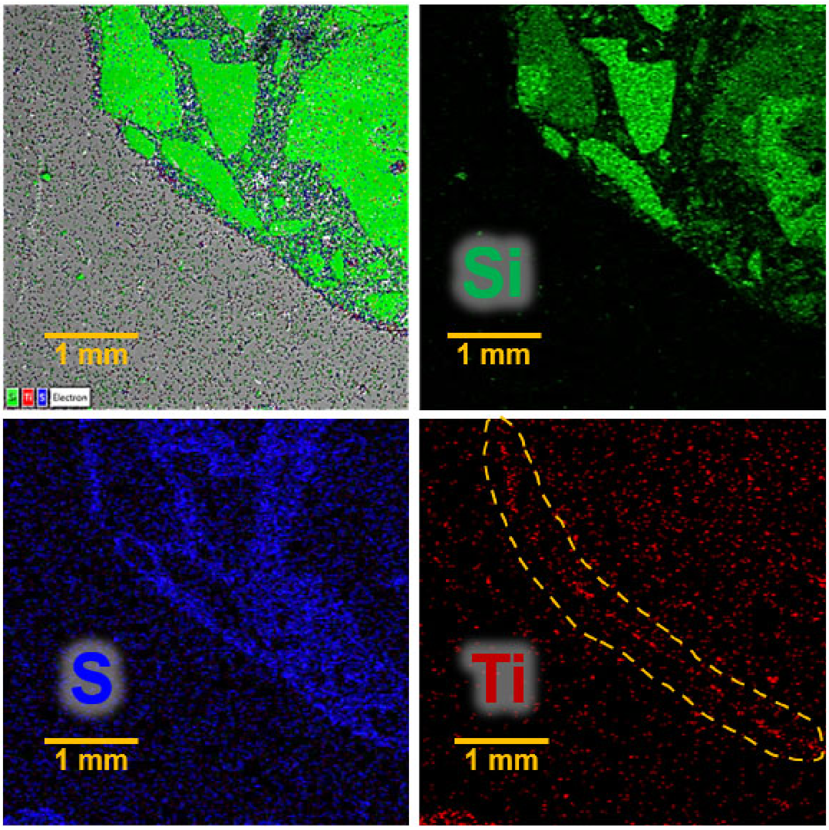

(b)

Figure 5.4 Consistency verification of characteristic elements: (a) SEM image; (b) EDS map scanning images.

Boundary identification of different components in PA specimen

Based on the EDS map scanning results, the EDS line scanning test was conducted around the areas of the applied ST emulsion to further identify different components. As shown in Figure 5.5, an EDS line scanning was performed from epoxy resin to aggregate to collect S/Ti/Si intensity data along the interesting line. The length of the line was controlled to be long enough to span the applied ST emulsion and old mortar film areas.

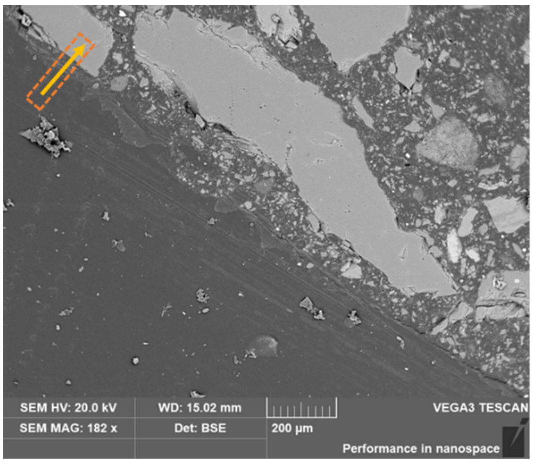

Figure 5.5 Example of an EDS line scanning test.

Figure 5.6(a) shows the enlarged image of the test area. The EDS line was controlled to be as perpendicular as possible to the aggregate for the convenience of internal comparisons. Figure 5.6(b) illustrates the scanning results along the EDS line. The Y-axis unit, namely counts per second (cps), represents the intensity of each element, which is only related to the element content. The element intensities of Ti and S began with low value and rapidly grew as the line scanned from the epoxy resin to the ST emulsion residue. However, when the line scanned from the ST emulsion residue to the aged asphalt mortar, the intensity of Ti suddenly reduced to a similarly low level, but that of S remained at a peak level as before. Subsequently, when the line scanned from the aged asphalt mortar to aggregate, especially at the interfacial transition zone (ITZ), the intensity of Si dramatically increased to a very high level while that of S rapidly decreased to a low level. Therefore, three boundaries between epoxy resin, ST emulsion residue, aged asphalt mortar, and aggregate can be clearly distinguished and identified at the ITZs based on the line scanning results of the three characteristic elements. It indicated that different components of PA specimens could be identified and demarcated by the EDS line scanning test, which makes it possible to continuously observe the potential diffusion of the ST emulsion residue in the aged asphalt mortar of PA.

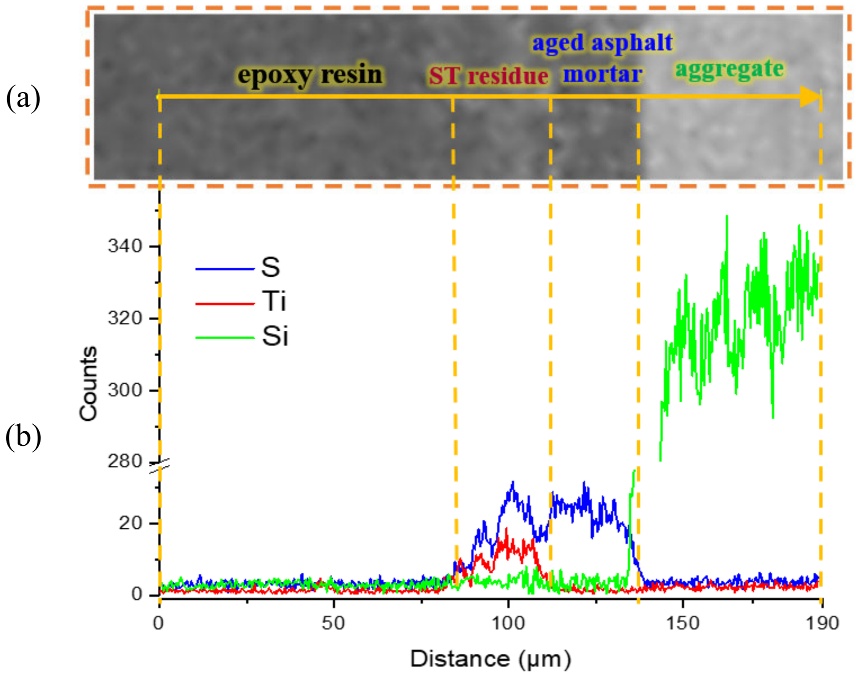

Figure 5.6 EDS line scanning results: (a) Test area; (b) Intensity distribution of elements.

Diffusion degree of ST emulsion residue in aged asphalt mortar

Since the mass of the applied ST emulsion is fixed, the mass of the added tracer TiO_2 is also a constant. In the asphalt binder area containing tracers, the tracer content is expected to alter as the curing condition changes, representing the diffusion phenomenon. A new statistical indicator, namely the diffusion degree (D_d), was proposed and calculated using Equation (5-1) to quantify the diffusion of ST emulsion residue in aged asphalt mortar. It is defined as the average ratio of Ti count number to S count number at each point in the asphalt binder area containing tracers. The line scanning test was repeated three times for each test area. At least 80 points per line were included in the calculation of D_d. It should be noted that the sulfur content of the asphalt binder used in ST emulsion is similar to the sulfur content of the asphalt binder used in the mixture based on the EDS line scanning test results.

$$D_d = \frac{1}{n}\sum_{i=1}^{n}\frac{C_{Ti}^{i}}{C_S^{i}} \tag{5-1}$$

where n is the number of points in the asphalt binder area containing TiO_2; C_{Ti}^{i} represents the count number of the Ti at the point of number i; and C_S^{i} is the count number of the S at the point of number *i*. A lower D_d indicates that more ST emulsion residues diffuse into the aged asphalt mortars.

5.2 Results and Discussions

5.2.1 Diffusion phenomenon at different curing conditions

When applying ST emulsion to PA pavement, the pavement surface temperature may affect the ravelling resistance recovery of PA pavement. The climate of Hong Kong is subtropical, with mild winter and hot summer. In this study, the curing temperatures of 25 ºC and 60 ºC were selected to represent room temperature and higher temperature for the road surface, respectively [139]. It should be noted that although the actual pavement surface cannot maintain a higher temperature, e.g. 60 ºC, all day long, it is meaningful to investigate the effect of curing temperature on the diffusion efficiency of ST emulsion in aged mortar, which can help guide the selection of maintenance environment. Besides, considering that the diffusion phenomenon in asphalt mixture might be a very slow process at aforementioned temperatures, the EDS line scanning test is repeated every 7 days until no visible signs of diffusion occur.

Figure 5.7 depicts two SEM images labeled with the yellow line scanning areas and the variations of two characteristic elements along the test path at two different curing temperatures. The asphalt binder area contains element S and the ST emulsion residue region contains element Ti. Based on the intensity variation of Ti along the scanning distance, the asphalt binder area containing the TiO_2 tracer was illustrated between two vertical dark dash lines in each figure. Figure 5.7(a) shows that when the curing temperature is 25 ºC, neither the intensity of Ti nor the length of the asphalt binder area containing tracers changed significantly over the whole continuous observation, indicating that there is no apparent diffusion of new ST emulsion residue in aged asphalt mortar. However, Figure 5.7(b) illustrates that when the curing temperature is 60 ºC, the shapes of red and blue patterns were constantly changing, especially the length of the red region representing element Ti gradually increased. Their boundaries also became blurred at 60 °C as the curing duration increased. In other words, the length of the asphalt binder area containing TiO_2 gradually extended toward the aged asphalt mortar region as the curing duration increased, suggesting that the ST emulsion residue gradually diffused into and fused with the aged asphalt binder. Such disparities between two different curing temperatures indicate that the curing temperature significantly affects the diffusion of ST emulsion residue in aged asphalt mortar. A higher curing temperature can promote diffusion efficiency and further rejuvenate the aged asphalt binder, which is helpful in improving the ravelling resistance of PA pavement. This also explains the relatively lower mass loss ratio of the treated PA specimen at 60 °C as presented in Figure 5.1. Therefore, it is recommended to spray ST emulsion on PA pavement in hot weather (e.g. summer) to achieve better maintenance efficiency. Due to the low reflectivity of road surface and the moderate heat conductivity of asphalt, the region near the pavement surface area usually has a relatively higher temperature than the air temperature [164]. The average temperature of pavement surface area in summer is higher than in other seasons, which is helpful to promote the diffusion efficiency of those penetrated ST emulsion residues near the top of road surface.

Furthermore, as shown in Figure 5.7(b), because the mass of added tracer is a certain value, the distribution of element Ti disperses with the diffusion of ST emulsion residue in aged asphalt mortar, resulting in a decrease in the intensity of Ti. Thus, the red color representing the Ti gradually fades from crimson to light red with the increase of the curing duration. These variations once again confirmed the existence of the diffusion of new ST residue in aged asphalt binder.

Besides, it was also found that the diffusion phenomenon is difficult to observe after curing for 21 days. One possible explanation is that due to the physisorption, chemisorption, and mechanical interlock, the adhesion between asphalt and aggregate is stronger as it gets closer to the aggregate surface area [165]. Thus, the diffusion phenomenon can hardly be observed on the side close to the aggregate surface.

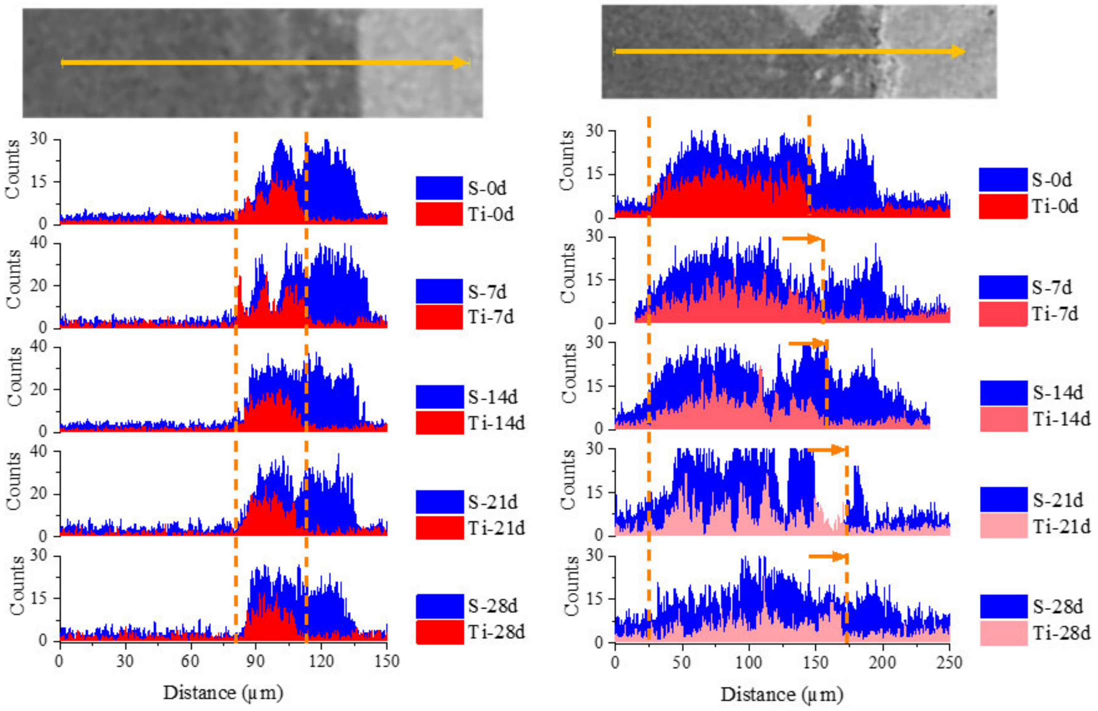

(a) (b)

Figure 5.7 Effect of curing temperatures on diffusion: (a) 25 °C; (b) 60 °C.

5.2.2 Diffusion degree of ST emulsion residue in aged asphalt mortar

As shown in Figure 5.8, the diffusion behaviors within the treated PA were further statistically analyzed by the D_d values under different curing conditions. The D_d values at 25 °C and 60 °C were similar at the beginning, which are around 0.54. However, they exhibited different changing trends at two curing temperatures as the curing duration increased. When the curing temperature is 25 °C, although no obvious diffusion behavior is shown in Figure 5.7(a) from a qualitative perspective, D_d presented a slightly decreasing trend from 0.54 to 0.49 throughout the curing duration. Meanwhile, when the curing temperature is 60 °C, D_d gradually decreased with the extension of diffusion area and then flattened out around 0.28 after 21 days of curing. The reductions in D_d over the entire test period at 25 °C and 60 °C are 0.05 and 0.25, respectively. Thus, the diffusion rate at 60 °C is around 5 times faster than that at 25 °C, which again proves that a higher curing temperature can accelerate the diffusion of ST emulsion residue in aged asphalt mortar.

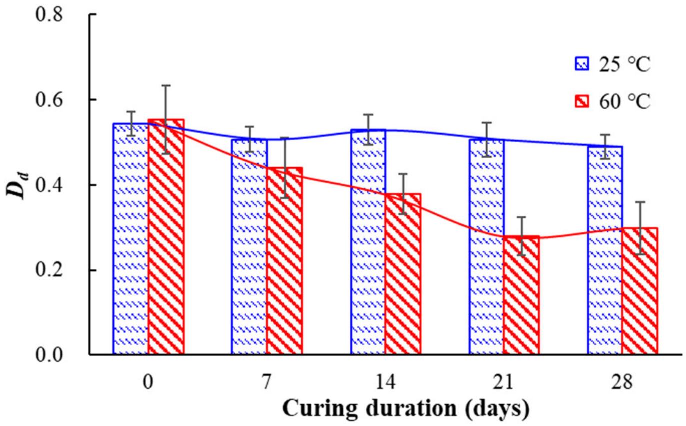

Figure 5.8 D_d under different curing conditions

5.2.3 Hindrance effect of fine aggregate on diffusion behavior

Asphalt mortar consists of fine aggregates, fillers, and asphalt binders, which adheres to the coarse aggregate surface and interconnects with other aggregates. The actual diffusion condition of the applied ST residue in aged asphalt mortar is not as simple as that in pure aged asphalt binder. As shown in Figure 5.9(a), the intensity of S decreased sharply, while the intensity of Si increased dramatically near the regions containing fine aggregates. Due to the hindrance effect of fine aggregates, the diffusion of the ST emulsion residue in aged asphalt mortar could be obstructed even at the high curing temperature of 60 ºC. In other words, the existence of fine aggregates in aged asphalt mortar may increase the diffusion path of new ST residue in aged asphalt mortar. Therefore, no obvious diffusion phenomenon was observed in Figure 5.9(b). Besides, the variations of D_d with and without fine aggregates in the diffusion path at 60 ºC are illustrated in Figure 5.10. The D_d remained relatively stable over the whole observation period when fine aggregates existed in the test area, indicating that the existence of fine aggregates in the diffusion path could significantly decrease the diffusion efficiency. Thus, the diffusion behavior in mortar is more complex than that in asphalt binder, which needs further study.

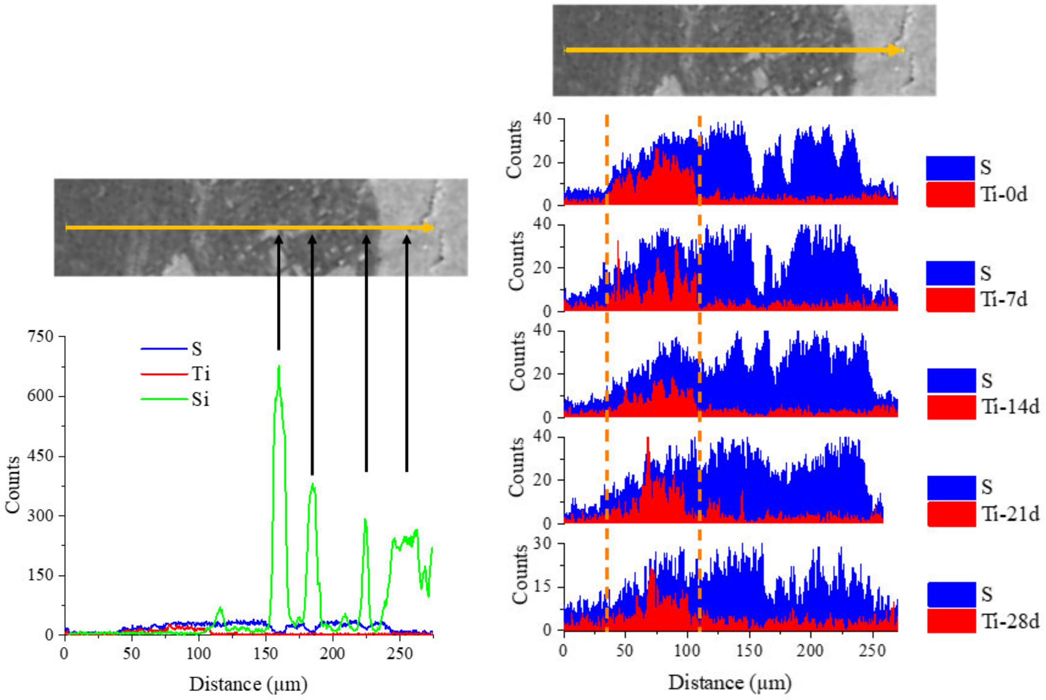

(a) (b)

Figure 5.9 Hindrance effect of fine aggregates on diffusion: (a) Intensity distribution of element; (b) EDS line scanning test results at 60 °C.

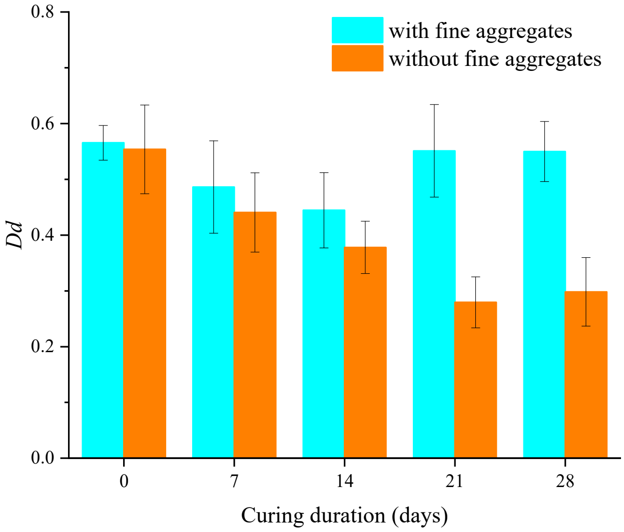

Figure 5.10 Variations of D_d with and without fine aggregates

5.3 Summary

In this chapter, a multi-step procedure was developed to prepare the treated PA specimens for the SEM/EDS test. The diffusion behavior was traced by the characteristic elements of different components in PA. The complex diffusion phenomena of the applied ST emulsion residues in aged asphalt mortars were investigated under different curing conditions. Moreover, a statistical indicator, D_d, was proposed to quantify the diffusion degree. The main findings and conclusions of this chapter are summarized below:

(1) The boundaries between the applied ST emulsion residues and other components of PA can be clearly distinguished through the SEM/EDS, which is an effective microscopic technique to directly observe the diffusion phenomenon within the PA mixture by careful specimen preparation.

(2) Curing temperature has a significant effect on the diffusion phenomenon and a higher curing temperature can accelerate this process based on the indoor test results. Considering that the average temperature near the pavement surface area in summer is higher than in other seasons, it is recommended to spray ST emulsions on PA pavement in hot weather (e.g. summer) to enhance the efficiency of this preventive maintenance technology in the field.

(3) The diffusion phenomenon was obvious after curing for 21 days at 60 °C, while it was not apparent after 28 days at 25 °C.

(4) D_d can quantify the diffusion degree of the ST emulsion residue in aged asphalt mortar. A lower D_d value indicates a better diffusion status. The diffusion rate at 60 °C was about 5 times faster than that at 25 °C for the case investigated in this study.

(5) The diffusion phenomenon of ST emulsion residue in aged asphalt mortar is complex. The existence of fine aggregates in mortar may increase the diffusion path due to the hindrance effect.

CHAPTER 6 OPTIMIZATION DESIGN OF ASPHALT EMULSION WITH REJUVENATOR TOWARDS A UNIFORM DISTRIBUTION IN DAMAGED PA MIXTURE FOR A BETTER RAVELLING RESISTANCE

Based on the main findings obtained from chapter 3 to chapter 5, it was found that spraying ST emulsion to PA road could effectively alleviate the ravelling distress. However, as a relatively new preventive maintenance material for PA pavements, several properties still need to be carefully clarified and optimized before widely promoting this technology.

First, some voids of PA mixtures might be blocked by ST emulsion residue, leading to water penetration deterioration and noise absorption property attenuation [166, 167]. Therefore, material optimization towards a low viscosity and a reasonable construction technique (such as blasting at a high temperature or spraying with high air pressure) are expected to be developed to preserve the pore structures to a large extent. Besides, the distribution of ST emulsion residues inside voids varies from each other. Chapter 4 found that a high percentage of coating area and a uniform coating film thickness helped improve the ravelling resistance. When the usage of ST emulsion is fixed, good wettability means the standard deviation of coating film thickness is small, and more aged asphalt binder areas can be coated by ST emulsion residues [168]. Therefore, a good wettability of ST emulsion is important to reach its potential. Third, the main demulsified component of the ST emulsion is fresh asphalt binder. However, the diffusion phenomenon between new asphalt binders and aged asphalt binders is very slow at room temperature, potentially restricting the recovery efficiency of the mechanical performance of ST treated PA pavement. Several studies proposed incorporating recycling agents into ST emulsion to enhance diffusion efficiency and alleviate the ravelling distress [116, 117, 169]. However, their maintenance effects are quite different in different studies. The application of rejuvenators as a preventive maintenance material for PA pavements is still in the preliminary exploration stage, which needs systematic investigations on the appropriate rejuvenator-adding methods, the optimal rejuvenator dosage and the reasonable evaluation indicators.

To satisfy the three demands mentioned above for optimizing the ST emulsion, rejuvenators are considered as the promising modifiers. Because most rejuvenators generally have lower viscosities than asphalt binders at room temperature, which is expected to improve the penetration depth of ST emulsion in PA mixture. Besides, rejuvenators may promote the coating efficiency of newly added asphalt binders due to their better wettability than pure asphalt binders [170]. Furthermore, adding rejuvenators could enhance the diffusion efficiency between new and aged asphalt binders [171]. Therefore, this study aims to 1) investigate the feasible preparation process and appropriate production parameters of adding rejuvenators; 2) determine the optimal formula of ST emulsion containing rejuvenators; 3) verify the effectiveness of optimized ST emulsion on the ravelling resistance of PA specimen. Figure 6.1 shows the flow chart of this chapter. Section 6.1 introduced that two kinds of rejuvenators were selected for incorporation into the asphalt emulsion. According to the orthogonal design table, eighteen rejuvenator emulsions were prepared after considering different compositions of pH values, emulsified temperatures, and emulsifier dosages. Section 6.2 summarized the test methods used in this chapter to evaluate the storage ability of rejuvenator emulsion and workability of rejuvenator-optimized asphalt emulsion. Section 6.3 discusses the design and selection of rejuvenator emulsions, focusing on their storage stability and particle size distribution as key control indicators. The appropriate parameter values for rejuvenator emulsion production were determined. Then, modified ST emulsions with different rejuvenator contents were prepared by mixing the asphalt emulsion and rejuvenator emulsion. The contact angle test was conducted to evaluate the wettability of modified ST emulsions. Meanwhile, the shear viscosity test was performed to investigate the viscosities of different ST emulsions. The water boiling test was also carried out to explore the bonding strength between ST emulsion residue and aggregate. The optimized dosage of rejuvenator emulsion was obtained based on the workability of modified ST emulsion. Lastly, the cantabro abrasion test was conducted to investigate the ravelling resistance of damaged PA specimens and verify the effectiveness of the optimized emulsion.

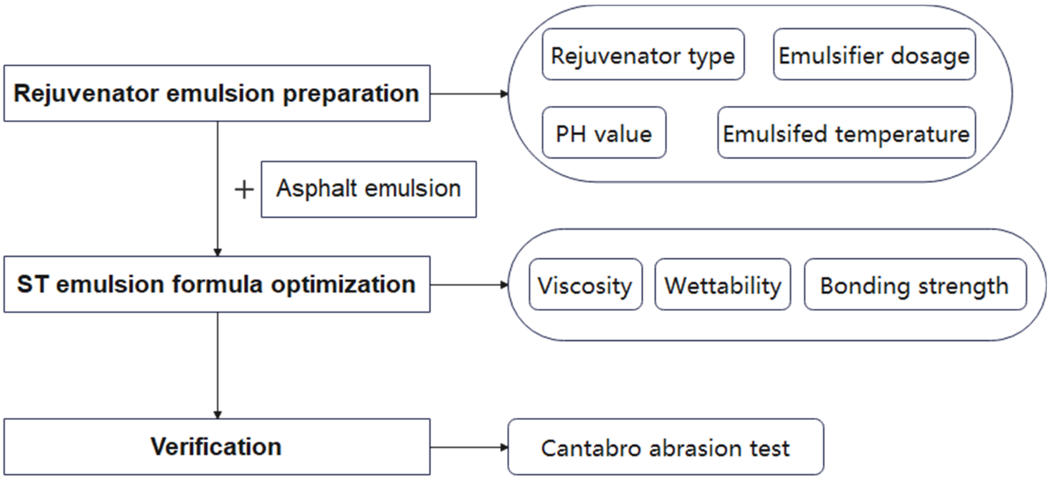

Figure 6.1 Flowchart of Chapter 6

6.1 Materials and Optimization Method

6.1.1 Emulsion preparation

Asphalt emulsion is the main component of the conventional ST emulsion. It usually consists of asphalt binder, distilled water, cationic emulsifier and stabilizer, where their mass percentages in this study are 60%, 36.8%, 3% and 0.2%, respectively. The main components of cationic emulsifier are lignin amine and its derivatives. Calcium chloride ($CaCl_2$) was used as the stabilizer to improve the storability of asphalt emulsion. The basic properties of asphalt emulsion are present in Table 6.1. Its preparation process has been introduced in Section 3.1. The rejuvenator emulsion preparation process is similar to that of asphalt emulsion except for several specific emulsifying parameters. The reasons why the rejuvenator needs to be emulsified and why it is recommended separately emulsification will be discussed as follows.

Figure 6.2 shows that there may be three ways to add a rejuvenator into asphalt emulsion. In method one, the asphalt emulsion is first prepared, and then a certain mass of rejuvenators is directly added to the asphalt emulsion to prepare the ST emulsion containing the rejuvenator. Although this method is easy to conduct, there is an obvious problem: the rejuvenator is generally an oil-based material, which is difficult to homogeneously disperse in the oil-in-water (O/W) system of asphalt emulsion without the emulsifier's help. Thus, the ST emulsion prepared according to method 1 tends to be unstable and gradually stratified. In method two, the asphalt binders and rejuvenators are emulsified separately by the colloid mill. The stable asphalt emulsion and rejuvenator emulsion are well prepared and then stored. One may artificially mix those two emulsions in the field at an appropriate mass ratio to prepare the final ST emulsion when the old PA pavements need maintenance. In method three, the rejuvenator and asphalt binder are first blended and then the mixtures are emulsified together to prepare the ST emulsion. Compared with method three, one advantage of method two is that the rejuvenator could be emulsified at an optimal condition, which might differ from the emulsifying parameters designed for the asphalt binder. The emulsified rejuvenator can stabilize and distribute uniformly in solvent, which will be discussed later in Section 3.1. Another advantage of method two is that the worker can precisely control the mix ratio of asphalt emulsion and rejuvenator emulsion to prepare various ST emulsions with different material compositions towards different functional needs. For example, suppose an old pavement surface has been used for many years and the asphalt binders were severely aged. In that case, the dosage of rejuvenator emulsion in ST emulsion should increase to ensure that aged asphalt binders are substantially rejuvenated. Therefore, method two, in which the rejuvenator was first emulsified and then mixed with asphalt emulsion, was adopted to prepare the ST emulsion.

Table 6.1 The basic properties of asphalt emulsion

	Evaporated residue				PSD		
	Residue content (%)	Penetration (25 °C, 0.1 mm)	Softening point (°C)	Ductility (5 °C, cm)	D_{50} (μm)	*Span*	D [4,3] (μm)

ST emulsion	60	64	50	67.2	1.55	1.26	1.82

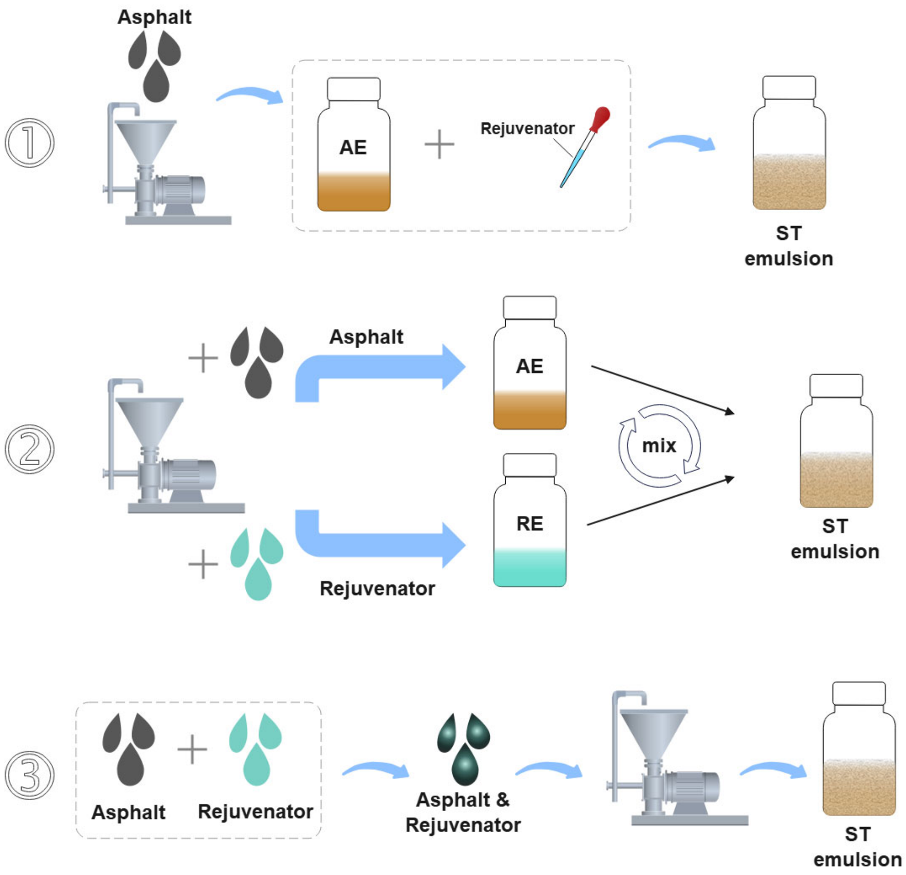

Figure 6.2 Three potential methods to prepare ST emulsion containing rejuvenator

Figure 6.3(a) shows that two kinds of rejuvenators were used in this section, which was selected from the five rejuvenators we used in the Chapter 3. One is a petrol-based rejuvenator named aromatic oil (AO), which is also the main light component in asphalt binders. The other one is a bio-based rejuvenator named tall oil (TO2), which is produced from a purified pine feed stock and is expected to soften aged asphalt binder. Their basic properties of AO and TO rejuvenators are also introduced in Table 3.3 denoted as the AO and TO2, respectively. Rejuvenators usually have significantly lower viscosities than asphalt binders at room temperature, making it easier to emulsify without such high temperatures. Besides, rejuvenators have different physical and chemical properties from asphalt binders. The optimal emulsifier dosage and the appropriate

PH value of emulsified soap should also be determined to prepare a stable and homogeneous rejuvenator emulsion. Figure 6.3(b) shows examples of AO and TO rejuvenator emulsions.

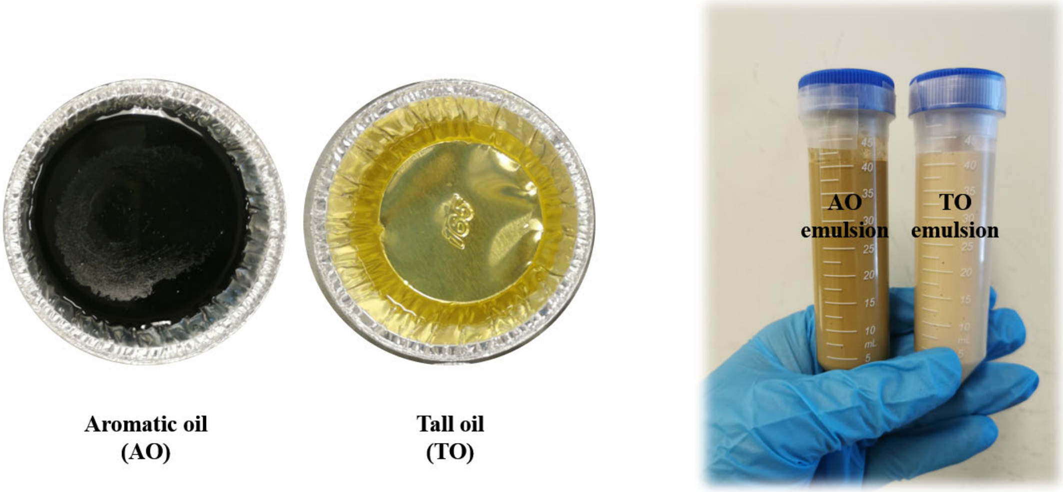

(a) (b)

Figure 6.3 Schematic graphs of (a) rejuvenators and (b) their emulsions used in this study.

6.1.2 Orthogonal experimental design

The orthogonal experimental design method is an efficient and fast experimental design method considering multivariate and multilevel factors. Several representative test points were selected based on the orthogonality. The features of those test points were uniformly distributed and neatly comparable, which is helpful in understanding the significance and interactions of different factors in a few experiments. Therefore, this statistical analysis method was used to optimize the preparation conditions of the rejuvenator emulsion.

A typical orthogonal array L9 was used to evaluate the emulsifying effects of various factors on rejuvenator emulsion. Table 6.2 shows a total of 9 experiments considering three factors (A/B/C) and three levels (1/2/3) for each factor. The meanings of test factors and values for each level are shown in Table 6.3. Factors of A, B, and C represent the PH value, emulsified temperature, and emulsifier dosage, respectively. The PH value is acidic and cationic rejuvenator emulsions were prepared in this study. The emulsifier dosage means the mass ratio of the emulsifier to the whole emulsion. The emulsified temperatures for those two rejuvenators are different as the viscosities of AO and TO vary from each other.

Table 6.2 L9 orthogonal array for preparing rejuvenator emulsion

No.	Control factors and their levels		
	A	B	C
1	1	1	1
2	1	2	3
3	1	3	2
4	2	1	3
5	2	2	2
6	2	3	1
7	3	1	2
8	3	2	1
9	3	3	3

Table 6.3 Meanings of test factors and their corresponding levels

Rejuvenator	Factors	Levels		
		1	2	3
AO	A. PH value	3	2	1
	B. Emulsified temperature, ºC	75	90	60
	C. emulsifier dosage, %	2	3	4
TO	A. PH value	3	2	1
	B. Emulsified temperature, ºC	40	60	20
	C. emulsifier dosage, %	2	3	4

6.2 Test Methods

6.2.1 Zeta potential test

One of the main concerns about rejuvenator emulsion's workability is storage stability. Owing to its convenience and high accuracy, Zeta potential is a useful indicator for describing the stability of an unknown colloidal dispersion. The electrical potential at the slipping plane describes the potential difference between the dispersion phase and the stationary layer of fluid attached to the dispersed particle. High Zeta potential means this interface could separate mobile fluid from slipping and keep attached to the surface. It is recognized that a solution sample is stable when the absolute value of Zeta potential is higher than 30 mV [86]. The Zetasizer with a type of Nano ZS90 manufactured by Malvern was used to conduct the Zeta potential test (Figure 6.4). All samples were diluted one thousand-fold with deionized water before testing. Three replicates were measured for each rejuvenator emulsion.

Figure 6.4 Zeta potential test

6.2.2 Particle size distribution (PSD) test

Appropriate particle size and a uniform PSD curve are crucial to the storage stability of rejuvenator emulsion. The Malvern Mastersizer 3000 was selected to measure the PSD of rejuvenator emulsion based on the laser diffraction technique. The PSD tests were performed in triplicate for each sample. D_{50} is calculated by Equation (6-1), which means the average particle size of the whole colloidal dispersion system. Span indicates the concentration of PSD range, which is calculated by Equation (6-2). The volume-weighted mean diameter of D [4,3] is calculated by Equation (6-3).

$$D_{50} = \sum_{i=1}^{n} d_i/n \tag{6-1}$$

$$Span = (D_{90} - D_{10})/D_{50} \tag{6-2}$$

$$D[4,3] = \sum_{i}^{n} n_i X_i^4 / \sum_{i}^{n} n_i X_i^3 \qquad (6\text{-}3)$$

Where d_i is the diameter of ith droplet, μm; D_{10} represents that droplet diameter such that 10 % of the total liquid volume is in drops of smaller diameter, μm; D_{50} is the volume median diameter, μm; D_{90} represents that droplet diameter such that 90 % of the total liquid volume is in drops of smaller diameter, μm; X_i is the center value of a size class, μm; n_i is the total particle number of each size class.

Figure 6.5 Particle size distribution test

6.2.3 Shear viscosity test

The viscosity of ST emulsion can affect its penetration depth in the PA pavement. The shear viscosity test was conducted by a dynamic shear rheometer (DSR, model MCR 302, Anton Paar) as shown in Figure 6.6(a). A concentric cylinder measuring system was used due to the liquid state of the rejuvenator emulsion. The test temperature is controlled at 23 ± 0.5 °C. The rotational spindle geometry is ribbed to alleviate the slippage phenomenon (Figure 6.6(c)). The inner diameter of the cylinder is 28.93 mm (Figure 6.6(b)), and the diameter of the outer contour of the spindle is 26.66 mm. Thus, the radial gap between the cylinder and spindle is 2.27 mm during the measurement. The protocol of the shear viscosity test is presented in Figure 6.6(d). Firstly, a 60 s pre-shear with a shear rate of 200 s^{-1} is conducted following by a 60 s rest to achieve a homogeneous emulsion. Then, the shear rate linearly increased from 0 s^{-1} to 200 s^{-1} within 2 minutes to obtain the shear viscosity curve of the rejuvenator emulsion. Two replicates were tested for each emulsion.

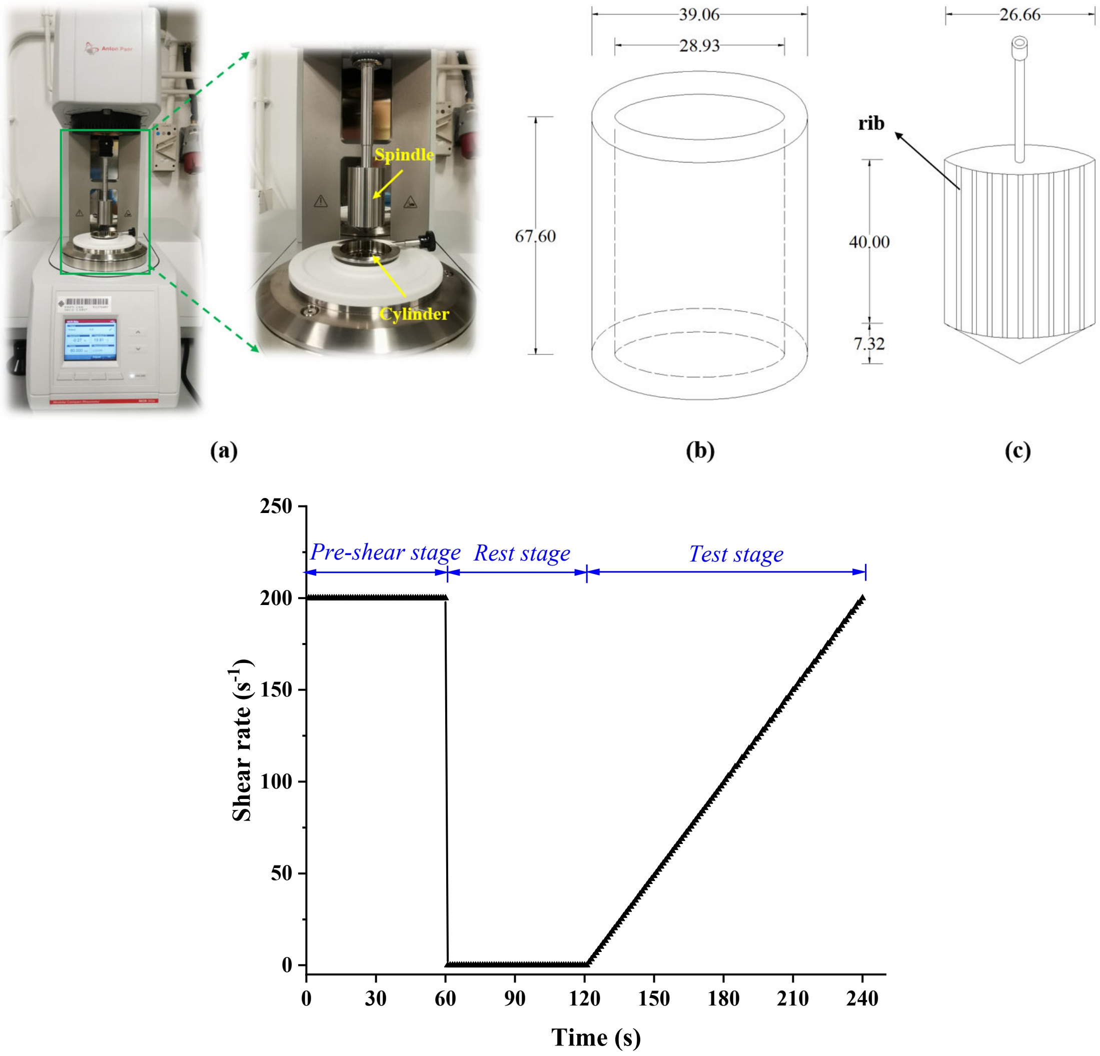

(a) (b) (c)

(d)

Figure 6.6 Shear viscosity test: (a) DSR device set-up; (b) the cylinder; (c) the ribbed rotational spindle (unit: mm); (d) the protocol of shear viscosity test.

6.2.4 Contact angle test

When the ST emulsion is sprayed to the aged PA pavement as a preventive maintenance material, most ST emulsions penetrate along the pore structure of PA pavement. Aged asphalt mastics, especially aged asphalt binders, are mainly distributed around the voids of PA mixtures. Consequently, penetrated ST emulsions will tightly contact aged asphalt binders and mastics. The wettability between ST emulsion and aged asphalt binder is of vital importance to the penetration depth of ST emulsion and distribution uniformity of ST emulsion residue thickness. Therefore, the contact angle of ST emulsion on aged asphalt binder is tested to compare the wettabilities of different ST emulsions. The long-term aged asphalt binders were first prepared according to the AASHTO R28. Then, some aged asphalt binders were dripped on the top surface of the hot glass slide. Afterward, the glass slide coated with asphalt binders was moved into the oven and cured at 150 ºC for self-leveling coating. A finished specimen is shown in Figure 6.7. During each contact angle test, a ST emulsion drop with 5.0 μL was dripped on the surface of aged asphalt binder. Three replicates were tested for each kind of ST emulsion. The test was conducted at room temperature with a humidity of around 70 % in the lab.

Figure 6.7 Glass slide coated with asphalt binder for contact angle test

6.2.5 Water boiling test

When adding rejuvenators into fresh asphalt binders to prepare the ST emulsion, although the rejuvenator is expected to replenish light components of aged asphalt binder so as to rejuvenate it, too many rejuvenators might weaken the bonding strength of ST emulsion residue. Therefore, the water boiling test was conducted to investigate the bonding strength of ST emulsion residue according to the Chinese standard of JTG E20-2011-T0654. Several granite coarse aggregates with a size larger than 19 mm were washed and dried at first (Figure 6.8(a)). The color of the prepared aggregate is greyish-white. Aggregates were dipped into distilled water for 1 minute and then moved to different ST emulsions for another 1 minute (Figure 6.8(b)). After the emulsion coated aggregates were cured for 24 hours at room temperature, those specimens were separately put into boiling water for 3 minutes. Finally, the boiled aggregates were dried and then photographed by a digital camera. Instead of conventional visual observation as described in a Chinese standard of JTG E20-2011-T0654, a grayscale-based image processing was performed by the Image Pro Plus software as shown in Figure 6.8(c). The coating ratio can be calculated by Equation (6-4). Four coarse aggregates were prepared for each kind of ST emulsion to evaluate its bond strength to aggregate.

$$Coating\ ratio = Residual\ area/(Aggregate\ area + Residual\ area) \times 100\% \quad (6\text{-}4)$$

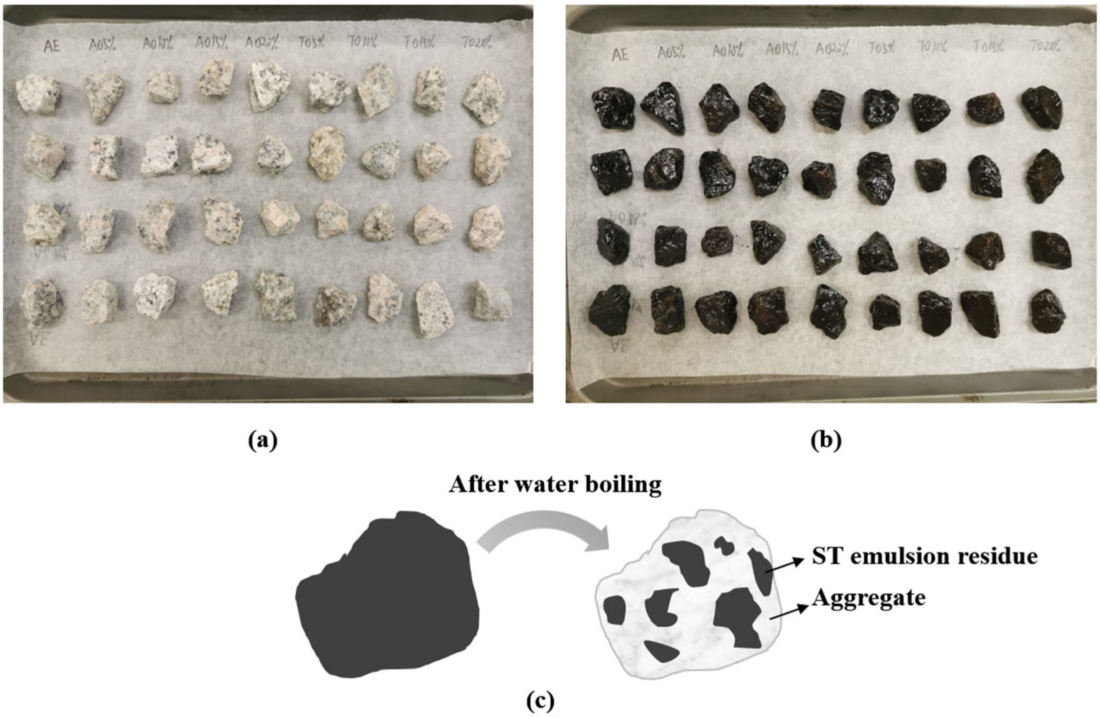

Figure 6.8 Water boiling test: (a) uncoated aggregates; (b) ST emulsion coated aggregates; (c) grayscale-based image processing.

6.2.6 Cantabro abrasion test

The ravelling resistance of the PA specimen treated with ST emulsion was evaluated by the cantabro abrasion test. PA mixtures were first subjected to long-term aging following by several freeze-thaw conditioning to prepare the damaged specimens. Subsequently, different

ST emulsions were applied to PA specimens with an application rate of 0.6 kg/m^2. Then, those emulsion treated PA specimens were cured at room temperature for 14 days and dry specimens were prepared for the cantabro abrasion test. More details about the sample preparation process can be found in Section 3.1. Four duplicate specimens were tested in each scenario. The mass loss ratios and lost masses were calculated.

6.3 Results and Discussions

6.3.1 Design and selection of rejuvenator emulsion

Particle size distribution

Particle size distribution of rejuvenator droplets in the aqueous phase is an important characteristic related to the storage stability of rejuvenator emulsion. Except for the fourth composition of AO emulsion, almost all kinds of AO emulsions have a similar D_{50} around 1.50 μm as shown in Table 6.4. It should be noted that the fourth kind of AO emulsion quickly coalesced, leading to the micro flocs, which is inapplicable for the PSD test. Besides, all TO emulsions have no significant differences of D_{50}, which is around 1.67 μm. Compared with the D_{50} of asphalt emulsion given in Table 6.1, both AO and TO emulsions have similar average particle sizes with the asphalt emulsion. Therefore, preparing a stable ST emulsion by mixing rejuvenator emulsion with asphalt emulsion is feasible based on their similar PSD conditions.

The indexes of Span and D [4,3] were also calculated, and their results are summarized in Table 6.4. It was found that the AO emulsions have higher *Span* values than TO emulsions, meaning that AO emulsion usually has a wider PSD range than TO emulsion. In other words, the particle size of TO emulsion distributes more uniformly than that of AO emulsion. Therefore, due to the relatively high proportions of coarse droplets in the AO emulsion, its D [4,3] values generally exhibited slightly bigger volume-weighted mean diameters than that of the TO emulsion.

Table 6.4 PSD of different AO and TO emulsions

No.	AO emulsion			TO emulsion		
	D_{50}, μm	*Span*	*D* [4,3], μm	D_{50}, μm	*Span*	*D* [4,3], μm
1	1.49	7.78	4.32	1.68	3.30	2.68
2	1.49	6.38	3.50	1.67	3.21	2.62
3	1.53	10.22	5.45	1.67	3.07	2.59
4	-	-	-	1.67	3.05	2.43
5	1.49	6.21	3.66	1.68	3.07	2.56
6	1.50	5.80	3.86	1.68	2.77	2.84
7	1.49	5.56	3.59	1.67	2.52	2.50
8	1.49	5.86	3.55	1.68	2.80	2.70
9	1.50	4.41	3.04	1.67	3.01	2.43

Storage stability

Good storage stability of emulsion facilitates production in large quantities and is ready for use in need. The zeta potential test results of different AO and TO emulsions are shown in the orthogonal experiment Table 6.5 and Table 6.6. k_i, (i=1,2 and 3) mean the average values at each factor level. *R* value represents the maximum variation range among k_i. The effect of each factor on the storage stability of the emulsion was evaluated by the k_i and *R*. A higher k_i value at one experimental level of a specific factor means better storage stability of the emulsion. A higher deviation of *R* for one factor means that its effect on the storage stability is more significant. Thus, k_i with the maximum values are considered the optimal conditions for preparing stable emulsions. The rankings of the effect of three factors on the zeta potential for AO emulsion and TO emulsion were B > A > C and A > C > B, respectively. That is to say, the critical factor affecting the stability of AO emulsion was the emulsifying temperature, while that for TO emulsion was the PH value of emulsified soap. The inconsistent critical factors for the two kinds of emulsions might be attributed to their differences in thermophysical properties. The optimal experimental condition for preparing the AO emulsion was $A_3B_2C_2$, in which the

PH value, emulsifying temperature and emulsifier dosage are 1, 90 °C and 3%, respectively. And the optimal experimental condition for preparing the TO emulsion was $A_3B_2C_3$, where the PH value, emulsifying temperature and emulsifier dosage are 1, 60 °C and 4%, respectively.

Table 6.5 Zeta potential results of different AO emulsions

No.	A (PH value)	B (Emulsifying temperature, °C)	C (Emulsifier dosage, %)	Zeta potential, mV
1	1 (3)	1 (75)	1 (2)	60.3
2	1 (3)	2 (90)	3 (4)	70.2
3	1 (3)	3 (60)	2 (3)	63.5
4	2 (2)	1 (75)	3 (4)	18.9
5	2 (2)	2 (90)	2 (3)	66.9
6	2 (2)	3 (60)	1 (2)	72.2
7	3 (1)	1 (75)	2 (3)	70.7
8	3 (1)	2 (90)	1 (2)	67.8
9	3 (1)	3 (60)	3 (4)	67.4
*k*1	64.7	50.0	66.8	
*k*2	52.7	68.3	67.1	
*k*3	68.7	67.7	52.2	
R	16.0	18.3	14.9	
Factor ranking		B > A > C		
Optimal scheme		A3B2C2		

Table 6.6 Zeta potential results of different TO emulsions

No.	A (PH value)	B (Emulsifying temperature, °C)	C (Emulsifier dosage, %)	Zeta potential, mV
1	1 (3)	1 (40)	1 (2)	43.2
2	1 (3)	2 (60)	3 (4)	52.6
3	1 (3)	3 (20)	2 (3)	49.9
4	2 (2)	1 (40)	3 (4)	56.8
5	2 (2)	2 (60)	2 (3)	55.9
6	2 (2)	3 (20)	1 (2)	39.3

7	3 (1)	1 (40)	2 (3)	61.4
8	3 (1)	2 (60)	1 (2)	60.0
9	3 (1)	3 (20)	3 (4)	58.7
k1	48.6	53.8	47.5	
k2	50.7	56.2	55.7	
k3	60.0	49.3	56.0	
Range	11.4	6.9	8.5	
Factor ranking		A > C > B		
Optimal scheme		A3B2C3		

Determination of optimal production conditions for rejuvenator emulsion

The orthogonal experiments were conducted to determine the optimal production parameters for the AO and TO emulsion. As discussed earlier, there are no significant differences in average particle size among AO, TO, and asphalt emulsions, which lays the foundation for their homogeneous mixing to prepare the ST emulsion as depicted in Figure 6.2. The optimal parameters of AO emulsion and TO emulsion were determined based on the orthogonal statistical analysis of zeta potential data, which will be verified in this section. Table 6.7 shows the zeta potential and PSD results of the asphalt emulsion and two optimized rejuvenator emulsions. It was found that both the optimized AO emulsion and TO emulsion have the highest Zeta potential values after orthogonal experiments, indicating that their storage stabilities are significantly improved. Meanwhile, two kinds of optimized rejuvenator emulsions have similar average particle sizes with asphalt emulsions, indicating that the emulsifying conditions are appropriate for the AO and TO rejuvenators. Therefore, a stable and homogeneous ST emulsion is expected to be acquired by directly mixing AO or TO emulsion with asphalt emulsion.

Table 6.7 Zeta potential and PSD results of optimized rejuvenator emulsions

Type	Zeta potential, mV	PSD		
		D_{50}, μm	*Span*	D [4,3], μm

AO emulsion	75.02	1.48	5.91	3.33
TO emulsion	62.00	1.63	2.11	2.29
Asphalt emulsion	64.12	1.55	1.26	1.82

6.3.2 ST emulsion formula optimization

Apparent viscosity

To ensure that as many ST residues as possible can alleviate the ravelling distress of PA pavement, the solid content of ST emulsion was fixed at 60% based on previous studies [168, 172]. Different ST emulsions were prepared by mixing AO or TO emulsions with asphalt emulsions. This study selected eight kinds of mixing proportions by mass of the whole ST emulsion, ranging from 0% to 50%. Figure 6.9 (a) and (c) show the apparent viscosity versus shear rate of different ST emulsions. The apparent viscosity rapidly declined in a narrow range at first when the shear rate increased from 0 s^{-1} to around 25 s^{-1}. And then, it slowly decreased as the shear rate increased from 25 s^{-1} to 200 s^{-1}. It is obvious that the apparent viscosities of all ST emulsions exhibited the shear-thinning behavior, indicating that those ST emulsions belong to the Bingham plastic fluid. Specifically, as the dosage of AO emulsion increased, the apparent viscosity of ST emulsion gradually decreased. It was reported that an emulsion with a wider PSD range usually has a relatively lower apparent viscosity [173]. Compared with asphalt emulsion, the AO emulsion has a similar mean particle size and a slightly higher Span value. Thus, the ST emulsions containing AO emulsions had a relatively lower apparent viscosity than that of the pure asphalt emulsion. However, another kind of ST emulsion presented an opposite trend, where its apparent viscosity gradually thickened as the proportion of TO emulsion increased. One possible explanation was that the AO mainly contains fatty acids and polyol esters [174]. Large amounts of acid ions and carboxyl groups came from AO, which would combine with the heavy metal ions originating from asphalt binder, leading to the increase of apparent viscosity.

The shear stress versus shear rate results of different ST emulsions are shown in Figure 6.9 (b) and (d). Initially, ST emulsions didn't exhibit flow until the shear stress exceeded yield stress. Then the shear stress linearly increased with the shear rate, which corresponds with the characteristics of Bingham plastic fluid. As mentioned above, the more AO emulsions mixed with asphalt emulsions, the more apparent viscosity of ST emulsion decreased, which was consistent with the descending trend of shear stress as shown in Figure 6.9 (b). By contrast, Figure 6.9 (d) shows that the shear stress of ST emulsion gradually increased as the addition of TO emulsion augmented, which accounts for the thickening of apparent viscosity.

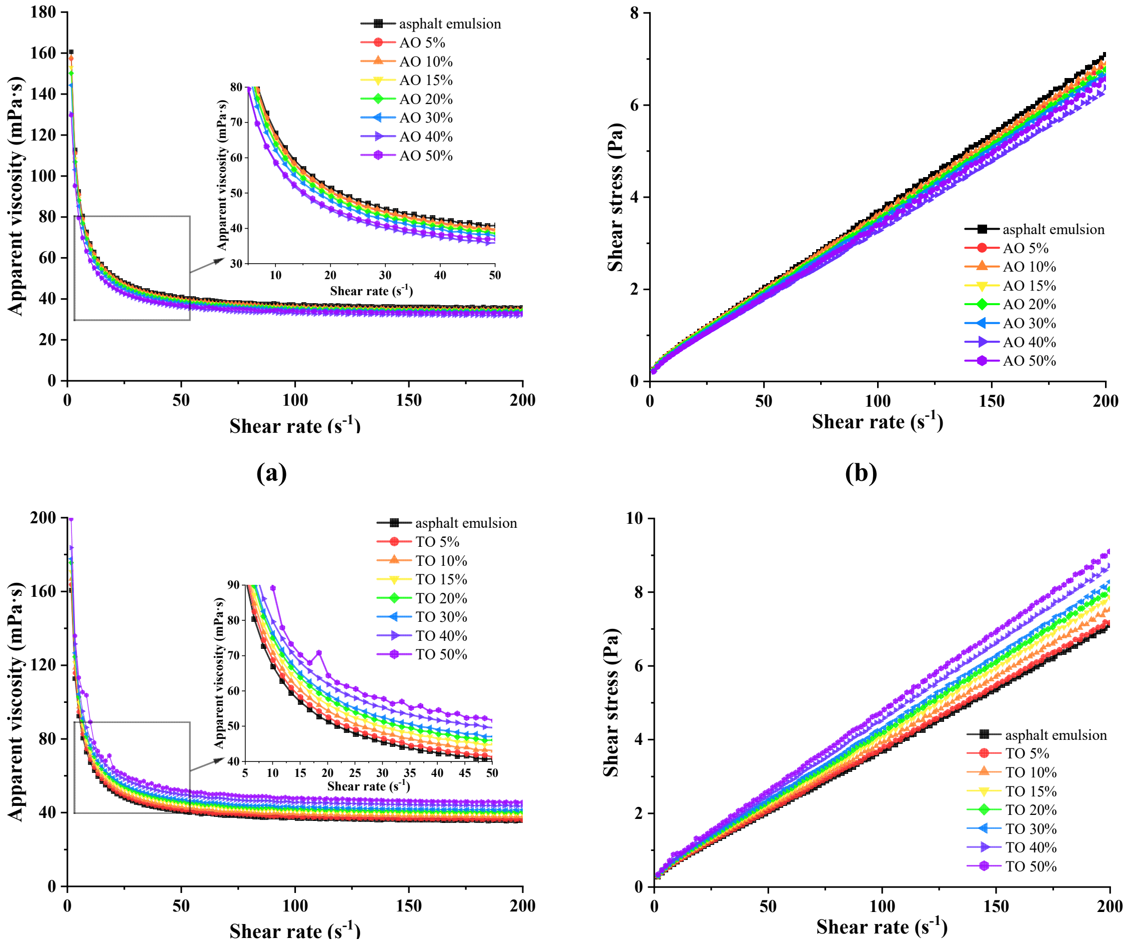

(a) (b)

(c) (d)

Figure 6.9 Shear viscosity test results: (a) apparent viscosity curves of AO emulsions; (b) shear stress curves of AO emulsions; (c) apparent viscosity curves of TO emulsions; (d) shear stress curves of TO emulsions.

Wettability

The wettability of the ST emulsion was evaluated by the contact angle test. The contact angles of pure asphalt emulsion, AO emulsion, and TO emulsion droplets on the aged asphalt binder were 71.5°, 47.5° and 44.6°, respectively, indicating that both AO and TO emulsion have a better wettability on the surface of aged asphalt binder than asphalt emulsion. Figure 6.10 shows that when adding AO emulsion or TO emulsion into asphalt emulsion to prepare the ST emulsion, the contact angle of mixed ST emulsion first rapidly decreased and then remained stable as the addition of rejuvenator emulsion increased. Especially, when the addition of rejuvenator emulsion was only 5% by the weight of ST emulsion, the contact angles of AO-5% and TO-5% emulsions declined to 55.8 ° and 51.4°, which were reduced by 21.95% and 28.11% compared with pure asphalt emulsion. The incorporation of AO or TO emulsion in ST emulsion significantly improved the wettability, which is expected to help emulsion residue penetrate deeper and distribute more uniformly. Besides, it was observed that the TO emulsion has a lower contact angle than the AO emulsion, so the ST emulsion containing the TO emulsion always has a slightly better wettability than the ST emulsion containing the AO emulsion in each scenario.

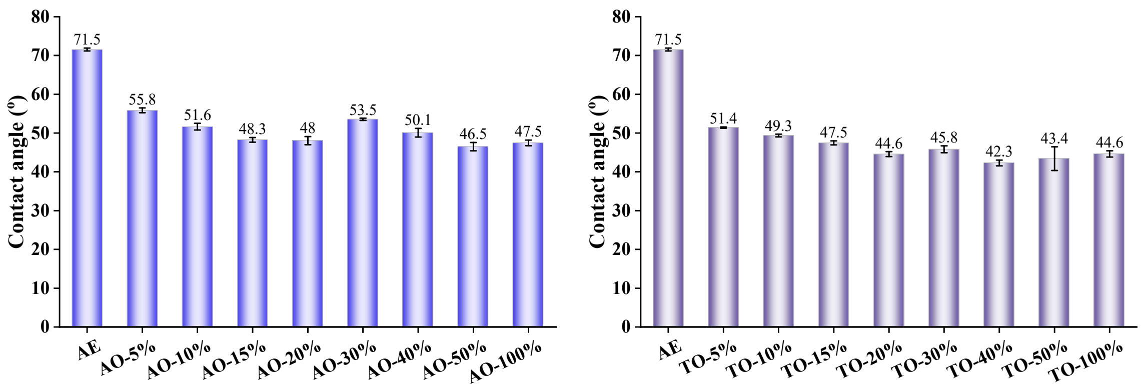

(a) (b)

Figure 6.10 Contact angles of (a) AO emulsion or (b) TO emulsion droplets on aged asphalt binder

Bonding strength

The coating ratio results after the water boiling test are depicted in Figure 6.11. The bonding strength between original aggregates and asphalt binders generally consists of two parts, which are the adhesive strength of asphalt to aggregate and the cohesive strength in asphalt binders. The results showed that the coating ratio decreased with the increase of rejuvenator emulsion, indicating the adhesive strength of composite emulsion residue to aggregate decreased. Meanwhile, it is well known that the cohesive strength of composite emulsion residues decreased with the increase of soft rejuvenating components. A high coating ratio means the ST emulsion residue has a good bonding strength with aggregate. The more rejuvenator emulsions were added into ST emulsion, the worse the bonding strength of ST residue was, which is similar to others' findings [175, 176]. As the Chinese standard of JTG E20-2011-T0654 stipulated, the minimum coating ratio should not be lower than 2/3 to ensure the bonding strength between ST residue and aggregate. Therefore, it was recommended that the dosages of AO or TO emulsion used in this study should be controlled within 10% and 5%, respectively.

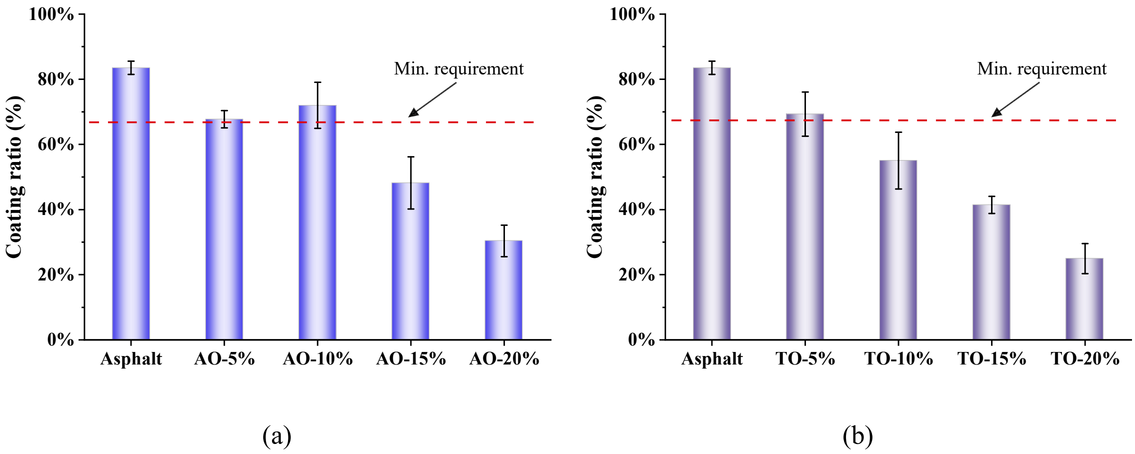

Figure 6.11 Coating ratios of (a) AO emulsion or (b) TO emulsion residues on aggregate

Determination of ST emulsion composition

The primary goal of adding rejuvenating agents into asphalt emulsion is to improve the wettability and permeability of ST emulsion in PA mixture. Then, under the premise of guaranteeing the bonding strength of ST emulsion residue, rejuvenators can be added more to help revitalize more aged binders in the long term. Here comes a frequently asked question related to the ST emulsion formula. How do we determine the optimal dosage of rejuvenator emulsion in ST emulsion? Three points need to be considered for the ST emulsion formula optimization.

First, the apparent viscosity variation of ST emulsion should be controlled in a reasonable range. A sticky emulsion with a high viscosity might be difficult to penetrate inside PA pavement, leading to the accumulation of emulsion residue on the pavement surface. In contrast, the ST emulsion with a low viscosity could account for the quick draindown and the waste of emulsion residue. It was found that the apparent viscosities of ST emulsions containing different proportions of AO or TO emulsion did not show significant statistical differences. Thus, the incorporation of rejuvenator emulsion to asphalt emulsion could not change the apparent viscosity of ST emulsion.

Second, the wettability of ST emulsion is expected to be improved to deepen the penetration depth and make the ST emulsion distribute uniformly. Previous studies found that the sprayed unmodified ST emulsion had a nonuniform distribution of ST residue film [168], which not only increased the risk of blocking micro-voids to some extent, but also didn’t coat the aged asphalt binder areas as much as possible. Therefore, a good wettability of ST emulsion is needed. Here, both AO and TO emulsions can significantly reduce the contact angles of ST emulsions, even at small addition amounts.

Third, the bonding strength of ST residue is a vital important performance as a preventive maintenance material. One of the motivations for using rejuvenators was replenishing light components of aged asphalt binders to rejuvenate them. If rejuvenator usage was calculated based on the effective penetration depth of emulsion and asphalt content of aged PA mixture, it was found that the needed rejuvenator content is too high to provide enough bonding strength of ST emulsion residue. However, different from the conventional hot recycling asphalt mixture, in which rejuvenators can effectively blend with and diffuse in aged asphalt binders of reclaimed asphalt pavement (RAP) at a high mixing temperature within several minutes [177, 178], this study sprayed the ST emulsions containing fresh asphalt binder and rejuvenators to aged PA pavement without external heating. The diffusion behaviors between rejuvenators and aged asphalt binders are slow at outdoor temperatures. Rejuvenators were mixed with fresh asphalt binders in ST residues after the demulsification of ST emulsion, which could sacrifice the initial strength of ST residue. Take the micro-cracks in PA mixtures filled with ST residues as an example, the dosage of AO or TO rejuvenator should be carefully controlled within a certain range to ensure the bonding strength of ST residue.

To sum up, after comprehensively considering the apparent viscosity, wettability, and bonding strength performances of the ST emulsion, the optimal dosages of AO and TO emulsions in ST emulsions were 10% and 5% in our scenarios, which were denoted by AO-10% and TO-5%, respectively.

6.3.3 Ravelling resistance verification

Three kinds of ST emulsions, named pure asphalt emulsion, asphalt emulsion containing AO emulsion (AO-10%), and asphalt emulsion containing TO emulsion (TO-5%), were sprayed to the top surface of damaged PA specimens to investigate their recovery efficiencies of the ravelling resistance. Specimens without emulsion treatment were also tested as a control group. Figure 6.12 shows the lost masses and mass loss ratios after conducting the cantabro abrasion test. All PA specimens treated with ST emulsions exhibited significantly lower lost masses and mass loss ratios than those of the control group, indicating a better recovery effectiveness of ravelling resistance. Furthermore, compared with the results of damaged PA specimens treated with asphalt emulsion, the lost masses of specimens treated with AO-10% and TO-5% reduced by 25.4% and 11.2%, respectively, indicating that the AO-10% and TO-5% showed better recovery efficiencies than asphalt emulsion. This phenomenon can be explained by the fact that the incorporation of AO emulsion or TO emulsion could significantly improve the wettability of the ST emulsion as discussed above, which helps the emulsion penetrate deeper and distribute more uniformly inside a specimen as well as coat on more areas of aged binders surrounding the internal voids. Besides, AO-10% and TO-5% emulsion residues might have better diffusion efficiencies than asphalt emulsion residues due to the occurrence of rejuvenators, which is helpful in rejuvenating aged binders. Therefore, it is verified that the optimized ST emulsion containing rejuvenators could improve the ravelling resistance than pure asphalt emulsion in our cases.

In addition, compared with pure AE treated specimens, the TO-5% treated PA specimens showed slightly lower mass loss ratios, while the AO-10% treated PA specimens showed relatively lower mass loss ratios than the TO-5% treated specimens, which could be explained by the following two aspects. On the one hand, Figure 6.9 shows that the AO-10% emulsion has a slightly lower apparent viscosity than that of TO-5% emulsion. Although the addition of rejuvenator emulsion into pure asphalt emulsion didn’t cause an order of magnitude change of apparent viscosity, the slight difference may affect the penetration depth of emulsion residues in PA mixture, which will further influence the recovery efficiency of ravelling resistance of PA mixture. On the other hand, the rejuvenator contents of AO-10% and TO-5% emulsions are different. Assuming the rejuvenating ability of AO and TO are similar, emulsion residues containing more rejuvenators theoretically could diffuse in and revitalize more aged asphalt binders, which benefits the recovery of the bonding strength of aged asphalt binders.

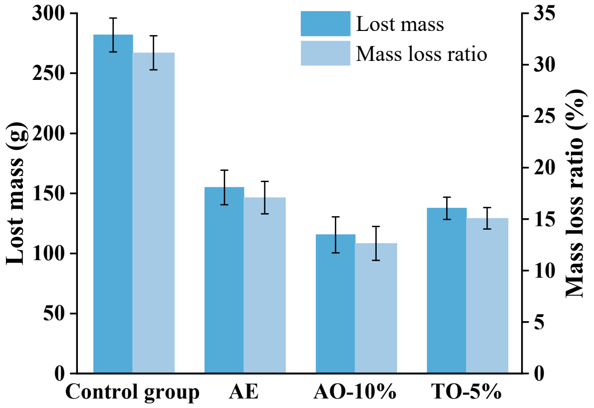

Figure 6.12 Cantabro abrasion test results

6.4 Summary

In this chapter, feasible methods of adding rejuvenators in ST emulsions were discussed first. The appropriate parameter values were determined by the orthogonal design method to prepare stable and homogeneous rejuvenator emulsions. The viscosities, wettability, and bonding strengths of different ST compositions were analyzed to determine the optimal formula. The ravelling resistances of damaged PA specimens treated with optimized ST emulsions were verified. The main findings and conclusions are summarized as follows:

(1) It is recommended that the rejuvenator be emulsified first to achieve better compatibility with asphalt emulsion.

(2) Based on the PSD and zeta potential results, the appropriate PH values, emulsified temperatures and emulsifier dosages to prepare stable and homogeneous AO and TO emulsions were 1, 90 °C, 3%, and 1, 60 °C, 4%, respectively.

(3) Mixing AO or TO emulsion with asphalt emulsion didn’t obviously change the apparent viscosity of the modified ST emulsion. Both AO and TO emulsions significantly improved the wettability of modified ST emulsions. The bonding strength of ST residue rapidly degraded as the dosage of rejuvenator emulsion increased. The optimal dosages of AO and TO emulsions are 10% and 5% by mass of the ST emulsion.

(4) AO-10% and TO-5% emulsions ultimately reduced the lost masses of PA mixtures by 25.4% and 11.2% compared with the cantabro abrasion test results of damaged PA specimens treated with asphalt emulsion, demonstrating that incorporation of AO and TO emulsion into asphalt emulsion could further improve the ravelling resistance of PA.

CHAPTER 7 MAINTENANCE MECHANISMS OF REJUVENATOR-OPTIMIZED ST EMULSION IN DAMAGED PA MIXTURE: MORPHOLOGICAL, PHYSICOCHEMICAL, AND RHEOLOGICAL CHARACTERIZATIONS

Recent studies [28, 96, 179] found that the ST emulsion containing rejuvenator ingredients may have a better recovery efficiency of ravelling resistance for old asphalt pavement than conventional asphalt emulsion. These studies claimed that the incorporation of a rejuvenating agent improved the rejuvenation ability of ST emulsion so as to efficiently revitalize aged asphalt binders. Adding rejuvenators to ST emulsions appears to make the ST emulsions penetrate deeper and distribute more uniformly in PA pavements. However, quantitative evidence regarding the distribution morphology of rejuvenator-optimized ST emulsion in old PA mixtures was still missing. Little information is available regarding the working mechanisms of rejuvenator in ST emulsion as a preventive maintenance material for old PA pavement. Thus, this chapter aims to comprehensively investigate the maintenance mechanisms of rejuvenator-optimized ST emulsion in old PA mixtures from morphological, physicochemical, and rheological perspectives.

As the flowchart shown in Figure 7.2, the distribution of ST residues in PA mixtures was first identified using X-ray CT. Penetration depth of ST residues was calculated based on the variations in air voids before and after the ST emulsion. Two indicators, thickness (T_c) and percentage of coating area (P_c) of emulsion residues, were developed to evaluate the distribution uniformity of ST residues in the PA mixture. Then, the same PA specimen was cut into four slices, and their binders, including asphalt binders and rejuvenators, were extracted using the solvent extraction method. Subsequently, the molecular weight compositions of extracted binders from different layers of the PA specimen were analyzed by the gel permeation chromatography (GPC) test. Meanwhile, Fourier Transform Infrared Spectroscopy (FTIR) was used to detect the penetration depth of rejuvenator-optimized ST emulsion based on the unique functional groups of the selected rejuvenator. In addition, relevant rheological tests were carried out to investigate the maintenance effects of rejuvenator-optimized ST residues on the anti-rutting and anti-cracking performances of old asphalt binders. Master curves were built to further analyze the rheological properties of extracted binders. The outcomes of this study hope to shed more light on the understanding of maintenance mechanisms of rejuvenator-optimized emulsion in damaged PA mixture, ultimately guiding the material design of ST emulsions and extending the service life of old PA pavement.

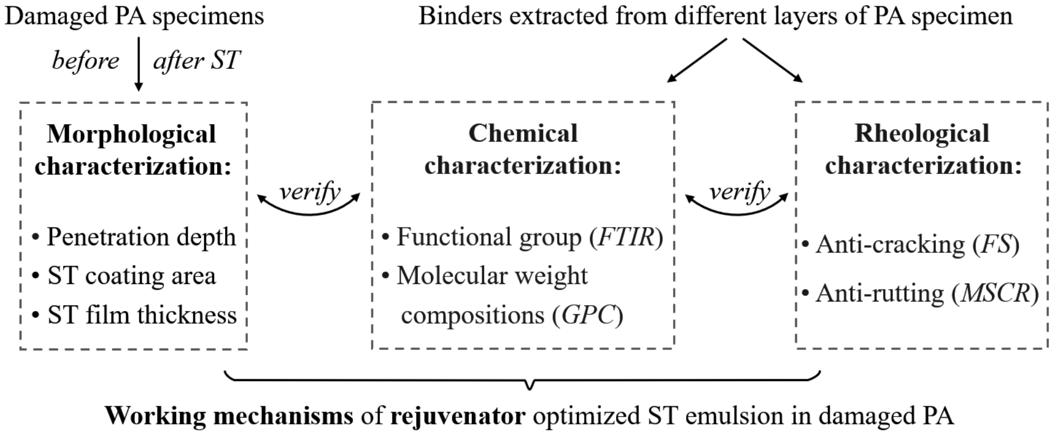

Figure 7.1 Flowchart of Chapter 7

7.1 Materials and Methodology

7.1.1 Materials and specimen preparation

ST emulsion preparation

A pure asphalt emulsion (AE) was prepared to serve as the control group. One petrol-based rejuvenator named aromatic oil (AO) and another bio-based rejuvenator named tall oil (TO) were separately emulsified to prepare two rejuvenator emulsions. The mass compositions and production conditions for those three kinds of emulsions are summarized in Table 7.1. Then, the AO emulsion, with a mass content of 10%, was directly added to AE to prepare the aromatic oil-optimized asphalt emulsion (AOAE). Similarly, the TO emulsion, with a mass percentage of 5%, was mixed with AE to prepare the tall oil-optimized asphalt emulsion (TOAE). So, three kinds of ST emulsions, designated AE, AOAE, and TOAE, were used in this study.

Table 7.1 Basic information about the ST emulsions

	Weight composition				Production condition	
Item	Solid content	Emulsifier	Stabilizer	Water	Heating temperature for binder (°C)	pH value
AE	60%	3%	0.2%	36.8%	135	2.5
AO	60%	3%	0.2%	36.8%	90	1
TO	60%	4%	0.2%	35.8%	60	1

PA mixture preparation

The SBS modified asphalt fulfilled with the Superpave performance grading of 76-16 (PG76-16) was used. The target air void is 22.5% and the nominal maximum aggregate size is 13.2 mm. The designed asphalt content of PA mixture was 4.1% by weight of aggregates. The loose asphalt mixtures were first heated in an oven at 135 °C for 8 hours to simulate the long-term aging effect on the asphalt pavement [180, 181]. Then, several cylindrical PA mixture specimens with a diameter of 100 mm and a height of 60 mm were fabricated by the Superpave gyratory compactor. Subsequently, three cycles of freezing and thawing conditioning were applied to all PA specimens to add some micro-cracks into PA mixtures. Finally, different ST emulsions were sprayed onto the surfaces of damaged PA specimens for maintenance purposes. The binder content and spraying rate of ST emulsion are 60% and 0.6 kg/m^2, respectively [167], which were determined in Chapter 3.

Figure 7.2 shows the schematic diagram of this study including the sample preparations and experimental methods. Firstly, the same PA specimen was scanned by X-ray CT for morphological characterization before and after the application of ST emulsion. It should be noted that the second scan was conducted only after the water had completely evaporated and the emulsion had fully demulsified. Three kinds of ST emulsions were tested, and two specimens were prepared for each kind of ST emulsion. Then, the ST treated specimens were cut into 4 slices with thicknesses of 10 mm, 10 mm, 20 mm, and 20 mm from the top surface to the bottom. Later on, each slice of PA mixture was immersed in dichloromethane (DCM) solvent to dissolve the asphalt binders and rejuvenators. Given that the boiling point of DCM is 39.6 °C at 1 atm, the solutions were placed in an oven at 45 °C for 24 hours to ensure thorough evaporation of the DCM. The extracted binder mixture, including asphalt binders and rejuvenators, was then used for the physicochemical and rheological tests.

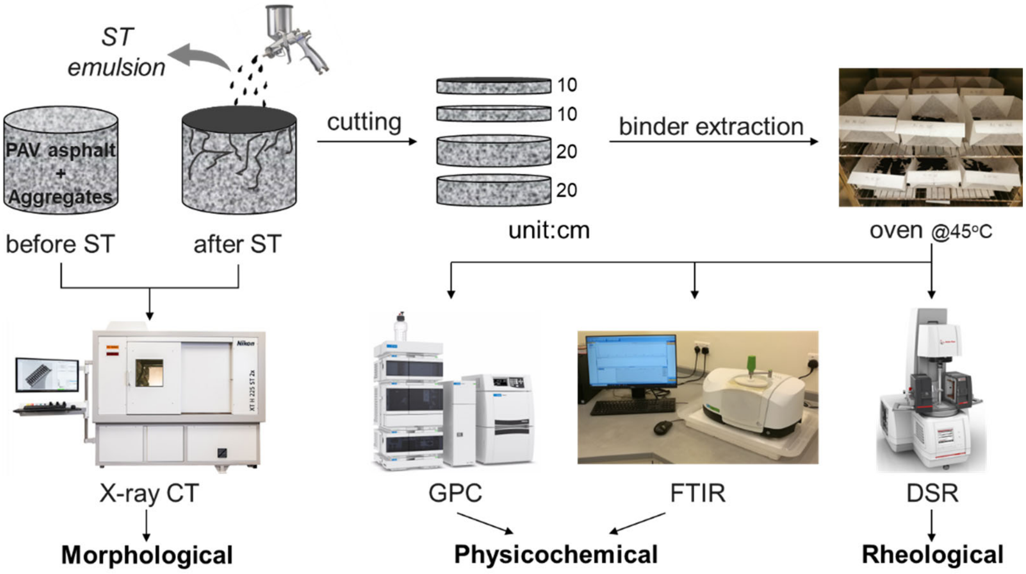

Figure 7.2 Sample preparations and experimental methods in this chapter

Ravelling resistance evaluation

The Cantabro Abrasion test was performed to evaluate the maintenance effects of different ST emulsions on the ravelling resistance of damaged PA specimens. The mass loss ratio (M_r) is calculated by Equation (3-1) and the results are shown in Table 7.2. The damaged PA specimen without ST presented the highest M_r value than that of ST treated specimen, demonstrating the effectiveness of ST emulsions in enhancing the anti-ravelling property of damaged PA. In particular, incorporating rejuvenator emulsion into AE helped decrease the M_r values of damaged PA specimens, so the damaged PA mixtures treated with either AOAE or TOAE exhibited slightly better ravelling resistance than those only treated with AE. Reasons why adding rejuvenator emulsion to AE can help further improve the anti-ravelling property of PA specimens will be explained in the following sections of this study.

Table 7.2 Mass loss ratios of damaged PA before and after ST application

	Without ST	AE	AOAE	TOAE
Mass loss ratio, %	31.2	17.1	12.6	15.1
St.d, %	1.7	1.6	1.7	1.0

7.1.2 Test methods

X-ray CT test

Cross-sectional images of PA specimens treated without and with ST emulsions were obtained using the X-ray CT machine, which is an effective and high-precision equipment to recognize the penetration status of ST residue in the PA mixture. The scanning system operated at a working voltage and current were 120 kV and 105 μA. The horizontal resolution of CT images varied slightly between 36.873 to 37.175 μm/pixel, due to the minor placement differences among different scanning operations. The minimum vertical interval of CT images is 100 μm, and a total of 600 pieces of images were exported for analyzing volumetric characteristics from the mesoscopic perspective. After conducting the smooth, denoising, and thresholding processes for CT images, the air voids and asphalt mixtures can be easily distinguished based on their gray values from the scanning images due to their significant density differences. Then, the images were rescaled, centered, and rotated to precisely match two groups of CT images for the same PA specimen before and after the application of ST emulsion. Thereafter, the newly added ST residues could be identified through the Boolean operation. In other words, the distribution of ST residues within a PA specimen can be recognized by subtracting the CT images of the PA specimen without ST from the corresponding slice images of the same PA specimen containing ST. All CT image processing was performed using a series of customized MATLAB algorithms.

The percentage of coating area (P_c) was proposed to evaluate the coating efficiency of ST residue in PA mixture. The average thickness of ST residues (T_c) and its standard deviation (Sd_c) were proposed to evaluate the uniformity of ST residue within PA mixture. More details about these indexes can be found in Section 4.1.2.

Gel permeation chromatography (GPC) test

An Agilent 1260 GPC assembled with two different pore sizes of chromatographic columns (PLgel 3 μm Mixed-E and PLgel 5 μm 10^3 Å) was adopted to measure the molecular weight distribution of the binder extracted from ST treated PA mixture. Each binder sample with a mass of 0.05g ± 0.002g was dissolved into 50 ml tetrahydrofuran (THF) solvent for preparing the binder solution. The injection volume was 20 μl for each test, with a 1 ml/min flow rate of the mobile phase. This test was performed at 30 °C. A refractive index differential detector was used to measure the molecular weight. The molecular weight corresponding to the highest percentage of the total molecular composition (M_p) and the number average molecular weight (M_n) are two representative statistical parameters, which are widely used in the GPC analysis [182]. The calculation equation of M_n is shown below.

$$M_n = \frac{\sum n_i M_i}{N} \tag{7-1}$$

where i represents a molecular with a specific molecular weight; n_i is the total weight and the total number of molecular i in each test; N means the total number of all kinds of molecules; M_i is the molecular weight of molecular i.

Fourier-transform infrared spectroscopy (FTIR) test

A PerkinElmer FTIR spectrometer operating in attenuated total reflectance (ATR) mode was selected to analyze the binders extracted from different layers of ST treated PA mixtures. Rejuvenators may contain some unique functional groups that respond with specific absorbance bands, allowing for differentiation from the asphalt binders. Theoretically, these distinct absorbance bands can serve as tracers to investigate the penetration depth of rejuvenator-optimized asphalt emulsions within PA specimens.

Dynamic shear rheometer (DSR) test

Asphalt binder acts as the important bonding material between aggregates in a mixture. Its rheological property highly affects the mechanical properties of asphalt mixture [183, 184]. Different ST emulsions may produce different maintenance effectiveness on the mechanical properties of the damaged PA mixture. So, the frequency sweep (FS) test and multiple stress creep recovery (MSCR) tests were conducted using a DSR to investigate the rheological property of the extracted binder from PA. Two replicates were prepared for each kind of extracted binder.

FS test

The phase angles (δ) and complex shear moduli (G^*) of different binder samples extracted from different ST treated PA specimens were measured in the FS test with a frequency range of 100-0.01Hz. The test temperatures are set from 10 °C to 60 °C with an increasing interval of 10 °C. The test strain was controlled at 0.1% to ensure the asphalt-based binder was within its linear viscoelastic range. The 25 mm parallel plate with a 1 mm gap and the 8 mm parallel plate with a 2 mm gap were used at test temperature ranges of 40-60 °C and 10-30 °C, respectively. Based on the time-temperature superposition principle, the shift factor was calculated using the Williams-Landel-Ferry (WLF) formula as given in Equation (7-2). The reference temperature was set at 10 °C.

$$\log a_T = \frac{-C_1(T-T_0)}{C_2+(T-T_0)} \tag{7-2}$$

where a_T is the shift factor; T and T_0 are the experimental temperature and the reference temperature, respectively; C_1 and C_2 are constants.

The viscoelastic response of asphalt binder can be fitted by the Modified Huet-Sayegh (MHS) model [185], whose mathematical expression is shown in Equation (5). The MHS model is optimized from Huet-Sayegh (HS) model by adding a linear dashpot in series, which can improve the goodness of fit of the master curve data at the low frequency region and help to describe the viscous behavior.

$$j^*(\omega) = \frac{G'}{|G^*(\omega)|^2} - i\left[\frac{G''}{|G^*(\omega)|^2} + \frac{1}{\eta\omega}\right] = J'(\omega) - ij''(\omega) \tag{7-3}$$

where $j^*(\omega)$, $J'(\omega)$ and $J''(\omega)$ represent the complex creep compliance, storage creep compliance, and loss creep compliance of the MHS model, respectively; ω and η mean the reduced frequency and the linear dashpot parameter, respectively; $G^*(\omega)$, G' and G'' are the complex shear modulus storage shear modulus and loss shear modulus of the original HS model, respectively.

Besides, the Glover-Rowe parameter (G-R) is calculated by Equation (7-4). The G^* and δ values at 0.005 s^{-1} and 15 °C were directly obtained from the constructed master curve. G-R parameter was used to evaluate the ductility and cracking resistance of asphalt binders at a low temperature [186, 187].

$$G - R = \frac{G^*(\cos\delta)^2}{\sin\delta} \tag{7-4}$$

Multiple stress creep recovery (MSCR) test

It is proved that the MSCR test can effectively evaluate the rutting resistance of asphalt binder [188, 189]. According to the standard of AASHTO M 332-23, a specimen with a diameter of 25 mm and a thickness of 1 mm undergoes the creep test at 60 °C and two different stress levels of 0.1 kPa and 3.2 kPa. In each stress level, a constant stress creep of 1s duration followed by a recovery period lasting 9s was applied to the specimen and ten cycles were repeated. $J_{nr0.1}$ and $J_{nr3.2}$ represent the average nonrecoverable creep compliances at two stress levels, which can be calculated by Equation (7-5). In addition, the average percent recovery of strain at both stress levels, $R_{0.1}$ and $R_{3.2}$, was calculated to evaluate the resilience of the binder after repeated stretching and relaxation.

$$J_{nr,\sigma} = \frac{\varepsilon_{nr}}{\sigma} \tag{7-5}$$

where $J_{nr,\sigma}$ is the nonrecoverable creep compliance at a specific stress level, kPa^{-1}; ε_{nr} is the average nonrecoverable strain of ten cycles; σ is the stress level, kPa.

7.2 Results and Discussions

7.2.1 Morphological analysis

Air void variations of different ST emulsions treated specimens

The air void contents along the depth direction within PA mixtures before and after applying different ST emulsions were depicted in Figure 7.3 with blue and red colors, respectively. It was found that the vertical profile of air voids within a PA mixture before and after ST showed a bath shape, which was consistent with other studies [111, 190]. Besides, after the water evaporation of ST emulsion, the newly added ST residues partially filled the air voids and accounted for the reduction of air voids. This change was identified by conducting the Boole operation on the CT images of PA mixture obtained before and after ST emulsion. The volume distribution of ST residues is depicted in Figure 7.3 in black color. It showed a vertical gradient decreasing profile in PA, with a relatively higher ST value near the top surface of PA due to the accumulation effect. Despite the same application rate and solid content of three different ST emulsions, their distributions within PA specimens exhibited different characteristics. Specifically, most AE residues penetrated approximately 20 mm into the PA specimen, while the other two rejuvenator-optimized ST residues could penetrate around 40 mm with relatively smoother profiles.

An indicator, named the reduction percentage of air voids (P_{ra}), was introduced to further describe the penetration status of ST residues in PA. It refers to the ratio of the area occupied by ST residues within air voids to the entire void regions before ST in each cross-section image, which can be calculated by Equation (7-6). Figure 7.4 shows average P_{ra} values with a depth interval of 5 mm in PA. It indicated that all ST residues mainly accumulated near the top surface of PA specimens at first with a peak value observed in the 5 to 10 mm depth region. Then the P_{ra} of ST residues gradually decreased as the vertical depth increased. Interestingly, both the rejuvenator-optimized ST residues (AOAE and TOAE) showed a relatively gentle declining trend along the vertical depth direction compared to the AE residues. Due to the good wettability and permeability of the AOAE and TOAE emulsions, rejuvenator-optimized emulsions penetrated deeper into PA than the pure asphalt emulsion under the same spraying conditions. If using a P_{ra} value greater than 5% as a reference indicator for penetration depth, AE penetrated nearly 25 mm into the PA specimen, while the penetration depths of AOAE and TOAE in PA mixtures are around 45 mm.

$$P_{ra} = \frac{V_{ST}^{i}}{V_{AV-b}^{i}} = \frac{V_{AV-b}^{i} - V_{AV-a}^{i}}{V_{AV-b}^{i}} \times 100\% \tag{7-6}$$

where i means the number i of the processed cross-section slice; V_{ST}^{i} is the volume of ST residue which can be calculated by subtracting the volume of air voids in PA after ST (V_{AV-a}^{i}) from the volume of air voids in PA before ST (V_{AV-b}^{i}).

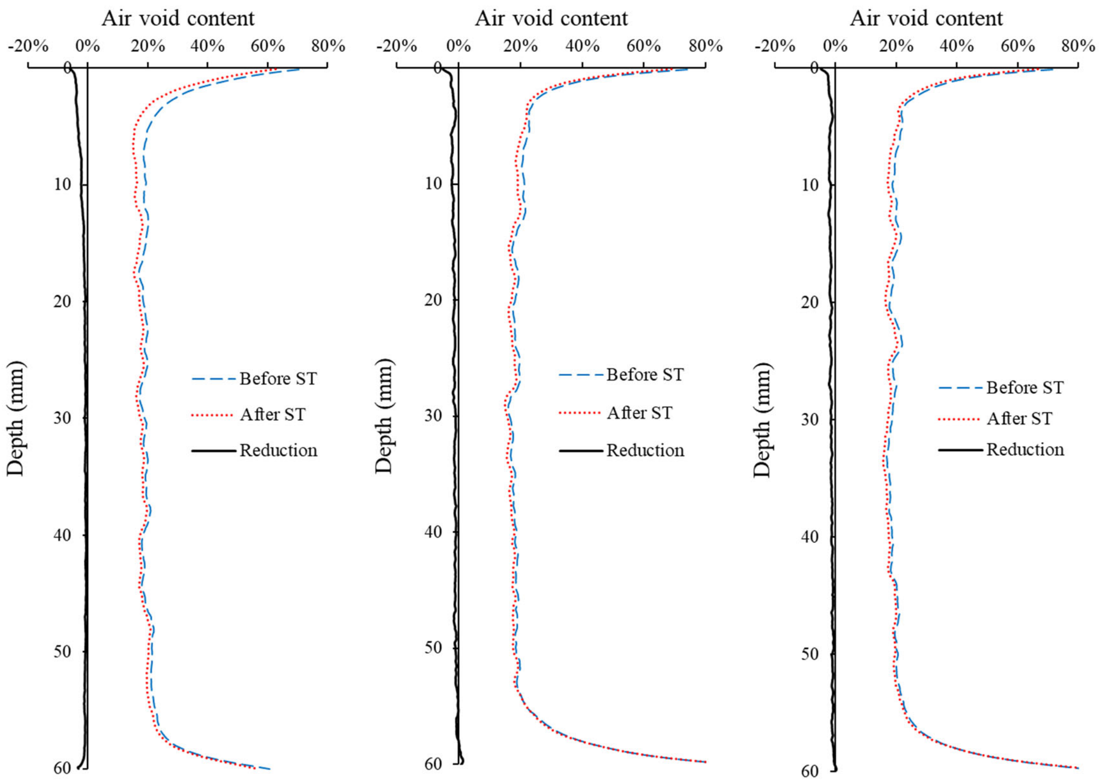

(a) AE (b) AOAE (c) TOAE

Figure 7.3 The air void contents along the depth direction within a PA specimen before and after the application of ST emulsions

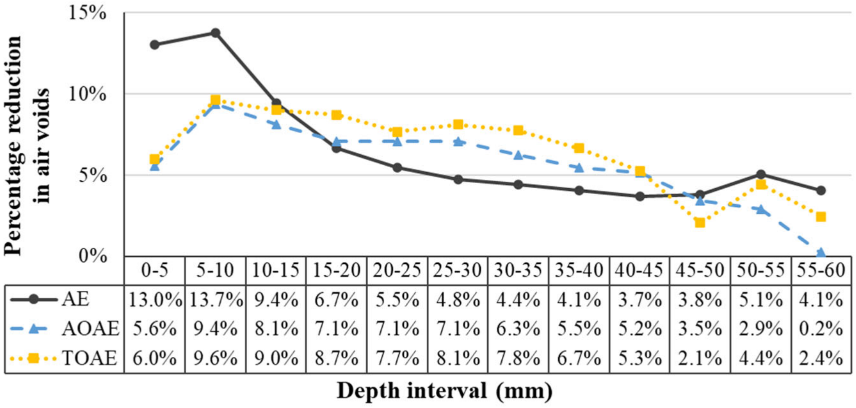

	0-5	5-10	10-15	15-20	20-25	25-30	30-35	35-40	40-45	45-50	50-55	55-60
AE	13.0%	13.7%	9.4%	6.7%	5.5%	4.8%	4.4%	4.1%	3.7%	3.8%	5.1%	4.1%
AOAE	5.6%	9.4%	8.1%	7.1%	7.1%	7.1%	6.3%	5.5%	5.2%	3.5%	2.9%	0.2%
TOAE	6.0%	9.6%	9.0%	8.7%	7.7%	8.1%	7.8%	6.7%	5.3%	2.1%	4.4%	2.4%

Figure 7.4 The percentage reduction in air voids along the vertical depth of the ST treated PA specimen

Distribution of ST residue

When ST emulsions penetrated PA mixtures along the air void, their residues coated the aged asphalt mortar areas, potentially revitalizing the aged asphalt binders in the long term. Theoretically, the more boundaries of air voids were coated by ST residues, the more aged binders surrounding the air voids could be covered and rejuvenated by new ST residues. Figure 7.5 illustrates the percentage of ST coating areas (P_c) in PA specimens at a 5 mm depth interval.

Considering the vertical gradient distribution characteristic of ST residues in the PA specimen, it is reasonable to observe that the P_c value gradually decreased as the depth increased. Interestingly, when the P_c is no less than 10%, the penetration depth is no more than 20 mm for the AE-treated PA specimen, but 35 mm for AOAE- and TOAE-treated PA specimens. This difference indicated that the rejuvenator-optimized ST emulsion can penetrate deeper and coat more air voids' boundaries within the PA specimen, which benefits the replenishment of fresh asphalt binders and the recovery of bonding strength of aged asphalt binder. This finding also explains why the mass loss ratio of rejuvenator-optimized ST emulsion-treated PA specimens exhibited lower values than that of AE-treated PA specimens as shown in Table 7.2.

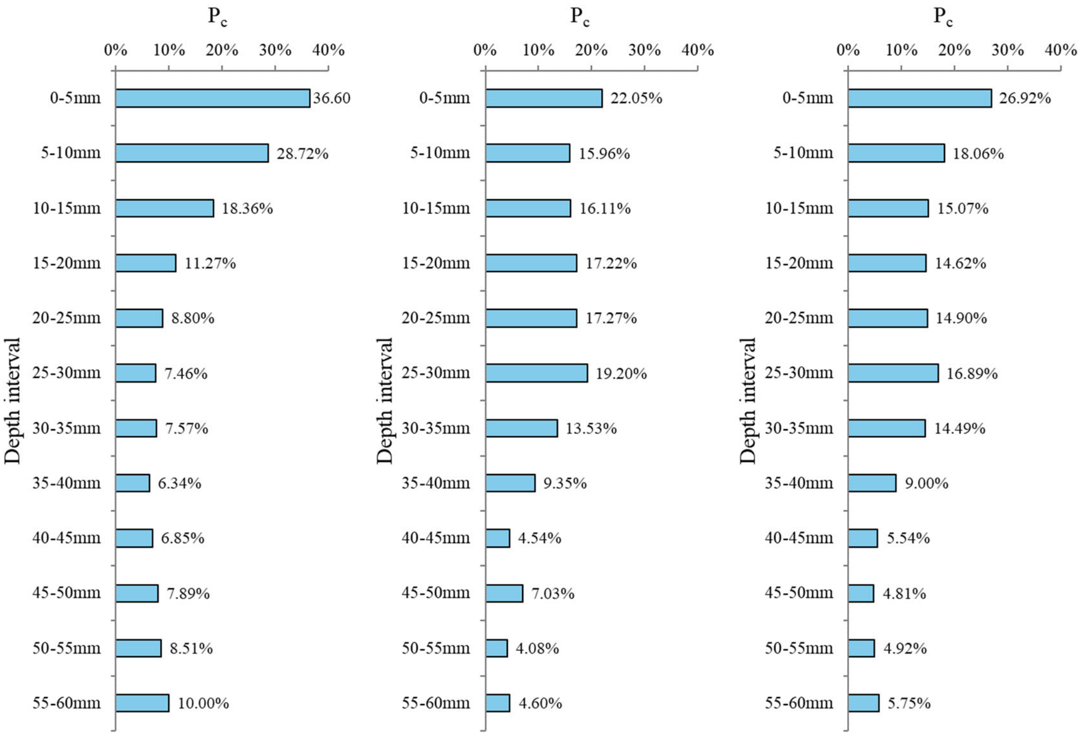

(a) AE (b) AOAE (c) TOAE

Figure 7.5 The percentage of ST coating areas on air voids along the vertical depth of PA specimens

Thickness of ST residue

The sprayed ST emulsions are mainly coated on the interfaces between aged asphalt mortars and air voids, forming new binder films after the demulsification of ST emulsions. The morphologies of ST residues in PA mixtures are complex. The average thickness of all ST residue droplets in each CT image was elaborately collected and a total of 600 data points were obtained from all CT slices of each PA specimen. These data points were summarized in a probability graph as illustrated in Figure 7.6. Both the film thickness curves of AOAE and TOAE residues displayed a single peak pattern with a relatively narrow distribution range. By contrast, the AE residues exhibited a double peak pattern with a slightly wider distribution range. In particular, approximately 37% of the AOAE and TOAE residues had a film thickness around 0.3 mm, while the AE curve exhibited the first and second peak values at film thicknesses around 0.4 mm and 0.7 mm, with a frequency of around 28% and 7%, respectively. Therefore, compared to the film thickness curve of AE residues, the peak values of curves for AOAE and TOAE residues moved to the low film thickness zone, and their frequencies of peak value significantly increased.

Furthermore, Table 7.3 shows the average thickness (T_c) of three different ST residues and their standard deviations (SD_c). The T_c values of AOAE and TOAE residues are around 0.280 mm, which was at least 22.5% lower than the T_c value of AE residues. This suggests that the rejuvenator-optimized ST emulsion formed a thinner film thickness than the conventional AE. That is to say, when the application rate of ST residue is constant, the rejuvenator-optimized ST residues could coat more aged binder areas surrounding air voids compared to conventional AE residues, thereby rejuvenating aged asphalt binders as much as possible. Besides, the SD_c values of AOAE and TOAE residues are 0.162 and 0.158 mm, respectively. Both are smaller than the SD_c value of AE residues, which is 0.179 mm, indicating that the AOAE and TOAE residues have a more uniform film thickness distribution than conventional AE residues.

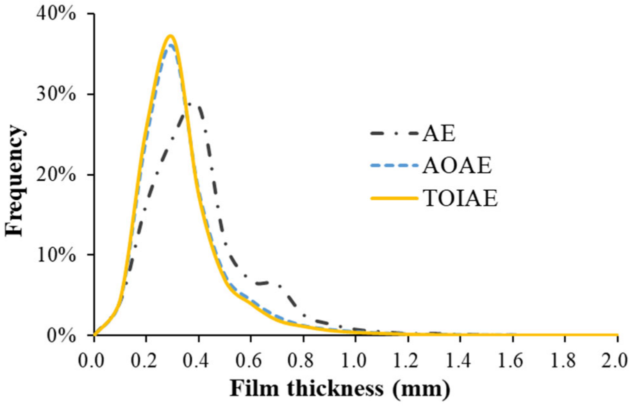

Figure 7.6 Probability graphs of the film thickness of three different ST residues

Table 7.3 Average film thickness and standard deviation of different ST residues in PA specimens

ST residue type	T_c (mm)	SD_c (mm)
AE	0.373	0.179
AOAE	0.289	0.162
TOAE	0.272	0.158

7.2.2 Physicochemical characterizations of asphalt binders from different layers of PA

GPC data analysis

The GPC test results are shown in Figure 7.7, where the first row and second row of stacked plots showed the M_p and M_n values of PA specimens treated with three different ST emulsions, respectively. Each plot includes four data points corresponding to depths of 5, 15, 30, and 50 mm, representing the average molecular weight compositions of binders extracted from four layers (0-10 mm, 10-20 mm, 20-40 mm, and 40-60 mm) within a PA mixture. All stacked plots of M_p and M_n values showed obvious vertical gradient trends. A turning point, marked by a red hollow circle in each plot, indicates where both indicators show smaller values before this point, followed by slight fluctuations thereafter. A smaller M_p value means that the new asphalt binders and rejuvenators diffused into and softened aged asphalt binders, breaking down the long and convoluted molecular chains into smaller molecules. Consequently, the percentage of small molecular weight increased, resulting in a lower M_n value in the upper layer of the emulsion-treated PA specimen. Therefore, based on the GPC test results, it was reasonable to speculate that the penetration depths of AE, AOAE, and TOAE are more than 20, 40, and 20 mm, respectively.

Here are two phenomena that need to be further discussed. On the one hand, although the CT scanning results showed that TOAE emulsion penetrated deeper than pure AE, Figure 7.7 shows that the turning points for AE and TOAE occurred in the third layer, which does not support this finding. After carefully comparing the variation trends of GPC results of AE- and TOAE-treated PA specimens, it was found that both the increase rates of M_p and M_n values of the AE-treated specimen gradually slowed down before the turning points, but the growth rates for the TOAE-treated specimen kept unchanged and even higher than the AE treated specimen at the same layer level. It suggests that the TOAE emulsion has a better permeability than AE, especially in the third layer at a depth ranging from 20 to 40 mm. To concisely describe the vertical gradient curve of M_p and M_n in future studies, it is recommended to increase the number of layers and reduce the thickness of each layer. On the other hand, the AOAE-treated specimen showed higher increase rates of M_p and M_n values in the third layer than the TOAE-treated specimen, indicating that the AOAE has better softening effectiveness on aged asphalt binders than TOAE, which benefits the recovery of bonding strength of aged asphalt binders. This also explains why the mass loss ratio of the treated PA mixture is lower than that of the TOAE-treated PA mixture as shown in Table 7.2.

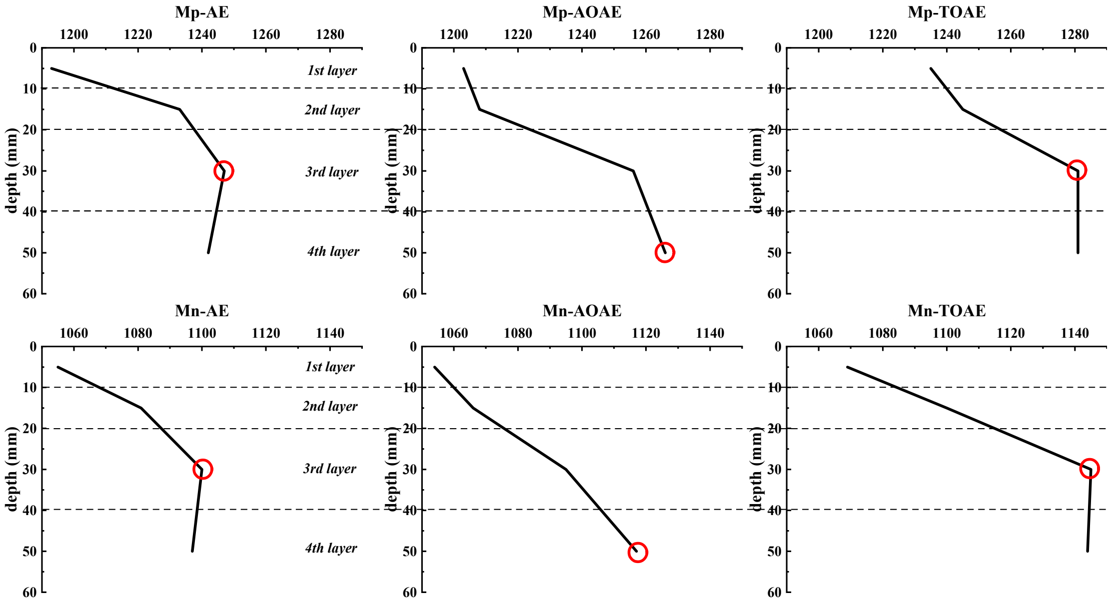

Figure 7.7 GPC test results of different layers of PA specimens treated with different ST emulsions

FTIR data analysis

The FTIR tests were carried out to investigate the penetration depths of different ST emulsions in PA mixtures from a chemical character perspective. The main effective components of three different ST emulsions contain asphalt binders, AO (if any), and TO (if any) materials. Their FTIR spectra are depicted in Figure 7.8. It was found that the rejuvenator TO has several significantly different functional groups from the asphalt binder. For example, a distinct peak at 1740 cm^{-1} in TO is attributed to the C=O stretching vibration of esters. However, another rejuvenator AO showed a similar FTIR spectrum to the asphalt binder. It is not unexpected because both AO and asphalt binder are usually derived from crude oil processing. They generally have similar chemical compositions, which accounts for insignificant differences in FTIR spectra between AO and asphalt binder.

Figure 7.9 shows the FTIR spectra of different binders extracted from different layers of a TOAE-treated PA specimen. The peak observed at 1740 cm^{-1} gradually decreased as the layer level increased from layer 1 to layer 4. The binders extracted from layer 4 of PA behaved at a slight peak around 1740 cm^{-1} compared with pure asphalt binder, indicating that the TOAE penetrated the fourth layer and its penetration depth at least 40 mm. This finding is also consistent with CT image analysis.

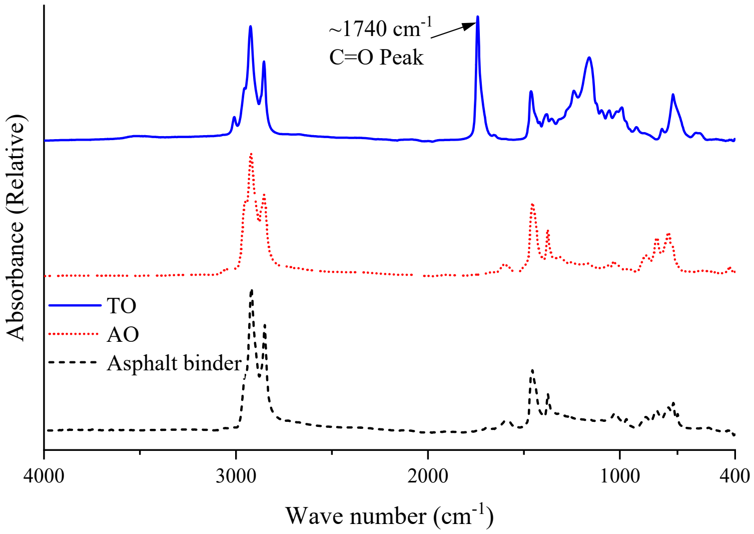

Figure 7.8 FTIR spectra of the asphalt binder and two rejuvenators

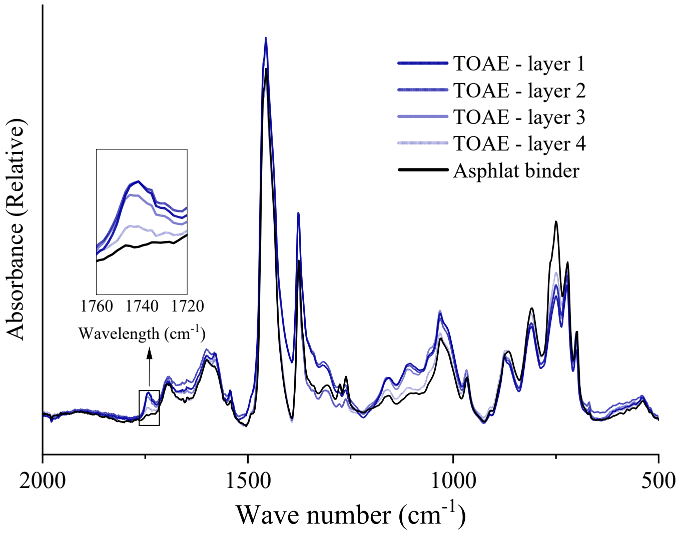

Figure 7.9 FTIR spectra of different binders extracted from different layers of TOAE-treated PA specimen

7.2.3 Rheological evaluations of asphalt binders from different layers of PA

FS analysis

To comprehensively evaluate and compare the maintenance effects of different ST emulsions on aged PA mixtures, the rheological performances of AE-, AOAE- and TOAE-treated PA specimens were investigated through the FS test. Master curves of binders extracted from four different layers of three different ST emulsions treated PA specimens are shown in Figure 7.10.

The PG 76 asphalt binder, processed by the pressure aging vessel (PAV) to prepare the long-term aged asphalt binder, was also included as a control group. It was found that the binders extracted from layer 4 showed very similar rheological behaviors (*G** and *δ* master curves) with aged asphalt binders. This similarity indicates that either almost no ST emulsion penetrated the fourth layer of the PA specimen, or maybe the quantity of penetrated ST emulsion in this layer was too low to have a noticeable impact on the rheological properties of the aged binders. Meanwhile, no matter which kind of ST emulsion was sprayed on the PA mixture, the *G** master curve consistently decreased from layer 4 to layer 1, and these differences are more significant in the low frequency range. This means that the newly added fresh asphalt binders and rejuvenators significantly softened the aged asphalt binders. Besides, all *δ* master curves shown in Figure 7.10(a)-(c) presented an upward trend from the fourth layer to the first layer across the whole frequency range, suggesting that the newly added different ST residues contributed to recovering the viscous characteristic of aged asphalt binders. A higher viscous component means a better stress relaxation property of asphalt binder, especially at a low service temperature.

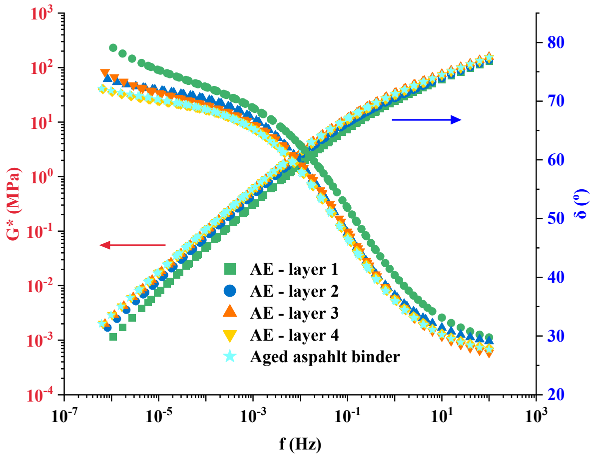

(a)

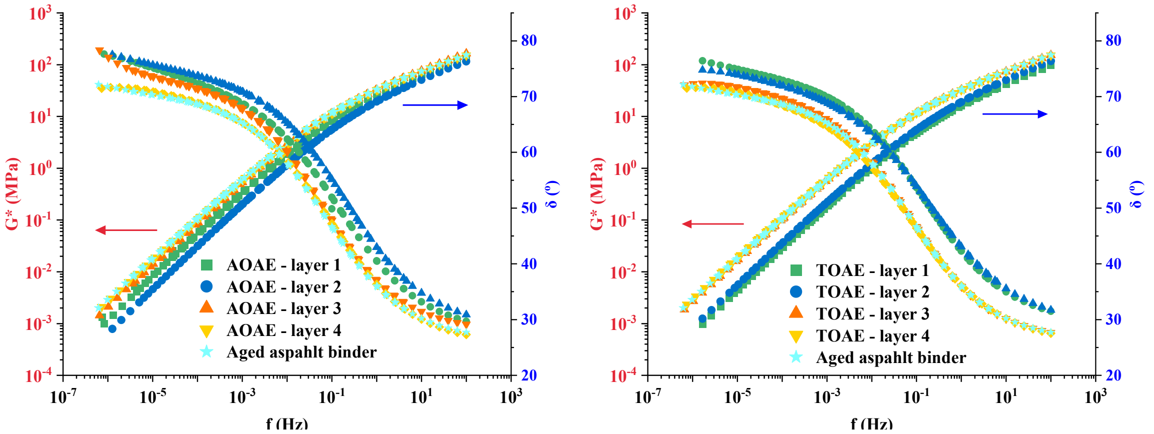

(b) (c)

Figure 7.10 *G and *δ* master curves of binders extracted from different layers of different ST emulsions treated PA mixtures**

The G-R parameter was calculated to further quantify the differences in rheological properties among three different ST emulsions treated PA specimens. As shown in Figure 7.11, the application of ST residues to the aged PA mixture indeed decreased the G-R values of extracted binders, especially in the first two layers of the PA specimen, which improved the ductility and cracking resistance of treated binders at a low temperature. Overall, most G-R values of extracted binders gradually increased from the first layer to the fourth layer, and the G-R values of three different emulsions treated specimens at the fourth layer were similar to the G-R value of aged asphalt binder after considering the experimental errors. Besides, both the AOAE- and TOAE-treated specimens showed relatively lower G-R values than AE-treated ones at the same layer level in most cases, suggesting that the addition of rejuvenator emulsion into pure asphalt emulsion could further enhance the low-temperature cracking resistance of aged asphalt binders.

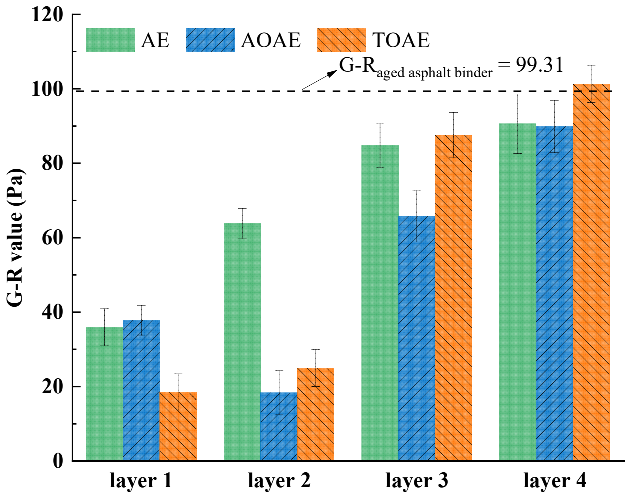

Figure 7.11 G-R values of binders extracted from different layers of different ST emulsions treated PA mixtures

MSCR analysis

MSCR test results of the nonrecoverable creep compliance (J_{nr}) and percent recovery of strain (R) at two stress levels are depicted in Figure 7.12. The long-term aged asphalt binder was also tested as a reference. For the tested binder from each layer, a high stress level at 3.2 kPa usually produced a higher J_{nr} and a lower R than the low stress level at 0.1 kPa. Overall, due to the penetration of ST emulsion in the PA specimen, almost all PA mixtures treated with three different emulsions showed a gradient descending trend of J_{nr} and a gradient augment trend of R from the first layer to the fourth layer. A higher J_{nr} value means the plastic deformation and viscous flow are more significant, and a lower R value represents the recoverable elastic deformation is smaller. The addition of fresh asphalt binders and rejuvenators not only replenished light components (e.g., naphthene aromatics, saturated hydrocarbons) and softened aged asphalt binders but also enhanced the risk of rutting disease of PA pavement to some extent. Besides, after making a comparison of the J_{nr} and R values between the aged asphalt binder and other binders extracted from different layers of PA, it was found that the conventional AE residues mainly changed the viscoelastic characteristics of binders extracted from the first layer, while the other two rejuvenator-optimized emulsion residues significantly changed the viscoelastic responses of tested binders from the first two layers and even the third layer. This enhanced rejuvenating effectiveness is consistent with the findings from the GPC and FS analyses, demonstrating that the incorporation of a rejuvenator into conventional AE not only increased the penetration depth but also promoted the maintenance effectiveness of aged asphalt binders.

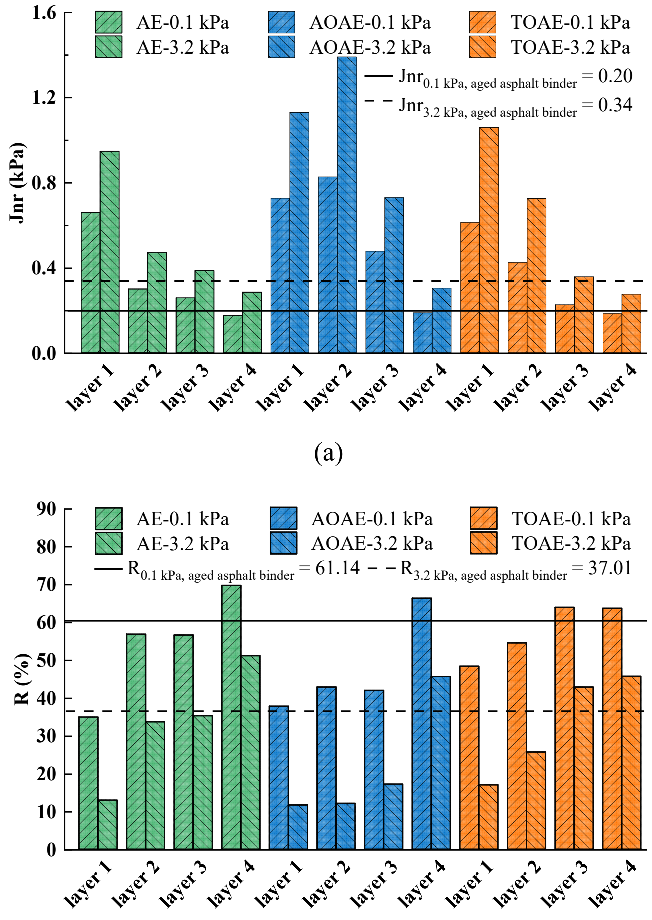

Figure 7.12 MSCR test results of binders extracted from different layers of different ST emulsions treated PA mixtures: (a) J_{nr}; (b) R.

7.3 Summary

In this chapter, three kinds of ST emulsions, including a conventional asphalt emulsion (AE) and two kinds of rejuvenator-optimized asphalt emulsions, were selected to evaluate their maintenance effectiveness for damaged PA mixtures. The working mechanisms of rejuvenator-optimized asphalt emulsion in PA were systematically investigated from morphological, rheological, and physicochemical perspectives. X-ray CT was selected to identify the distribution status of different emulsion residues in PA specimens. GPC and FTIR tests were conducted to characterize the physicochemical variations of the emulsion-treated PA specimen. FS and MSCR tests were carried out using a DSR to investigate the rheological properties of PA specimens treated with different ST emulsions. The relevant findings and conclusions were summarized as follows:

(1) All tests used in this chapter found that the distributions of different ST emulsion residues along the vertical depth of PA mixtures showed gradient decreasing trends, indicating that not all emulsion residues accumulated on the surface of PA mixture.

(2) From a morphological perspective, the penetration depth of rejuvenator-optimized asphalt emulsions was twice that of conventional AE, approaching 40 mm. P_c results showed that both AOAE and TOAE emulsions demonstrated better coating efficiencies and wettabilities by coating more aged asphalt areas. Consequently, the rejuvenator-optimized emulsions distributed more uniformly, which promotes the ravelling resistance of the damaged PA mixture.

(3) From a physicochemical perspective, the penetrated emulsion residues replenished new asphalt binders as well as light components, and softened aged asphalt binders, resulting in a decrease in the molecular weight at the highest occurrence frequency (M_p) and the number average molecular weight (M_n). The AOAE emulsion has a better maintenance effectiveness than the TOAE emulsion due to the lower M_p and M_n values of AOAE. Besides, utilizing a unique functional group as a tracer to qualitatively detect the penetration of rejuvenator-optimized asphalt emulsion in PA mixture is feasible. The FTIR spectra showed the penetration of TOAE is at least 40 mm, which is consistent with the findings based on the CT images.

(4) From a rheological perspective, compared with the conventional AE residue, the rejuvenator-optimized asphalt emulsion residue further significantly improved the viscoelastic property, especially the viscous aspect, of the aged asphalt binder. The AOAE and TOAE residues helped aged asphalt binder obtain a good stress relaxation property and cracking resistance at a low temperature, but they might compromise the rutting resistance of PA pavement.

CHAPTER 8 FINDINGS, CONCLUSIONS AND RECOMMENDATIONS

This study aims to reveal the working mechanism of ST emulsion in PA and optimize the material design of ST emulsion for improving maintenance effectiveness through a multiscale investigation. To achieve these objectives, the key factors affecting the ST emulsion on the ravelling resistance of damaged PA were first investigated, and the optimal application conditions of ST were determined. Subsequently, the effects of ST on the mechanical and functional properties of damaged PA were systematically explored. Then, the penetration and diffusion mechanisms of ST emulsion in PA mixture were investigated by the X-ray CT and SEM/EDS, respectively. Finally, rejuvenator was incorporated to optimize ST emulsion towards a better ravelling resistance of PA.

8.1 Findings and Conclusions

Based on the outcomes of this study, the following key findings have been obtained:

1. Both the application rate and solid content of the ST emulsion have significant effects on the ravelling resistance recovery of the damaged PA mixtures. For the CSS-1 emulsion and PA mixture evaluated in this study, the optimum application rate of 0.6 kg/m^2 and solid content of 60% were recommended, which could reduce the mass loss ratios from 31.2% to 17.4%.

2. The ST treated PA mixture exhibited a higher indirect tensile strength, a longer fatigue life, and a better anti-rutting performance than untreated PA specimen over 3 months of curing, which helps extend the service life of PA pavement.

3. Although a relatively high curing temperature accelerated the recovery efficiency of mechanical properties of damaged PA in the short term, a relatively fast aging phenomenon also accompanied it, which cannot be neglected.

4. When the appropriate ST emulsion material and application conditions were well designed, the rutting resistance of the ST treated PA specimen didn't deteriorate. Meanwhile, the negative effect of the ST emulsion on functional performance was limited.

5. The penetration of the ST emulsion presented gradient characteristics, and the penetration depths of different ST emulsions varied. The ST emulsion with an application rate of 0.6 kg/m^2 and solid content of 60% penetrated approximately 20 mm.

6. The ST application altered the size, number, and area distribution of the air voids in PA. Both the average equivalent diameter (D_e) and the number of air voids (N_a) reduced at the bottom of each PA specimen after ST, N_a increased while D_e decreased at the top of the specimens. Based on CT image analysis, the ST emulsion droplets can fill the micro-pores and separate the large air voids into multiple smaller ones.

7. The ST emulsion considerably lowered the interconnected factor (F_i) across the top surface of the PA specimen and the tortuosity (T) at both ends of the specimen. The smaller F_i value should be primarily responsible for the decreased permeability of the PA specimen caused by the ST emulsion.

8. The percentage of coating P_c value has a strong relationship with the mass loss ratio of the treated PA specimen. A larger P_c value implies improved coating effectiveness on the aged mortar surface and, potentially, improved recovery efficiency for the damaged PA, which inspired the wettability optimization of ST emulsion.

9. SEM/EDS is an effective microscopic technique to directly observe the diffusion phenomenon between the applied ST emulsion residues and aged asphalt mortars within PA mixtures.

10. The diffusion phenomenon was obvious after curing for 21 days at 60 ºC, but it was not apparent after 28 days at 25 ºC. The diffusion rate at 60 ºC was about 5 times faster

than that at 25 ºC. Thus, it is recommended to spray ST emulsions in the field during hot weather (e.g. summer) to enhance the recovery efficiency of ravelling resistance of PA.

11. Rejuvenator is highly recommended to be emulsified to prepare rejuvenator emulsion before mixing with asphalt emulsion. The appropriate produce parameters of rejuvenator emulsion were determined based on the particle size distribution and zeta potential tests.

12. Mixing rejuvenator emulsion with asphalt emulsion did not obviously change the apparent viscosity of rejuvenator-optimized ST emulsion, but significantly improved its wettability and weakened the bonding strength of rejuvenator-optimized ST residue. The optimal dosage of rejuvenator emulsion was determined by balancing the apparent viscosity, wettability, and bonding strength of ST.

13. The penetration depth of rejuvenator-optimized ST emulsion was twice that of conventional asphalt emulsion, approaching around 40 mm. The rejuvenator-optimized emulsion distributed more uniformly with a higher coating efficiency, which promotes the ravelling resistance of PA.

14. The penetrated rejuvenator-optimized ST residues replenished new asphalt binders as well as light components and softened aged asphalt binders, which decreased the molecular weight at the highest occurrence frequency (M_p) and the number average molecular weight (M_n). Besides, FTIR could qualitatively detect penetration depth using a unique functional group as a tracer.

15. Compared with the conventional asphalt emulsion residue, the rejuvenator-optimized asphalt emulsion residue further significantly improved the viscoelastic property of the aged asphalt binder, especially its viscous aspect. It also enhanced the stress relaxation property and cracking resistance at a low temperature but might compromise the rutting resistance of PA pavement.

Based on the findings listed above, the following general conclusions have been drawn:

1. ST asphalt emulsion is an effective preventive maintenance material for damaged PA pavements to alleviate the ravelling distress.

2. At the macroscopic scale, ST asphalt emulsion can improve the mechanical performances of damaged PA mixture, including anti-cracking, anti-fatigue, and anti-rutting performances, and its negative effect on the functional property of PA is limited.

3. At the mesoscopic scale, ST emulsion residue presents a gradient profile in damaged PA along the depth direction. It reshapes the interconnected pore microstructure, including the size, number, area, interconnectivity, and tortuosity of air voids. A higher coating efficiency and a more uniform coating film are the potential optimization strategies for ST emulsion.

4. At the microscopic scale, there is diffusion between ST residues and aged asphalt mortars within the damaged PA mixture, and a higher temperature is expected to promote a higher diffusion efficiency.

5. Due to the excellent wettability of rejuvenator-optimized ST asphalt emulsion, the incorporation of rejuvenator emulsion into asphalt emulsion achieves a more uniform penetration status of emulsion residues in PA mixture, which can coat more age binder areas so as to further improve the ravelling resistance of PA pavement.

8.2 Recommendations for Future Research

Since the preventive maintenance material for old PA pavement is a relatively new research topic, more research should be further explored to improve the ravelling resistance recovery efficiency of ST emulsion for PA mixtures. The following recommendations are proposed to promote the application of this preventive maintenance technique to old PA pavements:

1. Only one type of ST emulsion was selected in this study to investigate its diffusion characteristic in aged asphalt mortar of PA mixture. More ST emulsions containing different rejuvenators should be considered in the future to evaluate their diffusion efficiencies in PA mixtures.
2. The compatibility between different rejuvenators and asphalt emulsions should be investigated.
3. A field test is necessary to investigate the actual maintenance effectiveness of ST emulsion on old PA pavements.
4. Life cycle assessment (LCA) and life cycle cost analysis (LCCA) should be considered to evaluate the potential economic and environmental effects of the preventive maintenance materials of ST emulsion for old PA pavements.

REFERENCES

[1] Z. Chuanfeng, Z. Dajun, X. Nailiang, and S. Zhenfeng, "Mechanism of low-temperature adhesion failure in asphalt mixtures with dense-suspension and void-skeleton structures," *Construction and Building Materials,* vol. 36, pp. 711-718, 2012.

[2] G. Liu, D. Han, Y. Zhao, and J. Zhang, "Effects of asphalt mixture structure types on force chains characteristics based on computational granular mechanics," *International Journal of Pavement Engineering,* vol. 23, no. 4, pp. 1008-1024, 2022.

[3] R. B. Mallick, P. S. Kandhal, L. A. Cooley Jr, and D. E. Watson, "Design, construction, and performance of new-generation open-graded friction courses," 2000.

[4] J. TH, H. GRUIS, and J. SWART, "Porous Asphalt Wearing Courses in the Netherlands: State of the Art Review," *TRANSPORTATION RESEARCH RECORD,* vol. 1265, p. 95.

[5] U. Sandberg, "The global experience in using low-noise road surfaces: A benchmark report," ed, 2009.

[6] U. Sandberg, "Effect on noise reduction of repaving only the top layer in a double-layer porous asphalt pavement," in *Roads and Airports Pavement Surface Characteristics*: CRC Press, 2023, pp. 651-661.

[7] M. E. Barrett and C. B. Shaw, "Benefits of porous asphalt overlay on storm water quality," *Transportation Research Record,* vol. 2025, no. 1, pp. 127-134, 2007.

[8] H. Edmar Schulz, J. Edgar Curry, and A. L. Andrade Simões, "Water films and hydroplaning on highways: Hydrodynamic aspects," *Journal of Transportation Engineering, Part B: Pavements,* vol. 147, no. 4, p. 04021053, 2021.

[9] K. J. Kowalski, R. S. McDaniel, A. Shah, and J. Olek, "Long-term monitoring of noise and frictional properties of three pavements: Dense-graded asphalt, stone matrix

asphalt, and porous friction course," *Transportation Research Record,* vol. 2127, no. 1, pp. 12-19, 2009.

[10] A. Mohajerani, J. Bakaric, and T. Jeffrey-Bailey, "The urban heat island effect, its causes, and mitigation, with reference to the thermal properties of asphalt concrete," *Journal of environmental management,* vol. 197, pp. 522-538, 2017.

[11] J. J. Stempihar, T. Pourshams-Manzouri, K. E. Kaloush, and M. C. Rodezno, "Porous asphalt pavement temperature effects for urban heat island analysis," *Transportation Research Record,* vol. 2293, no. 1, pp. 123-130, 2012.

[12] Z. Zhang *et al.*, "State-of-the-art of porous asphalt pavement: Experience and considerations of mixture design," *Construction & building materials,* vol. 262, p. 119998, 2020, doi: 10.1016/j.conbuildmat.2020.119998.

[13] E. T. Hagos, "The effect of aging on binder proporties of porous asphalt concrete," 2008.

[14] R. Rahbar-Rastegar, J. S. Daniel, and E. V. Dave, "Evaluation of Viscoelastic and Fracture Properties of Asphalt Mixtures with Long-Term Laboratory Conditioning," *Transportation research record,* vol. 2672, no. 28, pp. 503-513, 2018, doi: 10.1177/0361198118795012.

[15] A. Gupta, D. Castro-Fresno, P. Lastra-Gonzalez, and J. Rodriguez-Hernandez, "Selection of fibers to improve porous asphalt mixtures using multi-criteria analysis," *Construction and Building Materials,* vol. 266, p. 121198, 2021/01/10/ 2021, doi: https://doi.org/10.1016/j.conbuildmat.2020.121198.

[16] X. Ma, Q. Li, Y.-C. Cui, and A.-Q. Ni, "Performance of porous asphalt mixture with various additives," *International Journal of Pavement Engineering,* vol. 19, no. 4, pp. 355-361, 2018/04/03 2018, doi: https://doi.org/10.1080/10298436.2016.1175560.

[17] J.-S. Chen, Y.-C. Sun, M.-C. Liao, and C.-C. Huang, "Effect of Binder Types on Engineering Properties and Performance of Porous Asphalt Concrete," *Transportation Research Record,* vol. 2293, no. 1, pp. 55-62, 2012, doi: https://doi.org/10.3141/2293-07.

[18] B. Shirini and R. Imaninasab, "Performance evaluation of rubberized and SBS modified porous asphalt mixtures," *Construction and Building Materials,* vol. 107, pp. 165-171, 2016/03/15/ 2016, doi: https://doi.org/10.1016/j.conbuildmat.2016.01.006.

[19] "Guidance notes on road surface requirement for expressways and high-speed roads," Highways Department, Hong Kong, RD/GN/032, 2007/06 2007.

[20] S. Shimeno, A. Oi, and T. Tanaka, "Evaluation and further development of porous asphalt pavement with 10 years experience in Japanese expressways," in *Proceedings of the 11th International Conference on Asphalt Pavements, Nagoya*, 2010, pp. 43-52.

[21] J. Voskuilen, F. Tolman, and E. Rutten, "Do modified porous asphalt mixtures have a longer service life?," in *Proceedings of the 3rd Eurasphalt and Eurobitume Congress Held Vienna, May 2004*, 2004, vol. 2.

[22] Y. Zhang, "Extending the Lifespan of Porous Asphalt Concrete," Delft University of Technology, Delft University of Technology, 2015. [Online]. Available: http://resolver.tudelft.nl/uuid:f9860e45-e28b-477b-8df9-a094b00fd703

[23] G. Lu, P. Liu, Y. Wang, S. Faßbender, D. Wang, and M. Oeser, "Development of a sustainable pervious pavement material using recycled ceramic aggregate and bio-based polyurethane binder," *Journal of Cleaner Production,* vol. 220, pp. 1052-1060, 2019/05/20/ 2019, doi: https://doi.org/10.1016/j.jclepro.2019.02.184.

[24] G. Lu, L. Renken, T. Li, D. Wang, H. Li, and M. Oeser, "Experimental study on the polyurethane-bound pervious mixtures in the application of permeable pavements,"

Construction and Building Materials, vol. 202, pp. 838-850, 2019, doi: https://doi.org/10.1016/j.conbuildmat.2019.01.051.

[25] Z. Qian and Q. Lu, "Design and laboratory evaluation of small particle porous epoxy asphalt surface mixture for roadway pavements," (in English), *Construction and Building Materials,* vol. 77, pp. 110-116, Feb 15 2015, doi: https://doi.org/10.1016/j.conbuildmat.2014.12.056.

[26] Q. Xiang and F. Xiao, "Applications of epoxy materials in pavement engineering," *Construction and Building Materials,* vol. 235, p. 117529, 2020/02/28/ 2020, doi: https://doi.org/10.1016/j.conbuildmat.2019.117529.

[27] R. Li, Z. Leng, Y. Zhang, and X. Ma, "Preparation and characterization of waterborne epoxy modified bitumen emulsion as a potential high-performance cold binder," *Journal of cleaner production,* vol. 235, pp. 1265-1275, 2019, doi: 10.1016/j.jclepro.2019.06.267.

[28] B. Xu, M. Li, S. Liu, J. Fang, R. Ding, and D. Cao, "Performance analysis of different type preventive maintenance materials for porous asphalt based on high viscosity modified asphalt," *Construction & building materials,* vol. 191, pp. 320-329, 2018, doi: 10.1016/j.conbuildmat.2018.10.004.

[29] Y. Zhang, M. F. C. Van De Ven, A. A. A. Molenaar, and S. Wu, "Increasing the service life of porous asphalt with rejuvenators," Sustainable Construction Materials 2012 - Proceedings of the 2nd International Conference on Sustainable Construction Materials - Design, Performance, and Application, 2013 2013, pp. 316-328.

[30] P. Li *et al.*, "Performance test and evaluation index recommendation of fog seal on airport asphalt pavement," *Case Studies in Construction Materials,* vol. 19, p. e02604, 2023.

[31] Y. Zhang, M. F. C. van de Ven, A. A. A. Molenaar, and S. P. Wu, "Assessment of effectiveness of rejuvenator on artificially aged porous asphalt concrete," *Construction & building materials,* vol. 110, pp. 286-292, 2016, doi: 10.1016/j.conbuildmat.2016.02.042.

[32] M. Van de Ven, J. Qiu, and Y. Zhang, "Increasing the functional service life of porous surfacings: Development of test methods to study the effect of rejuvenating binders," in *Proceeding of 15th International Flexible Pavements Conference of AAPA, Australian Asphalt Pavement Association, Queensland, Australia*, 2013.

[33] Y. Zhang and Z. Leng, "Quantification of bituminous mortar ageing and its application in ravelling evaluation of porous asphalt wearing courses," *Materials & Design,* vol. 119, pp. 1-11, 2017/04/05/ 2017, doi: https://doi.org/10.1016/j.matdes.2017.01.052.

[34] D. Whiting *et al.*, "Synthesis of current and projected concrete highway technology," *Strategic Highway Research Program, National Research Council, Washington, DC,* vol. 286, 1993.

[35] E. Thelen and L. Fielding Howe, *Porous pavements*. 1978.

[36] I. Drainfields, "Storm Water Technology Fact Sheet," 1999.

[37] E.-J. Elizondo-Martínez, V.-C. Andres-Valeri, D. Jato-Espino, and J. Rodriguez-Hernandez, "Review of porous concrete as multifunctional and sustainable pavement," *Journal of Building Engineering,* vol. 27, p. 100967, 2020.

[38] X. Guan, J. Wang, and F. Xiao, "Sponge city strategy and application of pavement materials in sponge city," *Journal of Cleaner Production,* vol. 303, p. 127022, 2021.

[39] S. Ling, F. Yu, D. Sun, G. Sun, and L. Xu, "A comprehensive review of tire-pavement noise: Generation mechanism, measurement methods, and quiet asphalt pavement," *Journal of Cleaner Production,* vol. 287, p. 125056, 2021.

[40] K. Iwao and I. Yamazaki, "A study on the mechanism of tire/road noise," *JSAE review,* vol. 17, no. 2, pp. 139-144, 1996.

[41] N. Neithalath, R. Garcia, J. Weiss, and J. Olek, "Tire-Pavement interaction noise: Recent research on concrete pavement surface type and texture," in *Proceedings of the 8th International Conference on Concrete Pavements*, 2005, vol. 2, pp. 523-540.

[42] M. Haider, G. Descornet, U. Sandberg, and F. Pratico, "Road traffic noise emission: recent developments and future prospects," *Int. SIIV,* 2007.

[43] U. Sandberg and G. Descornet, "Road surface influence on tire/road noise," ed: Statens väg-och transportforskningsinstitut, 1980.

[44] M. Shamsaei, A. Carter, and M. Vaillancourt, "A review on the heat transfer in asphalt pavements and urban heat island mitigation methods," *Construction and Building Materials,* vol. 359, p. 129350, 2022.

[45] Y. Liu, T. Li, and L. Yu, "Urban heat island mitigation and hydrology performance of innovative permeable pavement: A pilot-scale study," *Journal of cleaner production,* vol. 244, p. 118938, 2020, doi: 10.1016/j.jclepro.2019.118938.

[46] R. Field, H. Masters, and M. Singer, "AN OVERVIEW OF POROUS PAVEMENT RESEARCH 1," *JAWRA Journal of the American Water Resources Association,* vol. 18, no. 2, pp. 265-270, 1982.

[47] H. Nakanishi, M. Hamzah, M. M. Hasan, P. Karthigeyan, and O. Shaur, "Mix design and application of porous asphalt pavement using Japanese technology," in *IOP Conference Series: Materials Science and Engineering*, 2019, vol. 512, no. 1: IOP Publishing, p. 012026.

[48] S. Takahashi, "Comprehensive study on the porous asphalt effects on expressways in Japan: Based on field data analysis in the last decade," *Road Materials and Pavement Design,* vol. 14, no. 2, pp. 239-255, 2013.

[49] A. Moriyoshi, T. Jin, T. Nakai, H. Ishikawa, K. Tokumitsu, and A. Kasahara, "Construction and pavement properties after seven years in porous asphalt with long life," *Construction and Building Materials,* vol. 50, pp. 401-413, 2014.

[50] Y. Ma, X. Chen, Y. Geng, and X. Zhang, "Effect of clogging on the permeability of porous asphalt pavement," *Advances in Materials Science and Engineering,* vol. 2020, no. 1, p. 4851291, 2020.

[51] I. Holleran, D. J. Wilson, G. Holleran, L. F. Walubita, and B. James, "Porous Asphalt—More Than Just Safety," in *Proceedings of the IPENZ Transportation Group Conference, Auckland, NZ, USA*, 2016, pp. 7-9.

[52] A. Meng, C. Xing, Y. Tan, G. Li, J. Li, and H. Lv, "Investigation on the distributing behaviors of clogging particles in permeable asphalt mixtures from the microstructure perspective," *Construction and Building Materials,* vol. 263, p. 120531, 2020.

[53] L. Chu and T. Fwa, "Laboratory characterization of clogging potential of porous asphalt mixtures," *Transportation Research Record,* vol. 2672, no. 52, pp. 12-22, 2018.

[54] H. Deng, X. Gu, X. Wang, C. Wu, and C. Zhu, "Evaluation of high-temperature deformation of porous asphalt mixtures based on microstructure using X-ray computed tomography," *Construction and Building Materials,* vol. 227, p. 116623, 2019.

[55] Q. Li, H. Yang, X. Ma, and F. Ni, "Evaluation of microstructure and damage evolution for asphalt pavements in an advanced repeated load permanent deformation test using X-ray computed tomography," *Road Materials and Pavement Design,* vol. 18, no. 5, pp. 1135-1158, 2017.

[56] A. Abouelsaad and G. White, "Review of asphalt mixture ravelling mechanisms, causes and testing," *International Journal of Pavement Research and Technology,* pp. 1-15, 2021.

[57] L. Mo, M. Huurman, S. Wu, and A. Molenaar, "Mortar fatigue model for meso-mechanistic mixture design of ravelling resistant porous asphalt concrete," *Materials and structures,* vol. 47, pp. 947-961, 2014.

[58] L. Mo, M. Huurman, S. Wu, and A. Molenaar, "Ravelling investigation of porous asphalt concrete based on fatigue characteristics of bitumen–stone adhesion and mortar," *Materials & Design,* vol. 30, no. 1, pp. 170-179, 2009.

[59] L. Mo, "Damage development in the adhesive zone and mortar of porous asphalt concrete," 2010.

[60] L. Chu, R. Wang, C. Qin, and T. F. Fwa, "Laboratory study of cleaning effects of clogged porous asphalt mixtures," *Road materials and pavement design,* vol. 23, no. 8, pp. 1762-1777, 2022, doi: 10.1080/14680629.2021.1924234.

[61] X. Zhu, Y. Han, B. Li, and B. Tian, "Effect of Clogging and Cleaning on the Air Void Microstructure of Porous Asphalt Concrete," *Journal of materials in civil engineering,* vol. 36, no. 8, 2024, doi: 10.1061/JMCEE7.MTENG-17801.

[62] R. J. Winston, A. M. Al-Rubaei, G. T. Blecken, M. Viklander, and W. F. Hunt, "Maintenance measures for preservation and recovery of permeable pavement surface infiltration rate – The effects of street sweeping, vacuum cleaning, high pressure washing, and milling," *Journal of environmental management,* vol. 169, pp. 132-144, 2016, doi: 10.1016/j.jenvman.2015.12.026.

[63] Y. Yang, Z. Sun, Y. Yang, L. Yue, and G. Chen, "Effects of Freeze–Thaw Cycles on Performance and Microstructure of Cold Recycled Mixtures with Asphalt Emulsion," *Coatings (Basel),* vol. 12, no. 6, p. 802, 2022, doi: 10.3390/coatings12060802.

[64] M. Dinis-Almeida, J. Castro-Gomes, and M. d. L. Antunes, "Mix design considerations for warm mix recycled asphalt with bitumen emulsion," *Construction & building materials,* vol. 28, no. 1, pp. 687-693, 2012, doi: 10.1016/j.conbuildmat.2011.10.053.

[65] Z. Chen *et al.*, "Cyclodextrin as a green anti-agglomerant agent in oil–water emulsion containing asphalt," *Fuel (Guildford),* vol. 335, p. 127041, 2023, doi: 10.1016/j.fuel.2022.127041.

[66] A. James, "Overview of asphalt emulsion," *Transportation Research Circular E-C102: Asphalt Emulsion Technology,* pp. 1-15, 2006.

[67] I. Ishai and M. Livneh, "Functional and structural role of prime coat in asphalt pavement structures," in *Association of Asphalt Paving Technologists Proceedings*, 1984, vol. 53.

[68] J. R. Galaviz-González, D. A. Cueva, P. L. Covarrubias, and M. Z. Palacios, "Bonding evaluation of asphalt emulsions used as tack coats through shear testing," *Applied sciences,* vol. 9, no. 9, p. 1727, 2019, doi: 10.3390/app9091727.

[69] A. Abouelsaad, D. Swiertz, and H. U. Bahia, "Study of Factors Affecting Curing of Asphalt Emulsion Tack Coats," *Transportation research record,* vol. 2673, no. 12, pp. 619-627, 2019, doi: 10.1177/0361198118821932.

[70] L. Kiihnl and A. F. Braham, "Developing a particle size specification for asphalt emulsion," *Construction and Building Materials,* vol. 293, p. 123414, 2021.

[71] S. M. Hama, A. K. Manshad, and J. A. Ali, "Review of the application of natural surfactants in enhanced oil recovery: state-of-the-art and perspectives," *Energy & Fuels,* vol. 37, no. 14, pp. 10061-10086, 2023.

[72] L. O. de Guertechin, "Classification of surfactants," *Handbook of Cosmetic Science and Technology,* vol. 431, 2001.

[73] S. Wang, X. Chen, X. Zhang, F. Liu, Y. Gao, and F. Li, "Effect of ionic emulsifiers on the properties of emulsified asphalts: An experimental and simulation study," *Construction and Building Materials,* vol. 347, p. 128503, 2022.

[74] X.-D. Gong, L.-S. Shi, T.-Y. Wang, and X.-M. Yu, "The Synthesis and Characterization of a Novel Cationic Asphalt Emulsifier," *2ND INTERNATIONAL CONFERENCE ON COMPOSITE MATERIAL, POLYMER SCIENCE AND ENGINEERING (CMPSE2018),* vol. 264, p. 3006, 2019, doi: 10.1051/matecconf/201926403006.

[75] A. Yuliestyan, M. García-Morales, E. Moreno, V. Carrera, and P. Partal, "Assessment of modified lignin cationic emulsifier for bitumen emulsions used in road paving," *Materials & design,* vol. 131, pp. 242-251, 2017, doi: 10.1016/j.matdes.2017.06.024.

[76] Y. Wang, Y. Gao, Q. Zhang, and Q. Meng, "A novel cationic emulsifier used for preparing slow-cracking and rapid-setting asphalt: Synthesis, surface activity, and emulsification ability," *Journal of dispersion science and technology,* vol. 39, no. 4, pp. 478-483, 2018, doi: 10.1080/01932691.2015.1120676.

[77] H. Painter, "Anionic surfactants," in *Detergents*: Springer, 1992, pp. 1-88.

[78] Y. Yuan *et al.*, "How calcium and magnesium ions affect the stability of asphalt with anionic emulsifiers: A molecular dynamics study," *Construction & building materials,* vol. 400, p. 132770, 2023, doi: 10.1016/j.conbuildmat.2023.132770.

[79] F. L. Calderon, J. Biais, and J. Bibette, "Asphalt emulsions: Flocculation induced by a cationic surfactant and application to size partitioning," *Colloids and surfaces. A, Physicochemical and engineering aspects,* vol. 74, no. 2, pp. 303-309, 1993, doi: 10.1016/0927-7757(93)80274-I.

[80] L. You, Q. Dai, Z. You, X. Zhou, and S. Washko, "Stability and rheology of asphalt-emulsion under varying acidic and alkaline levels," *Journal of cleaner production,* vol. 256, p. 120417, 2020, doi: 10.1016/j.jclepro.2020.120417.

[81] B. Derjaguin, N. Churaev, V. Muller, B. Derjaguin, N. Churaev, and V. Muller, "The Derjaguin—Landau—Verwey—Overbeek (DLVO) theory of stability of lyophobic colloids," *Surface forces,* pp. 293-310, 1987.

[82] H. Ohshima, "The derjaguin–landau–verwey–overbeek (dlvo) theory of colloid stability," *Electrical Phenomena at Interfaces and Biointerfaces: Fundamentals and Applications in Nano-, Bio-, and Environmental Sciences,* pp. 27-34, 2012.

[83] X. M. Xie, L. L. Zhao, L. Zong, and Z. G. Liu, "Preparation and Storage Stability of Asphalt Emulsions Made from Modified Lignin Cationic Asphalt Emulsifiers," *ARCHITECTURE, BUILDING MATERIALS AND ENGINEERING MANAGEMENT, PTS 1-4,* vol. 357-360, pp. 781-785, 2013, doi: 10.4028/www.scientific.net/AMM.357-360.781.

[84] H. Collini and M. D. Jackson, "Zeta potential of crude oil in aqueous solution," *Advances in colloid and interface science,* vol. 320, pp. 102962-102962, 2023, doi: 10.1016/j.cis.2023.102962.

[85] A. Kumar and C. K. Dixit, "Methods for characterization of nanoparticles," in *Advances in nanomedicine for the delivery of therapeutic nucleic acids*: Elsevier, 2017, pp. 43-58.

[86] I. Pinto and A. Buss, "ζ Potential as a measure of asphalt emulsion stability," *Energy & Fuels,* vol. 34, no. 2, pp. 2143-2151, 2020.

[87] A. Sze, D. Erickson, L. Ren, and D. Li, "Zeta-potential measurement using the Smoluchowski equation and the slope of the current–time relationship in

electroosmotic flow," *Journal of colloid and interface science,* vol. 261, no. 2, pp. 402-410, 2003.

[88] R. Li, "Waterborne epoxy resin modified bitumen emulsion as a high-performance cold paving binder: working mechanism and engineering performance," 2021.

[89] J. Ouyang, P. Cao, Y. Meng, and T. Tang, "Investigation on the drying and demulsification process of filler–bitumen emulsion paste," *Materials and structures,* vol. 54, no. 1, 2021, doi: 10.1617/s11527-020-01600-x.

[90] J. Ouyang, Y. Meng, T. Tang, M. Miljković, and Y. Tan, "Characterization of the drying behaviour of asphalt emulsion," *Construction and Building Materials,* vol. 274, p. 122090, 2021.

[91] J. Ouyang, Y. Meng, S. Zarei, and H. Yang, "Film formation properties of asphalt emulsion under ambient temperature drying," *International Journal of Pavement Engineering,* vol. 24, no. 1, p. 2185239, 2023.

[92] J. Ouyang, P. Cao, T. Tang, and Y. Meng, "Investigation on maximum packing fraction of bitumen particles during emulsion drying," *Materials and Structures,* vol. 54, pp. 1-14, 2021.

[93] Y. Zhang, M. F. C. v. d. Ven, A. A. A. Molenaar, and S. Wu, "Increasing the Service Life of Porous Asphalt with Rejuvenators," in *Sustainable Construction Materials 2012*, 2012, pp. 318-330.

[94] C. Hu, R. Li, J. Zhao, Z. Leng, and W. Lin, "Performance of Waterborne Epoxy Emulsion Sand Fog Seal as a Preventive Pavement Maintenance Method: From Laboratory to Field," *Advances in materials science and engineering,* vol. 2020, 2020, doi: 10.1155/2020/6425817.

[95] Y. Zhang, W. Verwaal, M. Van de Ven, A. Molenaar, and S. Wu, "Using high-resolution industrial CT scan to detect the distribution of rejuvenation products in

porous asphalt concrete," *Construction and Building Materials,* vol. 100, pp. 1-10, 2015.

[96] B. Xu *et al.*, "Experimental investigation of preventive maintenance materials of porous asphalt mixture based on high viscosity modified bitumen," *Construction & building materials,* vol. 124, pp. 681-689, 2016, doi: 10.1016/j.conbuildmat.2016.07.122.

[97] L. Xu, C. Jiang, and F. Xiao, "Application of Fog-Seal Technology with Waterborne Thermosetting Additive in Asphalt Pavement," *Journal of Materials in Civil Engineering,* vol. 34, no. 8, p. 04022160, 2022.

[98] A. A. Kebede, "Asphalt pavement preservation using rejuvenating fog seals," Purdue University, 2016.

[99] Z. Fan, C. Wang, Y. Li, L. Feng, and Q. Chen, "State of the art review on fog seal for asphalt pavement: Material composition, classification, performance evaluation, and mechanism analysis," *Progress in organic coatings,* vol. 194, p. 108573, 2024, doi: 10.1016/j.porgcoat.2024.108573.

[100] C. Estakhri and H. Agarwal, "Effectiveness of Fog Seal and Rejuvenators for Bituminous Pavement Surfaces. Final Report," FHWA/TX-91/1156-1F, Res Rept 1156-1F, TTI: 2-18-87-1156, 1991.

[101] Y. Zhang, M. F. C. van de Ven, A. A. A. Molenaar, and S. P. Wu, "Assessment of effectiveness of rejuvenator on artificially aged porous asphalt concrete," *Construction and Building Materials,* vol. 110, pp. 286-292, 2016/05/01/ 2016, doi: https://doi.org/10.1016/j.conbuildmat.2016.02.042.

[102] X. Ma, J. Jiang, Y. Zhao, and H. Wang, "Characterization of the interconnected pore and its relationship to the directional permeability of porous asphalt mixture," *Construction and Building Materials,* vol. 269, p. 121233, 2021.

[103] J. Chen, H. Wang, and H. Zhu, "Investigation of permeability of open graded asphalt mixture considering effects of anisotropy and two-dimensional flow," *Construction and Building Materials,* vol. 145, pp. 318-325, 2017.

[104] A. Meng *et al.*, "Investigation on flow resistance of fluid in permeable asphalt mixture," *Construction and Building Materials,* vol. 395, p. 132040, 2023.

[105] S. Lee and J. Yang, "Modeling of Darcy-Forchheimer drag for fluid flow across a bank of circular cylinders," *International journal of heat and mass transfer,* vol. 40, no. 13, pp. 3149-3155, 1997.

[106] H. Li, H. Xu, F. Chen, K. Liu, Y. Tan, and B. Leng, "Evolution of water migration in porous asphalt due to clogging," *Journal of Cleaner Production,* vol. 330, p. 129823, 2022.

[107] H. Xu, F. Chen, X. Yao, and Y. Tan, "Micro-scale moisture distribution and hydrologically active pores in partially saturated asphalt mixtures by X-ray computed tomography," *Construction and Building Materials,* vol. 160, pp. 653-667, 2018.

[108] H. Xu, C. Xing, H. Zhang, H. Li, and Y. Tan, "Moisture seepage in asphalt mixture using X-ray imaging technology," *International Journal of Heat and Mass Transfer,* vol. 131, pp. 375-384, 2019.

[109] T. Fwa, E. Lim, and K. Tan, "Comparison of permeability and clogging characteristics of porous asphalt and pervious concrete pavement materials," *Transportation Research Record,* vol. 2511, no. 1, pp. 72-80, 2015.

[110] T. Fwa, S. Tan, and Y. Guwe, "Laboratory evaluation of clogging potential of porous asphalt mixtures," *Transportation Research Record,* vol. 1681, no. 1, pp. 43-49, 1999.

[111] A. Meng, C. Xing, Y. Tan, S. Xiao, J. Li, and G. Li, "Investigation on clogging characteristics of permeable asphalt mixtures," *Construction and Building Materials,* vol. 264, p. 120273, 2020.

[112] A. Meng, M. Sun, X. Zhang, B. Zheng, X. Xiong, and S. Xiao, "Research on morphology and distribution characteristics of clogging particles in permeable asphalt mixture," *Construction and Building Materials,* vol. 402, p. 132976, 2023.

[113] C. Liu, X. Qin, Z. Yang, H. Zhang, and S. Lv, "Assessing bio-oil cutback asphalt for prime coat on semi-rigid base asphalt pavement: Lab experiment & indoor test section application," *Construction & building materials,* vol. 422, p. 135814, 2024, doi: 10.1016/j.conbuildmat.2024.135814.

[114] J. Ouyang, Y. Sun, and S. Zarei, "Fabrication of solvent-free asphalt emulsion prime with high penetrative ability," *Construction and Building Materials,* vol. 230, p. 117020, 2020.

[115] J. Lin, J. Hong, C. Huang, J. Liu, and S. Wu, "Effectiveness of rejuvenator seal materials on performance of asphalt pavement," *Construction and Building Materials,* vol. 55, pp. 63-68, 2014.

[116] C.-T. Chiu and M.-G. Lee, "Effectiveness of seal rejuvenators for bituminous pavement surfaces," *Journal of Testing and Evaluation,* vol. 34, no. 5, pp. 390-394, 2006.

[117] J. Lee, S. Li, Y. Kim, and J. Lee, "Effectiveness of asphalt rejuvenator," *Journal of Testing and Evaluation,* vol. 41, no. 3, pp. 433-440, 2013.

[118] M. Orešković, G. Menegusso Pires, S. Bressi, K. Vasconcelos, and D. Lo Presti, "Quantitative assessment of the parameters linked to the blending between reclaimed asphalt binder and recycling agent: A literature review," *Construction and building materials,* vol. 234, p. 117323, 2020, doi: http://doi.org/10.1016/j.conbuildmat.2019.117323.

[119] P. Pirzadeh, S. Kapilan, and P. Kriz, "Blending Between Aged and Virgin Asphalt Binders in Recycled Pavements: A Review Study," *IOP conference series. Materials*

Science and Engineering, vol. 1075, no. 1, p. 12006, 2021, doi: 10.1088/1757-899X/1075/1/012006.

[120] J. W. Oliver, "Diffusion of oils in asphalts," *Industrial & Engineering Chemistry Product Research and Development,* vol. 13, no. 1, pp. 65-70, 1974.

[121] R. Karlsson and U. Isacsson, "Application of FTIR-ATR to Characterization of Bitumen Rejuvenator Diffusion," *Journal of materials in civil engineering,* vol. 15, no. 2, pp. 157-165, 2003, doi: http://doi.org/10.1061/(ASCE)0899-1561(2003)15:2(157).

[122] R. Karlsson and U. Isacsson, "Laboratory studies of diffusion in bitumen using markers," *Journal of materials science,* vol. 38, no. 13, pp. 2835-2844, 2003, doi: http://doi.org/10.1023/A:1024476217060.

[123] R. Karlsson, U. Isacsson, and J. Ekblad, "Rheological characterisation of bitumen diffusion," *Journal of materials science,* vol. 42, no. 1, pp. 101-108, 2007, doi: http://doi.org/10.1007/s10853-006-1047-y.

[124] B. Huang, G. Li, D. Vukosavljevic, X. Shu, and B. K. Egan, "Laboratory investigation of mixing hot-mix asphalt with reclaimed asphalt pavement," *Transportation research record,* vol. 1929, no. 1929, pp. 37-45, 2005, doi: http://doi.org/10.3141/1929-05.

[125] A. S. Noureldin and L. E. Wood, "Rejuvenator diffusion in binder film for hot-mix recycled asphalt pavement," *Transportation research record,* no. 1115, 1987.

[126] P. Kriz *et al.*, "Blending and diffusion of reclaimed asphalt pavement and virgin asphalt binders," *Road materials and pavement design,* vol. 15, no. 1, pp. 78-112, 2014, doi: http://doi.org/10.1080/14680629.2014.927411.

[127] F. Y. Rad, N. R. Sefidmazgi, and H. Bahia, "Application of diffusion mechanism: Degree of blending between fresh and recycled asphalt pavement binder in dynamic

shear rheometer," *Transportation Research Record,* vol. 2444, no. 2444, pp. 71-77, 2014, doi: http://doi.org/10.3141/2444-08.

[128] S. Zhao, B. Huang, X. Shu, and M. E. Woods, "Quantitative evaluation of blending and diffusion in high RAP and RAS mixtures," *Materials & design,* vol. 89, pp. 1161-1170, 2016, doi: http://doi.org/10.1016/j.matdes.2015.10.086.

[129] Y. Ding, B. Huang, X. Shu, Y. Zhang, and M. E. Woods, "Use of molecular dynamics to investigate diffusion between virgin and aged asphalt binders," *Fuel (Guildford),* vol. 174, pp. 267-273, 2016, doi: 10.1016/j.fuel.2016.02.022.

[130] S. Ren, X. Liu, P. Lin, S. Erkens, and Y. Gao, "Chemical characterizations and molecular dynamics simulations on different rejuvenators for aged bitumen recycling," *Fuel (Guildford),* vol. 324, p. 124550, 2022, doi: 10.1016/j.fuel.2022.124550.

[131] C. Castorena, S. Pape, and C. Mooney, "Blending Measurements in Mixtures with Reclaimed Asphalt: Use of Scanning Electron Microscopy with X-Ray Analysis," *Transportation Research Record,* vol. 2574, no. 1, pp. 57-63, 2016, doi: https://doi.org/10.3141/2574-06.

[132] S. E. Pape and C. Castorena, "Assessment of the impacts of sample preparation on the use of EDS for analysing recycled asphalt blending," *Journal of Microscopy,* vol. 283, no. 3, pp. 232-242, 2021, doi: https://doi.org/10.1111/jmi.13036.

[133] Y. Jiang, X. Gu, Z. Zhou, F. Ni, and Q. Dong, "Laboratory Observation and Evaluation of Asphalt Blends of Reclaimed Asphalt Pavement Binder with Virgin Binder using SEM/EDS," *Transportation Research Record,* vol. 2672, no. 28, pp. 69-78, 2018, doi: https://doi.org/10.1177/0361198118782023.

[134] H. U. Bahia *et al.*, "Field aging and oil modification study," Wisconsin. Dept. of Transportation, 2018.

[135] H. Chen, Y. Zhang, and H. U. Bahia, "The role of binders in mixture cracking resistance measured by ideal-CT test," *International journal of fatigue,* vol. 142, p. 105947, 2021, doi: 10.1016/j.ijfatigue.2020.105947.

[136] H.-C. Dan, C. Ling, W. Cao, Z. Wang, and J. Liu, "Fatigue behavior and phenomenological modeling of porous asphalt concrete under freeze–thaw cycling," *Materials and structures,* vol. 54, no. 6, 2021, doi: 10.1617/s11527-021-01829-0.

[137] R. Tarefder, H. Faisal, and G. Barlas, "Freeze-thaw effects on fatigue LIFE of hot mix asphalt and creep stiffness of asphalt binder," *Cold regions science and technology,* vol. 153, pp. 197-204, 2018, doi: 10.1016/j.coldregions.2018.02.011.

[138] J. Yi, S. Shen, B. Muhunthan, and D. Feng, "Viscoelastic–plastic damage model for porous asphalt mixtures: Application to uniaxial compression and freeze–thaw damage," *Mechanics of materials,* vol. 70, pp. 67-75, 2014, doi: 10.1016/j.mechmat.2013.12.002.

[139] J. Yang *et al.*, "A semi-empirical method for estimating complete surface temperature from radiometric surface temperature, a study in Hong Kong city," *Remote sensing of environment,* vol. 237, p. 111540, 2020, doi: https://doi.org/10.1016/j.rse.2019.111540.

[140] "D7064 Standard Practice for Open-Graded Friction Course (OGFC) Mix Design," ed, 2004.

[141] "C131/C131M Standard Test Method for Resistance to Degradation of Small-Size Coarse Aggregate by Abrasion and Impact in the Los Angeles Machine," ed, 2020.

[142] F. Zhou, S. Im, L. Sun, and T. Scullion, "Development of an IDEAL cracking test for asphalt mix design and QC/QA," *Road materials and pavement design,* vol. 18, no. sup4, pp. 405-427, 2017, doi: 10.1080/14680629.2017.1389082.

[143] C. Yan, Y. Zhang, and H. U. Bahia, "Comparison between SCB-IFIT, un-notched SCB-IFIT and IDEAL-CT for measuring cracking resistance of asphalt mixtures," *Construction and Building Materials,* vol. 252, p. 119060, 2020.

[144] "D6931 Standard Test Method for Indirect Tensile (IDT) Strength of Asphalt Mixtures," ed, 2017.

[145] H. Xu, W. Guo, and Y. Tan, "Permeability of asphalt mixtures exposed to freeze–thaw cycles," *Cold regions science and technology,* vol. 123, pp. 99-106, 2016, doi: 10.1016/j.coldregions.2015.12.001.

[146] "E303 Standard Test Method for Measuring Surface Frictional Properties Using the British Pendulum Tester," ed, 2022.

[147] R. M. Islam, S. Arafat, and N. M. Wasiuddin, "Quantification of Reduction in Hydraulic Conductivity and Skid Resistance Caused by Fog Seal in Low-Volume Roads," *Transportation research record,* vol. 2657, no. 1, pp. 99-108, 2017, doi: 10.3141/2657-11.

[148] B. Yang, Z. Leng, J. Jiang, R. Chen, and G. Lu, "Diffusion characteristics of surface treatment emulsion in aged asphalt mortar of porous asphalt mixture through SEM/EDS analysis," *International Journal of Pavement Engineering,* vol. 25, no. 1, p. 2290093, 2024.

[149] R. Y. Liang and S. Lee, "Short-term and long-term aging behavior of rubber modified asphalt paving mixture," *Transportation research record,* vol. 1530, no. 1, pp. 11-17, 1996.

[150] L. Raad, S. Saboundjian, and G. Minassian, "Field aging effects on fatigue of asphalt concrete and asphalt-rubber concrete," *Transportation Research Record,* vol. 1767, no. 1, pp. 126-134, 2001.

[151] N. A. Qureshi, N. H. Tran, D. Watson, and S. M. Jamil, "Effects of rejuvenator seal and fog seal on performance of open-graded friction course pavement," *Maejo International Journal of Science and Technology,* vol. 7, no. 2, p. 189, 2013.

[152] S. Kim, J. Musselman, and G. Sholar, "Evaluation of Fog Seal Preservation Technique on US-17 and US-27," *Tallahassee, FL: Florida DOT,* 2014.

[153] S. Li, S. Noureldin, Y. Jiang, and Y. Sun, "Evaluation of pavement surface friction treatments," Purdue University. Joint Transportation Research Program, 2011.

[154] X. Ma, J. Jiang, Y. Zhao, and H. Wang, "Characterization of the interconnected pore and its relationship to the directional permeability of porous asphalt mixture," *Construction & building materials,* vol. 269, p. 121233, 2021, doi: 10.1016/j.conbuildmat.2020.121233.

[155] Y. Zhao, X. Wang, J. Jiang, and L. Zhou, "Characterization of interconnectivity, size distribution and uniformity of air voids in porous asphalt concrete using X-ray CT scanning images," *Construction & building materials,* vol. 213, pp. 182-193, 2019, doi: 10.1016/j.conbuildmat.2019.04.056.

[156] J. Jiang, F. Ni, X. Gu, L. Yao, and Q. Dong, "Evaluation of aggregate packing based on thickness distribution of asphalt binder, mastic and mortar within asphalt mixtures using multiscale methods," *Construction & building materials,* vol. 222, pp. 717-730, 2019, doi: 10.1016/j.conbuildmat.2019.06.083.

[157] E. Masad, V. K. Jandhyala, N. Dasgupta, N. Somadevan, and N. Shashidhar, "Characterization of Air Void Distribution in Asphalt Mixes using X-ray Computed Tomography," *Journal of materials in civil engineering,* vol. 14, no. 2, pp. 122-129, 2002, doi: 10.1061/(ASCE)0899-1561(2002)14:2(122).

[158] A. E. Alvarez, A. E. Martin, and C. Estakhri, "Connected air voids content in permeable friction course mixtures," *Journal of testing and evaluation,* vol. 37, no. 3, pp. 254-263, 2009.

[159] J. Jiang, Y. Li, Y. Zhang, and H. U. Bahia, "Distribution of mortar film thickness and its relationship to mixture cracking resistance," *The international journal of pavement engineering,* vol. 23, no. 3, pp. 824-833, 2022, doi: 10.1080/10298436.2020.1774767.

[160] L. S. Perše, A. Bizjak, and B. Orel, "The role of rheological properties and spraying parameters on the spectral selectivity of Thickness Insensitive Spectrally Selective (TISS) paint coatings," *Solar energy materials and solar cells,* vol. 110, pp. 115-125, 2013.

[161] S. L. Toma, C. Bejinariu, R. Baciu, and S. Radu, "The effect of frontal nozzle geometry and gas pressure on the steel coating properties obtained by wire arc spraying," *Surface and Coatings Technology,* vol. 220, pp. 266-270, 2013.

[162] Q. Wang, J. Liu, J. Liu, and J. Li, "Experimental research on the impact of annular airflow on the spraying flow field: A source control technology of paint mist," *Building and Environment,* vol. 207, p. 108444, 2022.

[163] Y. Zhang, H. Chen, and H. U. Bahia, "Extended aging performance of high RAP mixtures and the role of softening oils," *International Journal of Pavement Engineering,* pp. 1-12, 2021, doi: https://doi.org/10.1080/10298436.2020.1870115.

[164] T. Asaeda, V. T. Ca, and A. Wake, "Heat storage of pavement and its effect on the lower atmosphere," *Atmospheric environment,* vol. 30, no. 3, pp. 413-427, 1996.

[165] X. Zhu, Y. Yuan, L. Li, Y. Du, and F. Li, "Identification of interfacial transition zone in asphalt concrete based on nano-scale metrology techniques," *Materials & Design,* vol. 129, pp. 91-102, 2017/09/05/ 2017, doi: https://doi.org/10.1016/j.matdes.2017.05.015.

[166] Y. Zhang, Q. Liu, M. Van de Ven, A. Molenaar, and S. Wu, "Identification of rejuvenators on porous-asphalt concrete using optical microscopy and nanoindentation technology," *Journal of Materials in Civil Engineering,* vol. 27, no. 8, p. C4014008, 2015.

[167] B. Yang, Z. Leng, J. Jiang, Z. He, and D. Li, "Recovery efficiency of the damaged porous asphalt mixture with emulsion-based surface treatment: Material optimization and performance verification," *Construction and Building Materials,* vol. 347, p. 128530, 2022, doi: https://doi.org/10.1016/j.conbuildmat.2022.128530.

[168] J. Jiang *et al.*, "Penetration mechanism of the emulsion-based rejuvenator in damaged porous asphalt mixture: Microstructure characterization and 3D reconstruction," *Materials & design,* vol. 221, p. 111014, 2022, doi: 10.1016/j.matdes.2022.111014.

[169] C. K. Estakhri and H. Agarwal, *Effectiveness of fog seals and rejuvenators for bituminous pavement surfaces*. Texas Transportation Institute, Texas A & M University, 1991.

[170] Y. Fang, Z. Zhang, H. Zhang, and W. Li, "Analysis of wetting behavior and its influencing factors of rejuvenator/old asphalt interface based on surface wetting theory," *Construction and Building Materials,* vol. 314, p. 125674, 2022.

[171] J. Yi, Y. Wang, Z. Pei, M. Xu, and D. Feng, "Mechanisms and research progress on biological rejuvenators for regenerating aged asphalt: Review and discussion," *Journal of Cleaner Production,* p. 138622, 2023.

[172] B. Yang, Z. Leng, J. Jiang, R. Li, and M. Han, "Investigation of bituminous emulsion's impact on the mechanical durability of damaged porous asphalt mixture," in *Advances in Functional Pavements*: CRC Press, 2024, pp. 273-277.

[173] F. Goodarzi and S. Zendehboudi, "A comprehensive review on emulsions and emulsion stability in chemical and energy industries," *The Canadian Journal of Chemical Engineering,* vol. 97, no. 1, pp. 281-309, 2019.

[174] S. Ren, X. Liu, S. Erkens, P. Lin, and Y. Gao, "Multi-component analysis, molecular model construction, and thermodynamics performance prediction on various rejuvenators of aged bitumen," *Journal of Molecular Liquids,* vol. 360, p. 119463, 2022.

[175] J. Ji *et al.*, "Effectiveness of vegetable oils as rejuvenators for aged asphalt binders," *Journal of Materials in Civil Engineering,* vol. 29, no. 3, p. D4016003, 2017.

[176] B. Cui, X. Gu, D. Hu, and Q. Dong, "A multiphysics evaluation of the rejuvenator effects on aged asphalt using molecular dynamics simulations," *Journal of Cleaner Production,* vol. 259, p. 120629, 2020.

[177] J.-F. Su, J. Qiu, E. Schlangen, and Y.-Y. Wang, "Investigation the possibility of a new approach of using microcapsules containing waste cooking oil: In situ rejuvenation for aged bitumen," *Construction and Building materials,* vol. 74, pp. 83-92, 2015.

[178] D. Li *et al.*, "Investigation of rejuvenation mechanisms of reclaimed asphalt rubber pavement through mortar tests," *International Journal of Pavement Engineering,* vol. 24, no. 1, p. 2235631, 2023.

[179] C. K. Estakhri, A. E. Alvarez, and A. E. Martin, "Guidelines on Construction and Maintenance of Porous Friction Courses in Texas," Texas Transportation Institute, FHWA/TX-08/0-5262-2, 2008.

[180] H. U. Bahia *et al.*, "Field aging and oil modification study," Wisconsin Deptament of Transportation, PDF 2018-09-01 2018. [Online]. Available: https://rosap.ntl.bts.gov/view/dot/40770

[181] C. Yan, Y. Zhang, and H. U. Bahia, "Predicting rutting performance of asphalt mixture from binder properties and mixture design variables," *Road Materials and Pavement Design,* vol. 23, no. 1, pp. 62-79, 2022.

[182] J. Ma, G. Sun, D. Sun, F. Yu, M. Hu, and T. Lu, "Application of gel permeation chromatography technology in asphalt materials: A review," *Construction and Building Materials,* vol. 278, p. 122386, 2021.

[183] Q. Lv, W. Huang, H. Sadek, F. Xiao, and C. Yan, "Investigation of the rutting performance of various modified asphalt mixtures using the Hamburg Wheel-Tracking Device test and Multiple Stress Creep Recovery test," *Construction and Building Materials,* vol. 206, pp. 62-70, 2019.

[184] C. Xing, G. Zheng, L. Zhang, and Y. Tan, "Thermoregulation Performance and Mechanical Properties of Phase Change Asphalt Mortars," *Journal of Materials in Civil Engineering,* vol. 36, no. 8, p. 04024213, 2024.

[185] M. Woldekidan, M. Huurman, and A. Pronk, "A modified HS model: Numerical applications in modeling the response of bituminous materials," *Finite Elements in Analysis and Design,* vol. 53, pp. 37-47, 2012.

[186] G. Rowe, G. King, and M. Anderson, "The influence of binder rheology on the cracking of asphalt mixes in airport and highway projects," *Journal of Testing and Evaluation,* vol. 42, no. 5, pp. 1063-1072, 2014.

[187] D. Li, Z. Leng, F. Zou, and H. Yu, "Effects of rubber absorption on the aging resistance of hot and warm asphalt rubber binders prepared with waste tire rubber," *Journal of Cleaner Production,* vol. 303, p. 127082, 2021.

[188] L. Zhang, C. Xing, F. Gao, T.-s. Li, and Y.-q. Tan, "Using DSR and MSCR tests to characterize high temperature performance of different rubber modified asphalt," *Construction and Building Materials,* vol. 127, pp. 466-474, 2016.

[189] H. Wang, X. Liu, P. Apostolidis, M. van de Ven, S. Erkens, and A. Skarpas, "Effect of laboratory aging on chemistry and rheology of crumb rubber modified bitumen," *Materials and Structures,* vol. 53, pp. 1-15, 2020.

[190] H. Li, H. Shi, H. Xu, Y. Tian, Y. Tan, and K. Liu, "Exploring freeze-thaw damage distribution of asphalt mixture through DIC in combination with CT," *International Journal of Damage Mechanics,* p. 10567895241245750, 2024.